Fractional Order Models of the Human Respiratory System

Fractionele-ordemodellen van het menselijke ademhalingssysteem

Clara-Mihaela Ionescu

Promotor: prof. dr. ir. R. De Keyser
Proefschrift ingediend tot het behalen van de graad van
Doctor in de Ingenieurswetenschappen: Biomedische Ingenieurstechnieken

Vakgroep Elektrische Energie, Systemen en Automatisering
Voorzitter: prof. dr. ir. J. Melkebeek
Faculteit Ingenieurswetenschappen
Academiejaar 2009 - 2010

UNIVERSITEIT
GENT

ISBN 978-90-8578-318-3
NUR 954, 978
Wettelijk depot: D/2009/10.500/76

To raise new questions, new possibilities, to regard old problems from a new angle, requires creative imagination and marks the real advance in science

A. Einstein

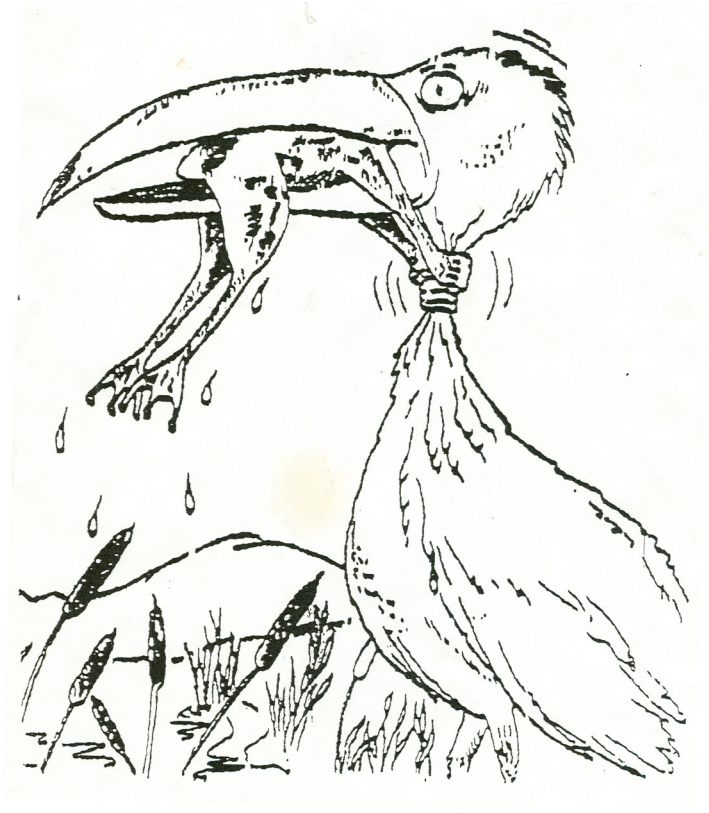

To those who encourage me to Never Ever Give Up.

Source: `http://www.wolfescape.com/Humour/Witty.htm`

Acknowledgment

If I had to mention all those who modeled in one way or another this quest for science, I would have to write another book. However, here I can only mention a few of those persons who directly supported me in my journey. The most courageous decision I took was in 2001, when for the first time I traveled out of my home-town and at the same time out of my home-country, to Belgium. I was an exchange student, who did not know much about life and had no specific career ambitions. Hence, I would like to thank Prof. Viorel Dugan from "Dunarea de Jos" University of Galati, Romania, for opening my eyes towards embracing an academic career. Secondly, I would like to express my gratitude and undivided appreciation for my mentor and promoter, Prof. Robin De Keyser, who supported my ambitions and who believed in my motivation and in my capabilities to pursue an academic career. Without the numerous opportunities he offered me in all these years, and without his spicy constructive criticism, this book would not exist.

Many thanks go to Prof. Kristine Desager from University Hospital in Antwerp and to Prof. Eric Derom from University Hospital in Gent for having the patience and good-will to help me in the clinical trials; I know now how complex the relationship doctor-patient is and how many efforts it requires. I cannot forget the many conversations and suggestions from Prof. Patrick Segers and Prof. Pascal Verdonck, who inspired me to embrace a biomedical application as my research topic. In the same line-of-thought, I thank Mr. Rudy Frigne, for providing the lung function testing device for research.

I would also like to thank Prof. Tenreiro Machado from the Institute of Engineering in Porto, Portugal, who gave me the first ideas on ladder networks on a paper-napkin, next to a delicious Bacalhao. Many thanks to Prof. Alain Oustaloup and his team in the University of Bordeaux, France, with whom I had many interesting and useful discussions.

I would like to thank my family, who encouraged me to go further whenever the light at the end of the tunnel seemed un-existent. My grandma, Buna, my aunt, Victoria, and my two cousins: Florina and Petrica. Their warmth and smile gave me strength to continue my journey.

I also express my gratitude to my colleagues from the Regeltechniek department, who provided a friendly atmosphere during the many hours of work. In particular I wish to thank dr. Bart Wyns for the support he provided on LaTex technicalities and numerous administrative details. And last but not least, I acknowledge my students and friends, with whom I shared many beautiful moments and discovered together many interesting research aspects of biomedical applications: Ramona Hodrea, Nele De Geeter, Niels Vannuffel and Ionut Muntean.

This dissertation presents research results which were financially supported by the following grants:

- Belgian Programme on Interuniversity Attraction Poles, SYSTeMS group, Ghent University, 2004;
- Verkennend Europees Onderzoek: Challenges for modelling and predictive control in biotechnological and biomedical engineering, project nr. 011/V0103, Ghent University, 2005-2007;
- BOF - Doctoraatsmandaten: Optimisation and implementation in a prototype medical apparatus of a routine evaluation technique for early detection of respiratory dysfunctions, project nr. 011/D04506, Ghent University, 2007-2009.

Contents

Summary

The fractional calculus is a generalization of classical integer-order integration and derivation to fractional (non-integer) order operators. Fractional order (FO) models are those models which contain such fractional order operators. A common representation of these models is in frequency domain, due to its simplicity. For an integer order system, the magnitude varies with an integer multiple of 20 dB/dec ($\pm$20 dB/dec, $\pm$40 dB/dec, etc), and the phase with an integer multiple of 90^o ($\pm 90^o$, $\pm 180^o$, etc). For a FO system of fractional order n, the magnitude varies with $n \cdot 20dB/dec$, with $0 \leq n \leq 1$. Similarly, the phase will vary with $n \cdot 90^o$.

The dynamical systems whose model can be approximated in a natural way using FO terms, exhibit specific features, such as viscoelasticity, diffusion and a fractal structure; hence the respiratory system is an ideal application for FO models. Although viscoelastic and diffusive properties were intensively investigated in the respiratory system, the fractal structure was ignored. Probably one of the reasons is that the respiratory system does not pose a perfect symmetry, hence failing to satisfy one of the conditions for being a typical fractal structure. Nonetheless, some degree of recurrence has been recognized in the airway generation models.

The respiratory system poses all three properties enumerated above and there is no reason why one should ignore either one of them. Moreover, with pathology, viscoelasticity is affected by changes at the cellular level, narrowing or occluding the airway, which in turn affects both the structure of the airway distribution, as well as the diffusion area. If a specific model (e.g. an electrical analogue) of the respiratory tree would exist, it would allow simulation studies in both healthy and pathology scenarios. Firstly, such an analogue would provide the means to investigate the appearance of the FO model and secondly, it would provide information upon how the FO model parameters are affected by changes in morphology.

In the 70s, the respiratory impedance determined by the ratio of air-pressure and air-flow, has been introduced in a model structure containing a resistance R_r, inertance L_r and compliance C_r element, whereas the latter contained a fractional order n: $1/C_r s^n$. The model proved to have a notorious success at low frequencies and has been used ever since by researchers to characterize the respiratory impedance. It has also been shown that the fractional order models outperform integer-order models on input impedance measurements. However, there is a lack of underpinning theory to clarify the appearance of the fractional order in the FO model structure.

Several attempts have been made to obtain an electrical equivalent of the respiratory tree, but the models reported hitherto are an approximation of the tree rather than a precise formulation, and do not preserve the intrinsic geometry. The clinicians prefer a simple, lumped, yet sufficiently accurate model from whose parameter values they are able to detect whether or not a lung function is normal. It is therefore interesting to characterize the lung function in terms of its mechanical properties, which can be directly related to changes in airway duct geometry and relate them to the non-integer order model parameters.

This thesis describes a physiologically consistent approach to reach twofold objectives:

- to provide a physiologically-based mathematical explanation for the necessity of fractional order models for the input impedance, and
- to determine the capability of the best fractional order model to classify between healthy and pathological cases.

Rather than dealing with a specific case study, the modelling approach presents a general method which can be used not only in the respiratory system application, but also in other similar systems (e.g. leaves, circulatory system, liver, intestines). Furthermore, we consider also the case when symmetry is not present (e.g. deformations in the thorax - kyphoscoliose) as well as various pathologies. We provide a proof-of-concept for the appearance of the FO model from the intrinsic structure of the respiratory tree. Several clinical studies are then conducted to validate the sensitivity and specificity of the FO model in healthy groups and in various pathological groups.

This thesis in organized as follows: chapter 1 describes what fractional-order models are and why they became so popular in characterizing the properties of the biological tissue, i.e. the lung parenchyma. A state of the art in the field of modelling and identification of the respiratory system is given and the

objectives and contributions of this work are stated. Some basic principles of lung physiology and pathology are introduced in order to provide support for later developments throughout the thesis. After introducing some concepts and results on the appearance of fractional-order in respiratory system models, the mathematical structure and the basic properties of such systems are presented.

The second chapter presents the principles of measuring the respiratory input impedance by means of FOT (Forced Oscillation Technique) lung function test. The chapter continues with an overview of the most representative parametric models reported in literature. Additionally, two alternative models are proposed. A comparison in terms of modelling performance is evaluated on typical patient data obtained with FOT, i.e. three averaged sets of representative diagnosed subjects: healthy, asthma and COPD (chronic obstructive pulmonary disease). It is shown that the FO model in four parameters from literature is unable to capture real parts of the impedance which are increasing with frequency. All identified model parameter values are discussed with respect to physiological insight.

The derivation of the mechanical parameters of the airways from morphological insight is presented in chapter 3. The approach consists of: 1) taking into account morphological and anatomical values such as: airway wall thickness, inner radius, tube length and tissue structure for each airway level and 2) combine them into a set of equations for modelling the pressure drop, flow, wall elasticity and air velocity (axial and radial). Both elastic and viscoelastic airways are investigated, in the context of a symmetric space-filling of the lung. Effects of pulmonary disease affecting the inner radius and elastic modulus of bronchial tree are discussed. The derived mechanical parameters (resistance, inertance, compliance and conductance) are used to gather insight into the recurrence of the respiratory tree.

Chapter 4 details the construction of the electrical ladder network equivalent, using the elements determined in chapter 3. The cases of an elastic tube wall and a viscoelastic tube wall are discussed, with supporting analytical and simulated results. A generalization of the analytical results is given, suggesting applicability to other branching systems (e.g. circulatory, neural, lymphatic, etc). The estimated results are successfully validated with measured data. The chapter ends with a special analysis of the asymmetric branching and its consequences on the total input impedance values.

In the 5th chapter, an equivalent mechanical representation is derived for the elastic and the viscoelastic electrical models developed in the previous chapter. Assuming a dichotomously branching tree, each airway tube is modeled

by a combination of Maxwell and Kelvin-Voigt elements calculated from morphological values. This will allow comparison to models reported in literature and provide the link between the appearance of the FO behaviour and both intrinsic fractal geometry, as well as the rheological properties of the lung parenchyma.

Next, chapter 6 presents an analysis of the modelling performance on several candidate fractional-order models. The models are presented on an evolutionary basis from the most simple to the most complex representation. The model with the least number of parameters which delivers the smallest modelling errors will be selected as the best candidate to model the impedance in the 4-48 Hz frequency interval. Further on, we investigate the ability of the selected FO model in classifying between healthy and pathologic patient data. The investigated groups are: healthy vs Chronic Obstructive Pulmonary Disease; healthy vs kyphoscoliosis; healthy vs asthma in children; healthy vs cystic fibrosis in children.

The main contributions of this work are pointed out in chapter 7, along with some further research directions.

Samenvatting

Fractionele calculus kan beschouwd worden als een veralgemening van afgeleiden en integralen, waarbij de orde nu ook niet-geheel kan zijn. Fractionele-orde (FO) systemen zijn dynamische systemen die gemodelleerd worden met behulp van differentiaalvergelijkingen waarin afgeleiden van niet-gehele orde voorkomen. Een gebruikelijke representatie van deze modellen is in het frequentie-domein. Voor een gehele-orde systeem, varieërt de magnitude in de Bode karakteristiek met een geheel veelvoud van 20 dB/dec ($\pm$20 dB/dec, $\pm$40 dB/dec, enz.), en de fase met een geheel veelvoud van 90^o ($\pm 90^o$, $\pm 180^o$, enz.). Voor een FO systeem met een fractionele orde n, varieërt de magnitude met $n \cdot 20dB/dec$, met $0 \leq n \leq 1$: evenzo zal de fase variëren met $n \cdot 90^o$.

De dynamische systemen die op een natuurlijke wijze met behulp van FO modellen kunnen gemodelleerd worden, vertonen specifieke kenmerken, zoals visco-elasticiteit, diffusie en een fractale structuur; het ademhalingssysteem is hiervan een ideaal voorbeeld. Hoewel de visco-elastische en diffuse eigenschappen van het ademhalingssysteem reeds intensief werden onderzocht, werd de fractale structuur tot nog toe genegeerd. Eén van de redenen is wellicht dat de luchtwegen geen perfecte symmetrie vormen, dus niet echt voldoen aan de voorwaarden om een typisch fractale structuur te zijn. Toch kan men een hoge mate van recurrentie herkennen in de luchtwegengeometrie.

Het ademhalingsstelsel bezit de drie hierboven genoemde eigenschappen en er is geen enkele reden waarom men één van hen zou moeten negeren. Bovendien wordt in het geval van aandoeningen de visco-elasticiteit beïnvloed door veranderingen op cellulair niveau; veranderingen die ook de oorzaak zijn van lokale vernauwingen en afsluitingen van de luchtwegen, die op hun beurt dan een invloed hebben op zowel de structuur van het luchtwegenstelsel als op het diffusiegebied. Als een specifiek model (een elektrisch analogon bv.) van de luchtwegen zou bestaan, dan zou dit kunnen gebruikt worden

voor simulatiedoeleinden, zowel bij gezonde als pathologische gevallen. Ten eerste, zou een dergelijk analogon nuttig zijn om het optreden van het FO verschijnsel te helpen verklaren, en ten tweede zou het ook informatie verstrekken over de wijze waarop de FO modelparameters worden beïnvloed door veranderingen in de morfologie.

In de jaren 70 heeft men de ademhalingsimpedantie - gedefinieerd als de verhouding tussen drukoscillaties en luchtstroomsnelheid - gemodelleerd met een RLC-structuur (een weerstand R_r, een inductie L_r en een condensator C_r) waarbij de condensator een fractionele orde n bevatte: $1/C_r s^n$. Het model bleek succesvol bij lage frequenties en wordt momenteel nog altijd gebruikt door onderzoekers om de luchtwegimpedantie te karakteriseren. Ook is gebleken dat de fractionele-orde modellen beter presteren dan gehele-orde modellen bij metingen van de ingangsimpedantie. Er was echter een gebrek aan theoretisch inzicht om het fractionele-orde verschijnsel in de structuur van het model te verklaren.

Verschillende pogingen werden gedaan om een elektrisch equivalent van de luchtweg-boomstructuur te verkrijgen, maar de modellen die tot nu toe gerapporteerd werden zijn gebaseerd op een ruwe benadering van de boom in plaats van een meer preciese formulering en ze behouden niet de intrinsieke geometrie. Artsen prefereren een eenvoudig maar toch voldoende accuraat model, waarvan de parameterwaarden kunnen dienstig zijn om te detecteren of de longfunctiemetingen normaal zijn. Het is daarom interessant om de longfunctie te karakteriseren in termen van mechanische eigenschappen - welke direct kunnen worden gerelateerd aan veranderingen in de luchtweggeometrie - en deze eigenschappen dan te relateren aan de FO modelparameters.

Dit proefschrift beschrijft een fysiologisch consistente aanpak om volgende twee doelstellingen te bereiken:

- het verstrekken van een theoretische verklaring - gebaseerd op fysiologisch inzicht - betreffende de noodzaak aan FO modellen voor de ademhalingsimpedantie
- het bepalen van de beste FO modelstructuur die toelaat om zo goed mogelijk gezonde en pathologische gevallen te classificeren.

Eerder dan een specifieke case te bestuderen, werd gekozen voor een meer algemene modelgebaseerde aanpak, die niet alleen kan worden gebruikt in de ademhalingssysteem, maar ook in andere vergelijkbare systemen (bijvoorbeeld bloedsomloop, lever, darmen, tot zelfs watertransport in de nerven van

bladeren). Verder beschouwen we ook het geval indien symmetrie niet aanwezig is (bijvoorbeeld vervormingen in de thorax - kyphoscoliose), evenals verschillende pathologieën. We brengen een proof-of-concept aan voor het optreden van het FO-fenomeen op basis van de intrinsieke structuur van de luchtwegenboom. Verschillende klinische studies worden vervolgens uitgevoerd voor de validatie van de gevoeligheid en specificiteit van het FO model in gezonde groepen en in verschillende pathologische groepen.

Dit proefschrift is als volgt opgebouwd: hoofdstuk 1 beschrijft wat fractioneleorde modellen zijn en waarom ze zo populair werden in de karakterisering van de eigenschappen van het biologische weefsel, dwz longparenchym. De state-of-the-art op het gebied van modellering en identificatie van de luchtwegen wordt gegeven, gevolgd door een opsomming van de doelstellingen en de bijdragen van dit proefschrift. Enkele basisprincipes van long fysiologie en pathologie worden ingevoerd om de steun voor latere ontwikkelingen in het proefschrift bieden. Na de introductie van een aantal concepten en resultaten omtrent het optreden van fractionele ordes in de modellen voor ademhalingswegen, worden de wiskundige structuur en de fundamentele eigenschappen van dergelijke FO systemen gepresenteerd.

Het tweede hoofdstuk begint met de principes van het meten van de ademhalingsimpedantie door middel van de geforceerde oscillometrie. Het hoofdstuk vervolgt met een overzicht van de meest representatieve parametrische modellen uit de literatuur. Daarnaast worden door ons twee alternatieve modellen gesuggereerd. Een vergelijking tussen al deze modellen voor wat betreft de modelperformantie wordt dan uitgevoerd op basis van typische patiëntgegevens die zijn verkregen met de geforceerde oscillometrie. Deze gegevens bestaan uit drie uitgemiddelde sets van representatieve groepen: gezond, astma en COPD (chronic obstructive pulmonary disease). Er wordt aangetoond dat het FO-model met 4 parameters uit de literatuur niet in staat is het reële deel van de opgemeten impedantie - dat toeneemt met de frequentie - te modelleren. Alle geïdentificeerde modelparameterwaarden worden geïnterpreteerd vanuit fysiologisch inzicht.

De afleiding van de mechanische parameters van de luchtwegen op basis van morfologisch inzicht is de kern van hoofdstuk 3. De aanpak bestaat uit: 1) rekening te houden met morfologische en anatomische waarden (zoals luchtweg-wanddikte, binnenstraal, buislengte, weefselstructuur) en dit voor elk luchtweg-niveau; en 2) deze te combineren in een stel vergelijkingen voor de modellering van de drukval, luchtdebiet, wandelasticiteit en luchtsnelheid (axiale en radiale). Zowel elastische als visco-elastische luchtwegen worden onderzocht, en dit in het kader van een symmetrische ruimte-opvulling. Ef-

fecten van longziekte die de straal en elasticiteitsmodulus van de bronchiale boom beïnvloeden, worden besproken. De afgeleide mechanische parameters (weerstand, inertie, capaciteit en geleiding) worden gebruikt om inzicht te verkrijgen in de recurrente structuur van de luchtwegenboom.

Hoofdstuk 4 beschrijft de opbouw van een equivalent elektrisch laddernetwerk met behulp van de basiselementen die bepaald werden in hoofdstuk 3. De 2 gevallen van een elastische en een visco-elastische buiswand worden besproken, met ondersteuning van analytische en gesimuleerde resultaten. Een veralgemening van de analytische resultaten wordt gegeven, wat wijst op de toepasbaarheid ervan in andere vertakkingsystemen (bijvoorbeeld de bloedsomloop, zenuwstelsel, lymfesysteem, enz.). De resultaten worden succesvol gevalideerd op basis van gemeten data. Het hoofdstuk eindigt met een speciale analyse van de a-symmetrische vertakking en de gevolgen daarvan op de totale waarde van de ingangsimpedantie.

In het 5e hoofdstuk wordt een equivalente mechanische representatie afgeleid voor de elastische en de visco-elastische elektrische modellen die werden ontwikkeld in het vorige hoofdstuk. Uitgaande van een dichotomisch-vertakkende boom, wordt elke luchtwegbuis gemodelleerd door een combinatie van Maxwell en Kelvin-Voigt elementen, berekend op basis van morfologische waarden. Dit laat toe een vergelijking te maken tussen ons model en andere modellen uit de literatuur. Het laat ook toe een verband te leggen tussen enerzijds het FO-verschijnsel en anderzijds zowel de intrinsieke fractale structuur van de longgeometrie als de rheologische eigenschappen van het longparenchym.

Hoofdstuk 6 start met een analyse van de prestaties van verschillende kandidaat FO modellen. De modellen worden voorgesteld van de meest eenvoudige tot de meest complexe structuur. Het model met het minste aantal parameters dat de kleinste modelfout oplevert wordt dan geselecteerd als het beste kandidaatmodel voor de ademhalingsimpedantie in het 4-48 Hz frequentie-interval. Verder onderzoeken we de mogelijkheden van het geselecteerde model voor wat betreft de indeling tussen gezonde mensen en patiënten. Dit gebeurt op basis van gegevens afkomstig van clinische metingen, waarbij de onderzochte groepen zijn: gezond versus COPD (Chronic Obstructive Pulmonary Disease); gezond vs astma bij kinderen; gezond vs cystic fibrosis bij kinderen; gezond vs kyphoscoliosis.

De belangrijkste bijdragen van dit proefschrift worden vermeld in een concluderend hoofdstuk 7, samen met enkele suggesties en ideëen voor vervolgonderzoek.

Chapter 1

Introduction

This chapter describes what fractional-order models are and why they became so popular in characterizing the properties of the biological tissue, i.e. the lung parenchyma. A state of the art in the field of modelling and identification of the respiratory system is given and the objectives and contributions of this work are stated. Some basic principles are given over the anatomy and physiology of the respiratory system along with its related pathologies. After introducing some concepts and results for the appearance of fractional-order in respiratory system models, the mathematical structure and the basic properties of such systems are presented. The chapter ends with an overview of this thesis.

1.1 Problem Statement

The concept of fractional order (FO) – or non-integer order – systems refers to those dynamical systems whose model parameters contain arbitrary order derivatives and/or integrals. The fractional order derivatives and integrals are tools of the Fractional Calculus theory (Oldham & Spanier 1974). The dynamical systems whose model can be approximated in a natural way using FO terms, exhibit specific features:

- viscoelasticity;
- diffusion;
- fractal structure.

Viscoelasticity has been shown to be the origin of the appearance of FO models in polymers (from the Greek: *poly* – many and *meros* – parts) (Adolfsson *et al.* 2005) and resembling biological tissues (Doehring *et al.* 2005, Suki *et al.* 1994, Ionescu & Chirita 2008).

Diffusion phenomena have been intensively studied in the field of chemistry and dielectrics (Jesus & Tenreiro Machado 2008, Reyes-Melo *et al.* 2004), hydrology (Benson *et al.* 2004) and in biology (Jesus *et al.* 2008, Hou *et al.* 2005, Losa *et al.* 2005).

Finally, the most remarkable property, the fractal structure, has been shown to lead to a FO model in some geometrical structures (Ramus-Serment *et al.* 2002, Elzbieta *et al.* 2005) and electrical networks (Tenreiro Machado & Jesus 2004, Ionescu & Tenreiro Machado in print).

Although viscoelastic and diffusive properties were intensively investigated in the respiratory system, the fractal structure was ignored. Probably one of the reasons is that the respiratory system does not pose a perfect symmetry, hence failing to satisfy one of the conditions for being a typical fractal structure. Nonetheless, some degree of recurrence has been recognized in the airway generation models (Mandelbrot 1983, Weibel 1963, Sauret *et al.* 1999).

The literature reports the existence of a FO model based on viscoelastic assumptions (Hantos *et al.* 1992*b*, *a*). The model provides an expression for the input impedance (measured at the mouth of the patient) by considering a series arrangement of a resistance, inertance and capacitance:

$$Z_r(s) = \frac{P(s)}{Q(s)} = R_r + L_r s + \frac{1}{C_r s^{\beta_r}} \tag{1.1}$$

with P – pressure in kPa; Q – flow in l/s; Z_r – the respiratory impedance; R_r – airway resistance kPa/(l/s); L_r – inductance kPa/(l/s^2); C_r – capacitance in l/kPa; $0 \leq \beta_r \leq 1$ the fractional order and s the Laplace operator (see details on units in Appendix A). In this representation, the last term is also referred to as *tissue viscance*. This model, although broadly used by researchers and providing valid parameter values in several groups of patients, is unable to characterize real part of the impedance values which increase with frequency (Ionescu 2003). As a result of this limitation, researchers have performed and reported studies in which the parameter values are meaningless from a physiological standpoint, i.e. negative (Hantos *et al.* 1982, Peslin *et al.* 1992, Suki *et al.* 1992).

The respiratory system poses all three properties enumerated above and there is no reason why one should ignore either one of them. Moreover, with pathology, viscoelasticity is affected by changes at the cellular level, narrowing or occluding the airway, which in turn affects both the structure of the airway distribution, as well as the diffusion area. If a specific model (e.g. an electrical analogue) of the respiratory tree would exist, it would allow simulation studies in both healthy and pathology scenarios. Firstly, such a model would provide the means to investigate the appearance of the FO model and secondly, would provide information upon how the FO model parameters are affected by changes in morphology.

Several attempts have been made to obtain an electrical equivalent of the respiratory tree (Farre *et al.* 1989, Diong *et al.* 2007, Ionescu 2003). However, the models reported hitherto are an approximation of the tree rather than a precise formulation, and do not preserve the intrinsic geometry. Thanks to advances in technology, information on airway radius, length and thickness is available (Sauret *et al.* 1999). This doctoral thesis provides a simulator for the dichotomous airway structure and verifies the appearance of a FO model.

The clinicians prefer a simple, lumped, yet sufficiently accurate model from whose parameter values they are able to detect whether or not a lung function is normal. It is therefore interesting to characterize the lung function in terms of its mechanical properties, which can be directly related to changes in airway duct geometry and relate them to the non-integer order model parameters. Consequently, an analysis of the respiratory tree in terms of its electrical and mechanical equivalent is another issue treated in this thesis.

1.2 State of the Art

The compliance is expressed as the volume increase in the lungs for each unit increase in alveolar pressure or for each unit decrease of pleural pressure. The most common representation of the compliance is given by the pressure-volume (PV) loops. Changes in elastic recoil (more, or less, stiffness) will affect these pressure-volume relationships. The initial steps undertaken by Salazar & Knowles to characterize the pressure-volume relationship in the lungs by means of exponential functions suggested a new interpretation of mechanical properties in lungs (Salazar & Knowles 1964). In their endeavor to obtain a relation for compliance which would be independent on the size of the lungs, they concluded that the pressure volume curve is a good tool in characterizing viscoelasticity. Shortly after, Hildebrandt used similar concepts to assess the viscoelastic properties of a rubber balloon (Hildebrandt 1969) as a model of the lungs. He obtained similar static pressure-volume curves by stepwise inflation in steps of 10ml (volume) increments in a one minute time interval. He then points out that the curves can be represented by means of a power law function (see figure 1.1).

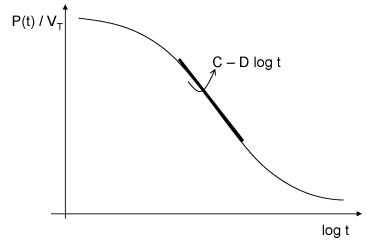

Figure 1.1: *Schematic representation of the quasi-linear dependence of the pressure-volume ratio with the logarithm of time.*

Instead of deriving the compliance from the PV curve, Hildebrandt suggests to apply sinusoidal inputs instead of steps and he obtains the frequency response of the rubber balloon. He considers the variation of pressure over total volume displacement also an exponentially-decaying function:

$$\frac{P(t)}{V_T} = A\,t^{-n} + B, \quad \frac{P(t)}{V_T} = C - D\,log\,t \tag{1.2}$$

with A, B, C, D arbitrary constants, V_T the total volume, t the time and n the power-law constant. The transfer function obtained by applying Laplace

to this stress relaxation curve is given by:

$$\frac{P(s)}{V_T} = A\frac{\Gamma(1-n)}{s^{1-n}} + \frac{B}{s} \tag{1.3}$$

with Γ the Gamma function. If the input is a step $v(t) = V_T u(t)$, then $V(s) = V_T/s$ and the output is given by $P(s) = T(s)V_T/s$ with $T(s)$ the unknown transfer function. Introducing this into (1.3) he obtains that

$$T(s) = \frac{P(s)}{V(s)} = As^n\Gamma(1-n) + B \tag{1.4}$$

By taking into account the mass of air introduced into the balloon, an extra term appears in the transfer function equation:

$$T(s) = \frac{P(s)}{V(s)} = As^n\Gamma(1-n) + B + L_r s^2 \tag{1.5}$$

with L_r the inductance. The equivalent form in frequency domain is given by:

$$\begin{aligned} T(j\omega) \quad &= A\Gamma(1-n)\omega^n \cos(\tfrac{n\pi}{2}) - L_r\omega^2 + B + \\ &+ j[A\Gamma(1-n)\omega^n \sin(\tfrac{n\pi}{2})] \end{aligned} \tag{1.6}$$

This function describes the behavior of the balloon in a plethysmograph, while undergoing sinusoidal forced oscillations (see Appendix B). One year later, in 1970, he published the results obtained by identifying such a model on excised cat lungs (Hildebrandt 1970). He then suggests to do the PV approximation with a transfer function which has an imaginary part independent on frequency. This special property gives a phase angle which decreases slightly with frequency (quasi-constant). Playing with these models on the data for the PV curves, he discusses the viscoelastic properties of the rubber balloon versus the excised cat lungs. In doing so, he combines several idealized mechanical elements to express viscoelasticity in a mechanical context. Some fragile steps are then directed towards concepts of stress relaxation and dynamic hysteresis of the lungs.

Two decades later, Hantos and co-workers in 1992*b* revise the work of Hildebrandt and introduce the impedance as the ratio of pressure and flow, in a model structure containing a resistance R_r, inertance L_r and compliance C_r element, as in (1.1) (Hantos *et al.* 1992*b*). This model proved to have a notorious success at low frequencies and has been used ever since by researchers to characterize the respiratory impedance.

In the same context of characterizing viscoelasticity, Suki *et al.* provided an overview of the work done by Salazar & Knowles, Hildebrandt and Hantos *et al.*, establishing possible scenarios for the origin of viscoelastic behavior in the lung parenchyma (Suki *et al.* 1994). The authors acknowledge the validity of the models from (1.2) and the FO impedance from (Hantos *et al.* 1992*b*):

$$Z_r(s) = \frac{1}{C_r s^{\beta_r}} \tag{1.7}$$

in which the real part denotes elastance and the imaginary part the viscance of the tissue. This model was then referred to as *the constant-phase model* because the phase is independent of frequency, implying a frequency-independent mechanical efficiency. In their paper, Suki *et al.* recognize five classes of systems admitting power-law relaxation or constant-phase impedance (Suki *et al.* 1994):

- **Class 1**: *systems with nonlinear constitutive equations*; a nonlinear differential equation may have a At^{-n} solution to a step input. Indeed, lung tissue behaves nonlinearly, but this is not the primary mechanism for having constant-phase behaviour, since the forced oscillations are applied with small amplitude to the mouth of the patient to ensure linearity.

- **Class 2**: *systems in which the coefficients of the constitutive differential equations are time-varying*; the linear dependence of the pressure-volume curves in logarithmic time scale does not support this assumption.

- **Class 3**: *systems in which there is a continuous distribution of time constants that are solutions to integral equations*. By aid of Kelvin bodies and an appropriate distribution function of their time constants, a linear model has been able to capture the hysteresis loop of the lungs, capturing the relaxation function decreasing linearly with the logarithm of time (Fung 1981). This is a class of systems which may be successful in acknowledging the origin of the constant-phase behaviour, but there is no micro–structural basis.

- **Class 4**: *complex dynamic systems exhibiting self-similar properties (fractals)*. This class is based on the fact that the scale-invariant behaviour is ubiquitous in nature and the stress relaxation is the result of the rich dynamic interactions of tissue strips independent of their

individual properties (Losa *et al.* 2005, Bates 2007). Although interesting, this theory does not give a straightforward explanation for the appearance of constant-phase behaviour.

- **Class 5**: *systems with input-output relationships including fractional order equations*; borrowed from fractional calculus theory, several tools were used to describe viscoelasticity by means of fractional order differential equations (Suki *et al.* 1994, Bates 2007, Craiem & Armentano 2007).

Referring to the specific application of respiratory mechanics, Classes 3–5 are most likely to characterize the properties of lung parenchyma. The work presented in this thesis deals primarily with concepts from Class 4, but addresses also several items from Class 5.

Following the direction pointed hitherto, several studies have been performed to provide insight on fiber viscoelasticity at macro– and microscopic levels, using tissue strips from animals (Yuan *et al.* 2000). For instance, Maksym & Bates attempt to provide a model based on Hookean springs (elastin) in parallel with a nonlinear string element (collagen) to fit measurements of stress-strain in tissue strips in dogs (Maksym & Bates 1997). Their theory is based on the seminal work of Salazar & Knowles and Hildebrandt and the results suggest that the dominant parameter in (1.2) is n. This parameter has been found increased in emphysema and decreased in fibrosing alveolitis. They interpret the changes in this variable as related to alterations in collagen and elastin networks.

About a decade later, Bates provides another mechanistic interpretation of the quasi-linear viscoelasticity of the lung, suggesting a model consisting of series spring-dashpot elements (Maxwell bodies) (Bates 2007). He also suggests the genesis of power-law behaviour arising from:

- the intrinsic complexity of dynamic systems in nature, ubiquitously present;
- the property of being self-organized critically, posing an avalanche behaviour (e.g. sandpile);
- the rich-get-richer mechanism (e.g. internet hubs).

whereas the common thread which sews all them together is *sequentiality*. By allowing two FO powers in the model of Maxwell bodies arranged in parallel (a spring in parallel with a dashpot), he discusses viscoelasticity in simulation

studies. Similar attempts have been done by Craiem & Armentano in models of the arterial wall (Craiem & Armentano 2007).

Hitherto, the research community focused on the aspect of viscoelasticity in soft biological tissues. The other property of the lungs which can be related to fractional-order equations is diffusion and some papers discuss this aspect (Losa *et al.* 2005).

Surprisingly, the plain fractal-like geometry of the airways has been completely ignored throughout the decades. Since Weibel and Mandelbrot there is no study reporting the influence of geometrical changes in airways with disease (Weibel 1963, Mandelbrot 1983). Perhaps one of the reasons for this lack of interest from the research community is that the lungs are not perfectly symmetric and even more, the quasi-symmetry disappears completely with disease. This doctoral thesis will also address this issue and will establish a direct relation between recurrent geometry (symmetric and asymmetric tree) and the appearance of the fractional order impedance function.

1.3 Objectives and contributions of this work

The seminal work of Mandelbrot and Weibel in the early 70s on the concept of self-similarity, iterative geometry and recursiveness tackled by fractal geometry have prompted innovative ways to promote real progress in biomedical sciences. While most biologic processes could be described by models based on power law behavior and quantified by a single characteristic parameter (the fractal dimension), the necessity arises to introduce multi–fractal models. The evaluation of airway tree geometry and morphology for deriving total impedance and validate the appearance of a FO term in the model is a primary task of this work. The concise objectives can be formulated as follows:

1. to employ the available knowledge from literature on airway geometry and morphology in order to derive a mathematical model of the respiratory impedance, using the fractal structure, in order to prove the necessity of a FO model;

2. to validate the reliability of the FO model in clinical studies.

Endeavoring the above enumerated objectives requires several specifications:

- the geometry and the morphology must be employed to derive an explicit formulation of the air pressure and air flow through the airways, e.g. by means of Navier-Stokes equations;
- the electrical equivalent of the Navier-Stokes model for respiratory ducts in terms of the equivalent electrical impedance must preserve the structure and morphology of the respiratory tree;
- the electrical equivalent must be analyzed in terms of its total input impedance, providing both theoretical and practical proof of fractional-order appearance;
- an equivalent mechanical model, preserving morphology and geometry, must be developed in order to analyze viscoelastic properties of lung parenchyma;
- the reduced model of fractional order(s), from the electrical and mechanical models, should preserve physiological interpretation and should be validated against measured data from healthy subjects;
- finally, the model parameter sensitivity should be tested on various groups of patients and the identified model coefficients should be discussed in relation to the respective pathologies.

This thesis describes a physiologically consistent approach to each of the afore-mentioned objectives. Rather than dealing with a specific case study, the modelling approach presents a general method which can be used not only in the respiratory system application, but also in other similar systems (e.g. leaves, circulatory system, liver, intestines). Furthermore, we consider also the case when symmetry is not present (e.g. deformations in the thorax - kyphoscoliose) as well as various pathologies. We provide a proof-of-concept for the appearance of the FO model from the intrinsic structure of the respiratory tree. Several clinical studies are then conducted to validate the sensitivity and specificity of the FO model in healthy groups and in various pathological groups.

The original contributions of this thesis are situated within the following:

- the theoretical study showing the appearance of the fractional order originated from the intrinsic geometry of the human respiratory tree;
- the simulations which validated the above theoretical considerations in both simplified and integral form of the respiratory tree;

- the physical interpretation which has been given to the fractional orders appearing in the lumped model of the total respiratory impedance; (this has been done for a generalized fractional-order model, as well as for several specific candidate models);
- the mathematical analysis on several fractional-order model candidates, suggesting one optimal structure which is valid in the frequency range of clinical interest;
- the FO model which has been evaluated on real clinical data (healthy, asthma and COPD), providing good separation between the groups and a valid assessment of the mechanical properties in lungs.

1.4 The Respiratory System

1.4.1 Anatomy and Physiology

Respiration is the act of breathing, namely inhaling (inspiration) oxygen from the atmosphere into the lungs and exhaling (expiration) into the atmosphere carbon dioxide (Guyton 1986). The respiratory system is made up of the organs involved in breathing, and consists of the nose, pharynx, larynx, trachea, bronchi and lungs, as depicted in figure 1.2 below.

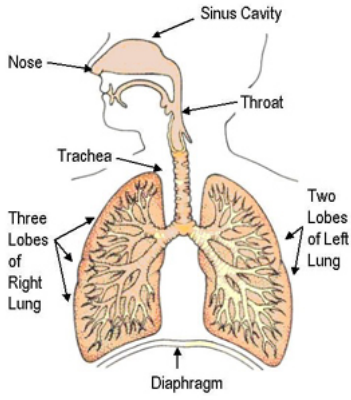

Figure 1.2: *Schematic representation of the respiratory system and its main components.*

The respiratory system can be divided into two major parts: the upper airways part and the lower airways part. The upper respiratory tract includes the nose,

with its nasal cavity, frontal sinuses, maxillary sinus, larynx and trachea. The lower respiratory tract includes the lungs, bronchi and the alveoli.

The lungs take in oxygen, which is required by all the cells throughout the body to live and carry out their normal functions. The lungs also get rid of carbon dioxide, a waste product of the body's cells. The lungs are a pair of cone-shaped organs made up of spongy, pinkish-gray tissue. They take up most of the space in the chest, or the thorax (the part of the body between the base of the neck and diaphragm).

The lungs are separated from each other by the mediastinum, an area that contains the following:

- heart and its large vessels;
- trachea;
- esophagus;
- thymus;
- lymph nodes.

The right lung has three sections, called lobes. The left lung has two lobes. When one breaths, the air enters the body through the nose or the mouth, travels down the throat through the larynx (voice box) and trachea (windpipe) and goes into the lungs through the tubes called main-stem bronchi. One main-stem bronchus leads to the right lung and the other one leads to the left lung. In the lungs, the main-stem bronchi divide into smaller bronchi and then into even smaller tubes called bronchioles, which finally end in tiny air sacs called alveoli. At this level, the act of diffusion takes place. Diffusion allows the oxygen from the alveoli to pass through the alveolar walls into the blood and the carbon dioxide to pass through the capillary walls into the alveoli. Hence, it is the act of gas exchange, as depicted in figure 1.3.

In order to move air in- and out- of the lungs, the volume of the thoracic cavity is increased (or decreases). The lungs do not contract but increase or decrease in volume. Muscles like intercostals or diaphragm contract during inspiration. Normally, the expiration is passive, the inpiration is active (= contraction of muscles). By increasing the thoracic cavity, the pressure around the lungs decreases, the lungs expand, and air is sucked in.

Normal quiet breathing (such as during the forced oscillation technique lung function test) is accomplished by contraction of the diaphragm, the parasternal muscles and the scaleni. During inspiration, the diaphragm pulls the

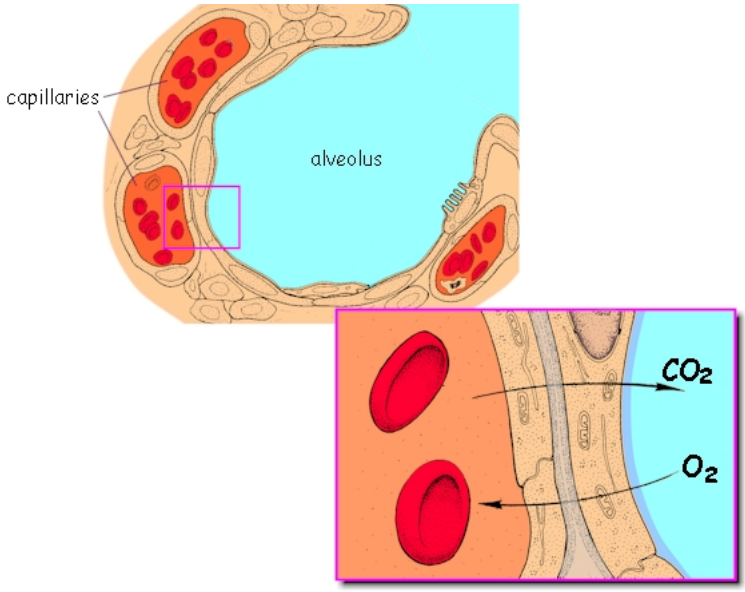

Figure 1.3: *Schematic representation of the respiratory system and its components.*

lower surfaces of the lung downwards. Expiration results from simple relaxation of these muscles. Changes in the elastic recoil of the lungs (more, or less, stiffness) will affect their normal function, in particular total lung volume and pressure-volume relationships.

Some measurements are performed during forced inspirations and forced expirations, i.e. the spirometry lung function test. A person's vital capacity can be measured by a spirometer. In combination with other physiological measurements, the vital capacity (VC) can help make a diagnosis of underlying lung disease. Vital capacity is the maximum amount of air a person can expel from the lungs after a maximum inspiration. It is equal to the inspiratory reserve volume plus the tidal volume plus the expiratory reserve volume. Force vital capacity (FVC) is the maximum volume of air that a person can exhale after maximum inhalation. It can also be the maximum volume of air that a person can inhale after maximum exhalation. Another important measure during spirometry is the forced expired volume in one second (FEV1). The FEV1/FVC ratio is used in the diagnosis of obstructive and restrictive lung disease, and normal values are approximately 80%. In obstructive lung disease, the FEV1 is reduced due to obstruction to air escape. Thus, the FEV1/FVC ratio will be reduced. In restrictive lung disease, the FEV1 and

FVC are equally reduced due to fibrosis or other lung pathology (not obstructive pathology). Thus, the FEV1/FVC ratio should be approximately normal.

The compliance is expressed as the volume increase in the lungs for each unit of trans-pulmonary pressure (which is the difference between the alveolar and pleural pressures). For instance, the compliance of the normal lungs and thorax combined is 0.13 liter per centimeter of water pressure (l/cmH_2O). This means that every time the alveolar pressure is increased by 1 cmH_2O, the lungs expand 130 ml. The most common representation of the compliance is given by the pressure-volume (PV) loops, as depicted in figure 1.4. The area between the inspiratory and expiratory PV curve is called the work of breathing; this will again vary with pathology.

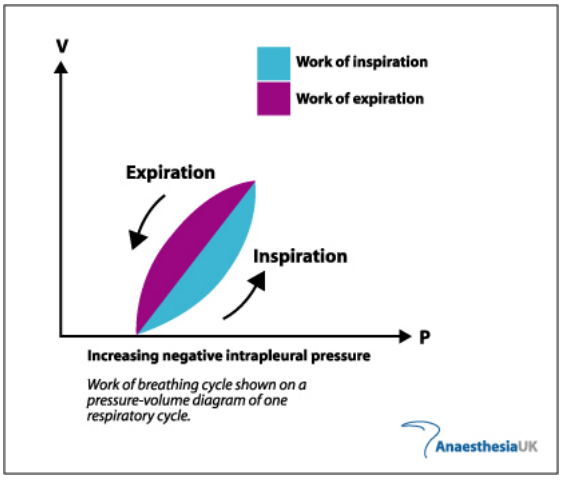

Figure 1.4: *Schematic representation of the work of breathing.*

Factors that cause abnormal compliance can be in fact anything which destroys the lung tissue, causing it to become fibrotic or edematous, blocks the bronchioli or in any other way impedes lung expansion and contraction. When considering the compliance of the lungs and thorax together, one should keep in mind any abnormality of the thoracic cage (e.g. kyphosis, scoliosis). In the next section we shall discuss some of the most important respiratory diseases and their effects on the normal functioning of the respiratory system.

1.4.2 Specific Pulmonary Abnormalities

Chronic Pulmonary Emphysema literally means excess air in the lungs (Guyton 1986, Hogg *et al.* 2004, Barnes 2000). It results from three major pathophysiological events in the lung:

- chronic infection, caused by inhaling smoke or other substances that irritate the bronchi and bronchioles;
- the infection, the excess of mucus, and inflammatory edema of the bronchiolar epithelium together cause chronic obstruction of smaller airways;
- the obstruction of the airways makes it especially difficult to expire, causing entrapment of air in the lungs (barrel chest effect) and overstretching the alveoli.

The physiological effects of chronic emphysema are extremely varied, depending on the severity of the disease and on the relative degree of bronchiolar obstruction versus parenchymal destruction at the alveolar level. Some tissue samples can be observed in figure 1.5.

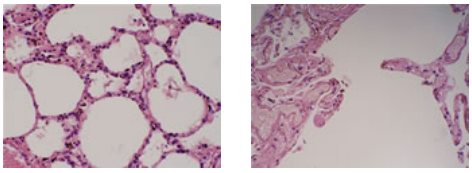

Figure 1.5: *Alveolar tissue in normal lungs (left) and disrupted alveolar walls in emphysematous lungs (right); pictures available at http://www.kuma.us/index.cfm/page/daily/emphysema.htm.*

The bronchiolar obstruction causes increased airway resistance and results in greatly increased work of breathing. It is especially difficult for the person to move air through the bronchioles during expiration, because the compressive force on the alveoli acts also on the bronchi, further increasing their resistance during expiration. Another physiological effect is that of a decreased diffusive capacity, from the marked loss of lung parenchyma (see figure 1.5 on the right). This will reduce the ability of the lungs to oxygenate the blood and to remove the carbon dioxide. Another effect is that of abnormal ventilation-perfusion ratio, i.e. portions of the lungs will be well ventilated, while others will be poorly ventilated, depending on the degree of the obstructive process.

Chronic emphysema progresses slowly over many years, leading to necessity of ventilatory assist devices and finally to death.

Asthma is characterized by spastic contraction of the bronchioles, which causes extremely difficult breathing (Guyton 1986, Busse & Lemanske 2001). The usual cause is bronchial hyperresponsiviness towards a variety of specific and a-specific stimuli. In fact, in younger patients, under the age of 30, the asthma is in about 70% caused by allergic hypersensitivity (i.e. plant polen, dust mite, cats, dogs). In elder persons, the hypersensitivity is to non-allergic types of irritants in air, such as smog.

Figure 1.6 depicts schematically the difference between normal and asthmatic airways.

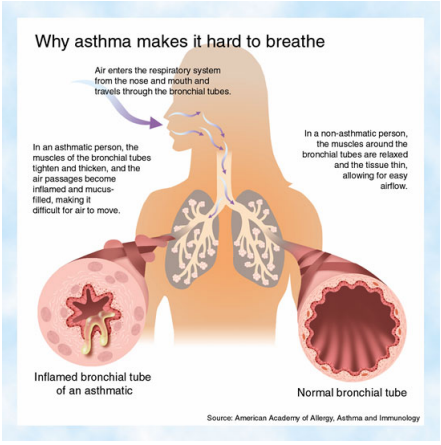

Figure 1.6: *Schematic representation of the normal and asthmatic airways.*

As a result of the irritants, the allergic person has a tendency to produce a high amount of antibodies, which attach to specific cells in the bronchioles and small bronchi. As a result of the antibodies reaction with the irritant, some substances are released (e.g. histamine). The combined effect of all these factors will produce:

- localized edema in the walls of the small bronchioles as well as secretion of thick mucus into bronchiolar airways, and
- spasm of the bronchiolar smooth muscle.

There may be a wheezing or whistling sound, which is typical of asthma. Wheezing occurs because muscles that surround the airways tighten, and the inner lining of the airways swells and pushes inward. It also occurs because

membranes that line the airways secrete extra mucus and furthermore the mucus can form plugs that may block the air passages. As a result, the rush of air through the narrowed airways produces the wheezing sounds. Usually, the asthmatic person can inspire quite easily, but has difficulty to expire air from the lungs. Also here the long-term effect of barrel chest will occur, similarly to chronic obstructive emphysema.

Although anyone may have an asthma attack, it most commonly occurs in children, by the age of 5, adults in their 30s, adults older than 65 and people living in urban communities (smog or allergic reactions). Other factors include: family history of asthma and personal medical history of allergies.

Cystic Fibrosis is an inherited disease characterized by an abnormality in the glands that produce sweat and mucus (Rogers & Doull 2005, Elizur *et al.* 2008). It is chronic, progressive, and may be fatal. Cystic fibrosis affects various systems in children and young adults, including the following: respiratory system, digestive system and the reproductive system.

Approximately 1 in 20 people in the US and Europe are carriers of the cystic fibrosis gene. These people are not affected by the disease and usually do not know that they are carriers.

Figure 1.7 depicts schematically the difference between normal and cystic fibrosis airways.

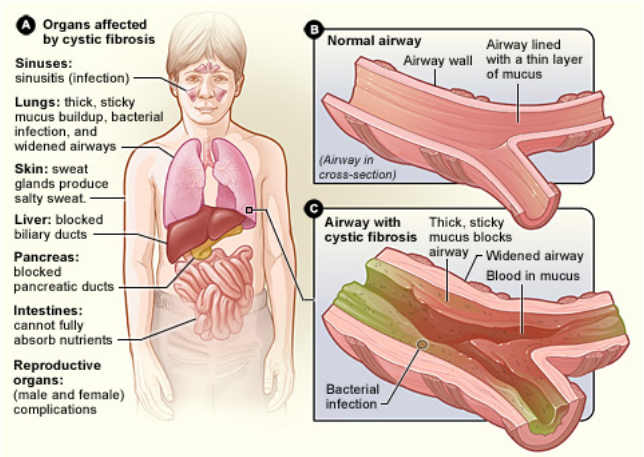

Figure 1.7: *Schematic representation of the normal and cystic fibrosis airways.*

Abnormalities in the glands that produce sweat and mucus can cause:

- loss of salt, which in turn can cause an upset in the balance of minerals in the blood, abnormal heart rhythms and possibly, shock;
- thick mucus that accumulates in lungs and intestines, which in turn can cause malnutrition, poor growth, frequent respiratory infections, breathing difficulties and in general, lung disease;
- other medical problems.

Under the item of medical problems one can enumerate: sinusitis, nasal polyps, clubbing of fingers and toes, pneumothorax - rupture of lung tissue, hemoptysis - coughing blood, enlargement of right side of heart, abdominal pain, gas in the intestines, liver disease, diabetes, pancreatitis and gallstones.

In addition to a complete medical history and physical examination, diagnostic procedures for cystic fibrosis include a sweat test to measure the amount of sodium chloride (salt) present. Higher than normal amounts of sodium and chloride will suggest cystic fibrosis.

Kyphoscoliosis is a deformation of the spine, as a combination effect of scoliosis and kyphosis (McCool & Rochester 2008). An example of an X-ray is given in figure 1.8, courtesy of Prof. Derom from Ghent University Hospital. The patient was hospitalized for severe breathing insufficiency.

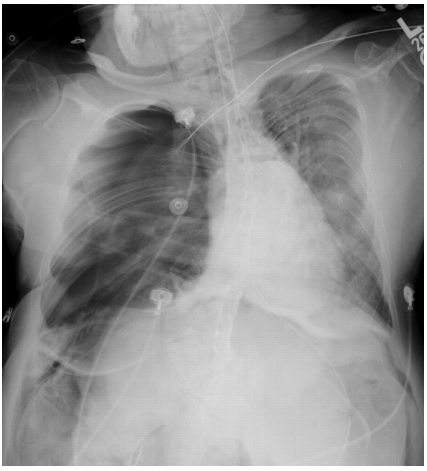

Figure 1.8: *X-ray of a patient presenting kyphoscoliosis.*

Scoliosis, is a medical condition in which a person's spine is curved from side to side, shaped like an *S* or *C*, and may also be rotated. To adults it can be very painful. It is an abnormal lateral curvature of the spine. On an X-ray,

viewed from the rear, the spine of an individual with a typical scoliosis may look more like an *S* or a *C* than a straight line. It is typically classified as congenital (caused by vertebral anomalies present at birth), idiopathic (sub-classified as infantile, juvenile, adolescent, or adult according to when onset occurred) or as neuromuscular, having developed as a secondary symptom of another condition, such as spina bifida, cerebral palsy, spinal muscular atrophy or due to physical trauma. Scoliotic curves of 10 degrees or less affect 3-5 out of every 1000 people.

Kyphosis, also called hunchback, is a common condition of a curvature of the upper (thoracic) spine. It can be either the result of degenerative diseases (such as arthritis), developmental problems, osteoporosis with compression fractures of the vertebrae, and/or trauma. In the sense of a deformity, it is the pathological curving of the spine, where parts of the spinal column lose some or all of their normal profile. This causes a bowing of the back, seen as a slouching back and breathing difficulties. Severe cases can cause great discomfort and even lead to death.

As a result of these deformities at the spinal level, the thorax cannot perform its normal function, leading to changes in airway resistance and total lung compliance.

1.5 Some concepts from Fractional Calculus

The fractional calculus is a generalization of integration and derivation to non-integer (fractional) order operators. At first, we generalize the differential and integral operators into one fundamental operator D_t^n (n the order of the operation) which is known as *fractional calculus*.

Several definitions of this operator have been proposed (see, e.g. (Podlubny 1999)). All of them generalize the standard differential–integral operator in two main groups: (a) they become the standard differential–integral operator of any order when n is an integer; (b) the Laplace transform of the operator D_t^n is s^n (provided zero initial conditions), and hence the frequency characteristic of this operator is $(j\omega)^n$. The latter is very appealing for the design of control systems by using specifications in the frequency domain (Oustaloup *et al.* 2000, Ionescu & De Keyser 2008*a*, 2009*a*, De Keyser *et al.* 2009).

A fundamental D_t^n operator, a generalization of integral and differential operators (*differintegration* operator), is introduced as follows:

$$D_t^n = \left\{ \begin{array}{cc} \frac{d^n}{dt^n}, & n > 0 \\ 1, & n = 0 \\ \int_0^t (d\tau)^{-n}, & n < 0 \end{array} \right\} \tag{1.8}$$

where n is the fractional order and $d\tau$ is a derivative function. Since the entire thesis will focus on the frequency-domain approach for fractional order derivatives and integrals, we shall not introduce the complex mathematics for time domain analysis. The Laplace transform for integral and derivative order n are, respectively:

$$L\left\{D_t^{-n} f(t)\right\} = s^{-n} F(s) \tag{1.9}$$

$$L\left\{D_t^{n} f(t)\right\} = s^{n} F(s) \tag{1.10}$$

where $F(s) = L\{f(t)\}$ and s is the Laplace complex variable. The Fourier transform can be obtained by replacing s by $j\omega$ in the Laplace transform and the equivalent frequency-domain expressions are:

$$\frac{1}{(j\omega)^n} = \frac{1}{\omega^n}\left(\cos\frac{\pi}{2} + j\sin\frac{\pi}{2}\right)^{-n} = \frac{1}{\omega^n}\left(\cos\frac{n\pi}{2} - j\sin\frac{n\pi}{2}\right) \tag{1.11}$$

$$(j\omega)^n = \omega^n\left(\cos\frac{\pi}{2} + j\sin\frac{\pi}{2}\right)^{n} = \omega^n\left(\cos\frac{n\pi}{2} + j\sin\frac{n\pi}{2}\right) \tag{1.12}$$

Thus, the modulus and the argument of the FO terms are given by:

$$Modulus(dB) = 20\log\left|(j\omega)^{\mp n}\right| = \mp 20n\log|\omega| \tag{1.13}$$

$$Phase(rad) = arg\left((j\omega)^{\mp n}\right) = \mp n\frac{\pi}{2} \tag{1.14}$$

resulting in:

- a Nyquist contour of a line with a slope $\mp n\frac{\pi}{2}$, anticlockwise rotation of the modulus in the complex plain around the origin according to variation of the FO value n;
- Magnitude (dB *vs* log-frequency): straight line with a slope of $\mp 20n$ passing through 0dB for $\omega = 1$;
- Phase (rad vs log-frequency): horizontal line, thus independent with frequency, with value $\mp n\frac{\pi}{2}$.

The respective sketches can be seen in figure 1.9.

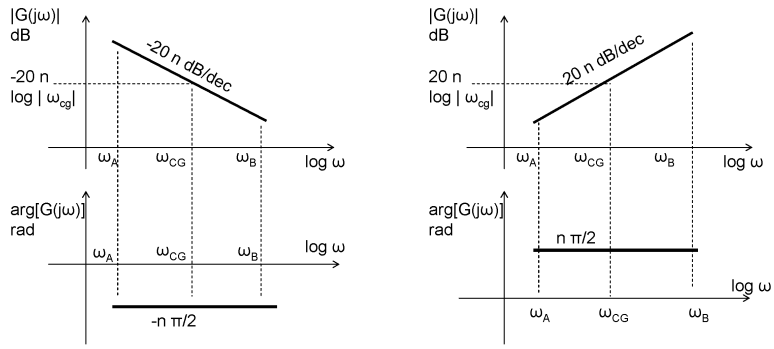

Figure 1.9: *Sketch representation of the FO integral and derivator operators in frequency domain, by means of the Bode plots (Magnitude, Phase)*

1.6 Fractional order dynamical systems

This section will discuss the most representative results in systems posing one of the three conditions for FO behaviour. These typical results will be used throughout the work presented by this thesis.

Let us firstly consider the rheological properties of soft biological tissue, i.e. viscoelasticity. Typical cases are the arterial wall (Craiem & Armentano 2007) and lung parenchyma (Bates 2007), which clearly pose viscoelastic behaviour. In these recent reports, the authors acknowledge that integer-order models to capture these properties can reach high orders and that fractional derivative models with fewer parameters have proven to be more efficient in describing rheological properties. Both of these authors define the complex modulus of elasticity as being determined by a real part, i.e. the storage modulus, capturing the elastic properties, and respectively by an imaginary part, i.e. the dissipation modulus, capturing the viscous properties:

$$E^*(j\omega) = \frac{\sigma(\omega)}{\varepsilon(\omega)} = E_S(\omega) + jE_D(\omega) \tag{1.15}$$

with σ the stress and ε the strain. This complex modulus $E^*(j\omega)$ shows partial frequency dependence within the physiologic range in both soft tissue examples. A typical example of integer-order lumped rheological model is the Kelvin-Voigt body, consisting of a perfectly elastic element (spring) in parallel with a purely viscous element (dashpot):

$$\sigma(t) = E\varepsilon(t) + \eta\frac{d\varepsilon(t)}{dt} \tag{1.16}$$

with E the elastic constant of the spring and η the viscous coefficient of the dashpot. One of the limitations of this model is that it shows creep but does not show relaxation, the latter being a key feature of viscoelastic tissues (Adolfsson *et al.* 2005, Ionescu & Chirita 2008). The classical definition of fractional order derivative (i.e. the Riemann-Liouville definition) of an arbitrary function $f(t)$ is given by (Oldham & Spanier 1974, Podlubny 1999):

$$\frac{d^n f}{dt^n} = \frac{1}{\Gamma(1-n)} \frac{d}{dt} \int_0^t \frac{f(\tau)}{(t-\tau)^n} d\tau \tag{1.17}$$

where Γ is the Euler gamma function. Hence, the FO derivative can be seen in the context of (1.16) as the convolution of $\varepsilon(t)$ with a t^{-n} function, anticipating some kind of memory capability and power-law response. It follows that the *spring-pot element* can be defined based on (1.17) as:

$$\sigma = \eta \frac{d^n \varepsilon}{dt^n}, \;\; 1 \geq n \geq 0 \tag{1.18}$$

in which the value for n can be adjusted to incorporate either a purely elastic component ($n = 0$), either a pure viscous one ($n = 1$). Both Bates and Craiem & Armentano acknowledge the fact that the soft biological tissue follows both elastic and viscous behaviour under baseline and stimulated case. Therefore, if one needs to derive a general model for characterizing soft tissue rheological properties, two instead of one spring-pot elements are necessary. This recent conclusion based on mechanical properties of soft tissues is very similar to a suggestion presented in my Master Thesis work based on frequency domain analysis of an electrical equivalent model (Ionescu 2003). Therefore, it would be of great interest to offer a validation of this suggestive remark in nominal and pathological case.

Secondly, let us consider the diffusive properties; e.g. heat transfer (Losa *et al.* 2005), gas exchange (Hou *et al.* 2005) and water transfer through porous materials (Benson *et al.* 2004, Losa *et al.* 2005). Diffusion is of fundamental importance in many disciplines of physics, chemistry, and biology. It is well known that the fractional order operator $\frac{d^{0.5}}{dt^{0.5}} \rightarrow s^{0.5}$ appears in several types of problems (Battaglia *et al.* 2001). The transmission lines, the heat flow, or the diffusion of neutrons in a nuclear reactor are examples where the half-operator is the fundamental element. Diffusion is in fact a part of transport phenomena, being one of the three essential partial differential equations of mathematical physics. Molecular diffusion is generally superimposed on, and often masked by, other transport phenomena such as convection, which tend to be much faster. However, the slowness of diffusion can be the reason

for its importance: diffusion is often encountered in chemistry, physics and biology as a step in a sequence of events, and the velocity of the whole chain of events is that of the slowest step. Transport due to diffusion is slower over long length scales: the time it takes for diffusion to transport matter is proportional to the square of the distance. In cell biology, diffusion is a main form of transport for necessary materials such as amino acids within cells. Metabolism and respiration rely in part upon diffusion in addition to bulk or active processes. For example, in the alveoli of mammalian lungs, due to differences in partial pressures across the alveolar-capillary membrane, oxygen diffuses into the blood and carbon dioxide diffuses out. Lungs contain a large surface area to facilitate this gas exchange process. Finally, the spreading of any quantity that can be described by the diffusion equation or a random walk model (e.g. concentration, heat, momentum, ideas, price) can be called diffusion. It is therefore a property ubiquitous in nature.

Thirdly, let us consider the fractal geometry; e.g. self-similarity and recurrence. Much work has been done on the fundamental property of percolation using self-similar fractal lattices such as the Sierpinski gasket and the Koch tree (see figures 1.10 and 1.11) (Mandelbrot 1983, Oustaloup 1995, Ramus-Serment *et al.* 2002, Losa *et al.* 2005). Examples from real-life include the coastline, invasion-front curve, lightning, broccoli and cauliflower, and several human organs such as lungs, vascular tree and brain surface. Other studies involve the temporal dynamics of biological signals and systems, which also pose recurrence (Eke *et al.* 2002, Suki & Frey 2003).

Figure 1.10: *The Sierpinski triangle, determined by a fractal dimension 1.58 from the ratio* $\log 3/\log 2$*. A similar example of this, entitled the Sierpinksi carpet is obtained using a ratio of* $\log 8/\log 2$ *and started by a square instead of a triangle.*

It is generally acknowledged that dynamical systems (e.g. electrical circuits) involving such geometrical structures would lead to the appearance of a fractional order transfer function. However, this topic has been investigated only in the case of an electrical analogue of the Sierpinski gasket (Ramus-Serment *et al.* 2002) and in the case of the vascular system (Elzbieta *et al.* 2005). In both cases, the calculated total impedance was of non-integer order. This

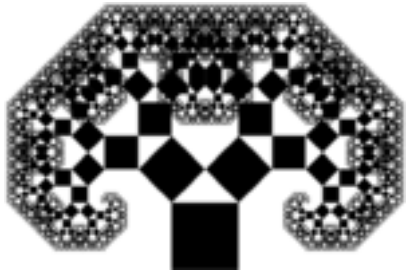

Figure 1.11: *The Koch tree is determined from a square by generating 2 other squares (dichotomous) with a reduction ratio of* $\sqrt{2}/2$*. The fractal dimension is given by the ratio* $\log 2/\log 2\sqrt{2}$

thesis proposes to investigate the case of the respiratory system impedance, whereas a fractal geometrical structure can be applied: the Koch tree.

1.7 Overview

This thesis offers a detailed investigation of three main issues:

- the appearance of the fractional order behaviour in a recurrent structure of the respiratory tree;
- the relation between the electrical network and mechanical network equivalents of such a tree; and
- the determination of an effective fractional order model for clinical studies and its validation on clinical data.

First, we start our quest for knowledge by introducing the principles of measuring respiratory impedance, which will set our background conditions for the next steps. This is done in chapter 2, next to a comparison of the most popular integer-order models for assessment of the respiratory impedance.

We proceed our pursuit with chapter 3, where the Navier-Stokes equations from fluid dynamics theory collaborate with Womersley assumptions to provide a set of differential equations for pressure and flow in laminar flow conditions. This chapter will also show that during restful breathing, the laminar flow condition is fulfilled, along with other simplifying assumptions.

Chapter 4 provides an electrical equivalent of the dichotomous respiratory tree, preserving morphological information using the pressure-flow equations

derived in chapter 3. Here we present the first proof that the geometrical structure of the tree leads to a fractional order behaviour and both recurrent and explicit cases are analyzed. The model determined in chapter 4 allows us to make changes in the morphology of the tree according to pathology and simulate changes from specific lung disease.

We continue our journey by discussing viscoelasticity with respect to the fractal structure of the lungs in chapter 5. Hence, a mechanical equivalent model is derived from our electrical network model from chapter 4.

Finally, a set of candidate fractional order models (also known by their specific property as constant-phase models) are evaluated in chapter 6. The best candidate is then further used in clinical studies on various groups of patients: Chronic Obstructive Pulmonary Disease (COPD), asthma, cystic fibrosis and kyphoscoliosis.

The main contributions of this work and conclusions are resumed in chapter 7, along with a short overview of the by-products of this investigation.

Chapter 2

The Respiratory Input Impedance

This chapter presents the principles of measuring the respiratory input impedance by means of FOT (Forced Oscillation Technique) lung function test. The chapter continues with an overview of the most representative parametric models reported in literature. Additionally, two alternative models are proposed. A comparison in terms of modelling performance is evaluated on typical patient data obtained with FOT, i.e. three averaged sets of representative diagnosed subjects: healthy, asthma and COPD (chronic obstructive pulmonary disease). It is shown that the FO model in 4 parameters from literature is unable to capture real parts of the impedance which are increasing with frequency. All identified model parameter values are discussed with respect to physiological insight.

Parts of the material presented in this chapter has been used and extended in the following publications:

- *Ionescu C., De Keyser R. (2008a), "Parametric models for the human respiratory impedance", Medical Engineering and Technology,* ***32(4)****, 315- 324;*
- *Ionescu C., De Keyser R. (2003), "A Novel Parametric Model for the Human Respiratory System", in : Proc. of the IASTED Int. Conf. on Modelling and Simulation, Palm Springs, CA USA, 246-251.*

2.1 Input Impedance Measurement

The impedance was measured using the FOT standard setup, commercially available, assessing respiratory mechanics from $4 - 48$ Hz. An **I2M** (Input Impedance Measurement) device produced by Chess Medical Technologies, The Netherlands (2000) and available in our laboratory has been used for pulmonary testing. The specifications of the device are: 11kg, 50x50x60 cm, 8 sec measurement time, European Directive 93/42 on Medical devices and safety standards EN60601-1. The standard measurement time of 8 seconds is attractive because it requires minimal cooperation from the subject, but the breathing period in this interval might not be considered as a stationary signal. Hence, to avoid biased estimates due to short measurement time, a second measurement line has been connected to a data acquisition PCMCIA card and the signals were recorded for 30 seconds. The subject is connected to the typical setup from figure 2.1 via a mouthpiece, suitably designed to avoid flow leakage at the mouth and dental resistance artifact. The oscillation pressure is generated by a loudspeaker connected to a chamber (DuBois *et al.* 1956, Oostveen *et al.* 2003). The loudspeaker is driven by a power amplifier fed with the oscillating signal generated by a computer. The movement of the loudspeaker's cone generates a pressure oscillation inside the chamber, which is applied to the patient's respiratory system by means of a tube connecting the loudspeaker's chamber and the bio-filter. A bias tube allows the patient to have fresh air circulation. Ideally, this pipeline will have high impedance at the excitation frequencies to avoid the loss of power from the LS pressure chamber. During the measurements, the patient wears a nose clip and keeps the cheeks firmly supported. Before starting the measurements, the frequency response of the transducers and of the pneumotachograph are calibrated (Van De Woestijne *et al.* 1994). The measurements of air-pressure P (cmH_2O) and air-flow Q (l/s) during the FOT lung function test is done at the mouth of the patient.

The global experimental set-up from figure 2.1-A can be modelled by the electrical analogy from figure 2.1-B, where: U_g denotes the generator test signal (known); U_r denotes the effect of spontaneous breathing (unknown); Z_r denotes the total respiratory impedance (to be estimated); Z_1 denotes the impedance (unknown) describing the transformation of driving voltage (U_g) to chamber pressure; Z_2 denotes the impedance (unknown) of both bias tubes and loudspeaker chamber; Z_3 denotes the impedance (unknown) of tube segment between bias tube and mouth piece (effect of pneumotachograph essentially). It follows that the respiratory impedance Z_r can be defined as

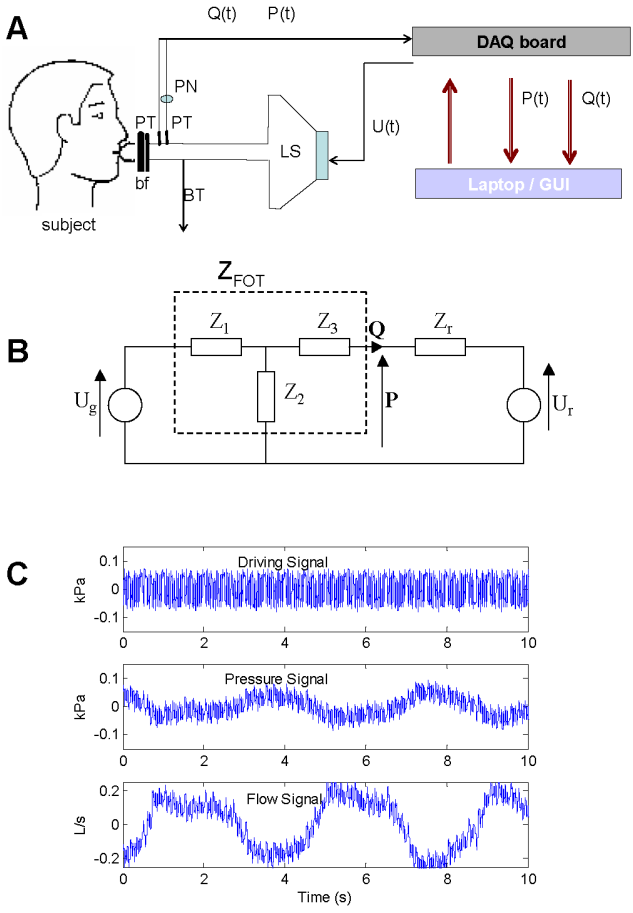

Figure 2.1: *A schematic overview* ***(A)*** *and an electrical analogy of the FOT setup* ***(B)****. Typical measured signals* ***(C)*** *from one subject: oscillatory driving air-flow; air pressure and air-flow. The breathing of the patient (low frequency) can be observed superimposed on the multisine signals. Symbols: LS - loudspeaker; PT - pressure transducer; PN - pneumotachograph; BT - bias tube; bf - biological filter; U(t) - generated pressure oscillations (4-48Hz); P(t) - measured pressure oscillations; Q(t) - measured flow; pressure unit conversion: 1* kPa *= 10* cmH_2O*.*

their spectral (frequency domain) ratio relationship (Daroczi & Hantos 1982, Ionescu & De Keyser 2003):

$$Z_r(j\omega) = \frac{S_{PU_g}(j\omega)}{S_{QU_g}(j\omega)} \tag{2.1}$$

where $S_{XY}(j\omega)$ denotes the cross-correlation spectra between the various input-output signals, $\omega = 2\pi f$ is the angular frequency and $j = \sqrt{-1}$, the result being a complex variable. The derivation of (2.1) from the measured signals is detailed in Appendix B. The FOT excitation signal is kept within a range of a peak-to-peak size of 1-3 (cmH_2O), in order to ensure linearity (Oostveen *et al.* 2003). Averaged measurements from 3-5 technically acceptable tests are taken into consideration for each subject, and typical recorded signals are depicted in figure 2.1-C.

2.2 Identification Methods

The spectral representation of Z_r is a fast, simple and fairly reliable evaluation. The algorithm can be summarized starting from the following equation from the electrical analogue in figure 2.1-B:

$$P(s) = Z_r(s)Q(s) + U_r(s) \tag{2.2}$$

where s denotes the Laplace operator. If the excitation signal is taken into account as proposed in (Daroczi & Hantos 1982, Ionescu & De Keyser 2003) and correlation analysis is applied to the measured signals, one can estimate the respiratory impedance as in (2.1). From the point of view of the forced oscillatory experiment, the signal components of respiratory origin (U_r) have to be regarded as pure noise for the identification task.

With the real Re and imaginary Im parts of the complex impedance from (2.1) at hand, parametric identification has been employed and the models parameters were estimated using a nonlinear least squares optimization algorithm, making use of the `MatLab` function `lsqnonlin`. The optimization algorithm is a subspace trust region method and is based on the interior-reflective Newton method described in (Coleman & Li 1996). The large-scale method for `lsqnonlin` requires that the number of equations (i.e., the number of elements of cost function) is at least as great as the number of variables. Every iteration involves the approximate solution using the method of preconditioned conjugate gradients, for lower and upper bounds. In this application, the lower bounds were set to 0 (negative values are meaningless)

and no upper bounds. The optimization stopped either when a high number of iterations reached 100 times the number of variables (i.e. 500), or a termination tolerance value of $10e^{-8}$. In all cases we obtained a correlation coefficient between data and model estimates above 80%.

Along with the corresponding model estimates, the error on the real and imaginary part respectively and the total error between the real patient impedance and the model estimated impedance are calculated according to the formula:

$$\begin{aligned} E_R &= \tfrac{1}{N_S}\sqrt{\textstyle\sum_1^{N_S}(Re - \hat{Re})^2} \\ E_X &= \tfrac{1}{N_S}\sqrt{\textstyle\sum_1^{N_S}(Im - \hat{Im})^2} \\ E_T &= \sqrt{E_R^2 + E_X^2} \end{aligned} \tag{2.3}$$

with Re denoting the real part of the impedance, Im denoting the imaginary part of the impedance and N_S the total number of data samples.

2.3 Parametric Models from Literature

Unlike non-parametric modeling, parameterization has the advantage of providing concise values for the variables of interest. With the frequency-dependent impedance curves at hand, by means of identification algorithms (Schoukens & Pintelon 2001), the non-parametric data may be correlated with the models consisting of electrical components that are analogous to the resistances, compliances and inertances inherent in the respiratory system (Oostveen *et al.* 2003). For this study, we selected 4 reported models closely related to the physiology of human lungs. The units are as follows: resistance in cmH_2O/(l/s); inertance in cmH_2O/(l/s^2) and compliance in l/cmH_2O.

One of the first models reported in the literature and also the simplest is based on analogy of the respiratory system as a tube denoting the central airways and a balloon accounting for the inspiration and expiration changes in volume of the lungs. This pipe-balloon analogy can be described as a series RLC electrical circuit (DuBois *et al.* 1956), as in figure 2.2.

In its initial attempts to characterize input impedance with a series RLC model structure, DuBois *et al.* observed that over the 1-15Hz frequency range, the inertance is a factor which must be negligible at ordinary breathing frequencies (0.0004 cmH_2O/(l/s^2)), but that inertia and compressibility of alveolar air become factors of increasing importance as the test frequency is increased. He also found rather high values for the airway resistance (3.8 cmH_2O/(l/s)) in the 2-10Hz frequency range. He concluded that the

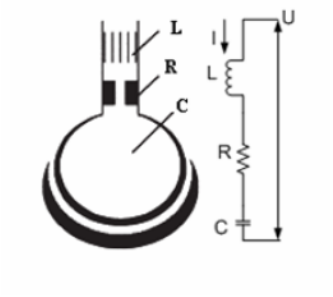

Figure 2.2: *Structure of the series RLC model from (DuBois* et al. *1956); R - airway resistance; L - air inertance; C - tissue compliance.*

mechano-acoustical (equivalent) system must be more complex in order to be able to capture the true properties of chest and lungs. The model is unable to represent the frequency-dependent real part of the complex impedance (resistance), and has not been included in the consequent discussion.

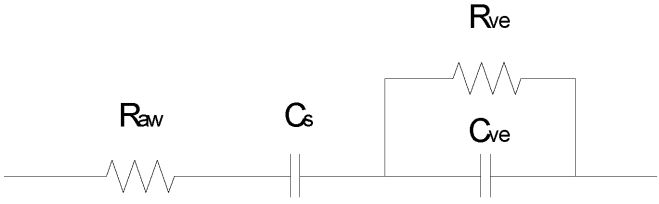

Figure 2.3: *Structure of the viscoelastic model from (Navajas* et al. *1990). R_{aw} - airway resistance; C_s - static compliance; R_{ve} - viscoelastic tissue resistance; C_{ve} - viscoelastic tissue compliance.*

A model which provides significant biased estimates at high frequencies, due to the absence of the inertance element, is the so-called *viscoelastic model*. This model consists of the overall airway resistance, the static compliance and the viscoelastic tissue resistance and compliance. The viscoelastic model (figure 2.3) implies that the respiratory system acts like a tree with uniform airways leading to identically distributed viscoelastic tissues (Navajas *et al.* 1990). The viscoelastic model gave best estimates for our data using the following initial values in the optimization procedure: $R_{aw} = 0.01$; $C_s = 0.06$; $R_{ve} = 0.4$; $C_{ve} = 0.45$; with: R_{aw} - airway resistance; C_s - static compli-

ance; R_{ve} - viscoelastic tissue resistance; C_{ve} - viscoelastic tissue compliance.

To characterize the respiratory mechanical properties at low frequencies, Navajas *et al.* proposed the above model, including a linear viscoelastic component for the tissues (figure 2.3) (Navajas *et al.* 1990). They assessed the impedance in seven anesthetized paralyzed patients with no respiratory disease. The advantage of this scenario is that the influence from upper airway shunt and muscular activity are not active and therefore do not bias the estimates. The R_{aw} is hypothesized to represent airways resistance plus a purely viscous component of tissue resistance, presumably in the chest wall. The C_s is the static compliance of the respiratory system. The R_{ve} and C_{ve} are related to viscoelastic properties of the tissue. As observed, there is virtually no inertance (air mass) quantified in this model, therefore it is expected that this model will provide biased estimates.

All patients exhibited a marked frequency dependence of effective respiratory resistance (real part of impedance) at low frequencies. The resistance fell sharply from 6.2 ± 2.1 cmH_2O/(l/s) at 0.25 Hz to 2.3 ± 0.6 cmH_2O/(l/s) at 2 Hz and decreased moderately with frequency, such that its value at 32 Hz was 1.5 ± 0.5 cmH_2O(l/s). The imaginary part of the impedance was -22.2 ± 5.9 cmH_2O/(l/s) at 0.25 Hz and increased with frequency, crossing zero line around 14 Hz and reached 2.3 ± 0.8 cmH_2O/(l/s) at 32 Hz. They observed that the inertance becomes important as early as with 4 Hz, which rather contradicts DuBois (DuBois *et al.* 1956, Lutchen & Costa 1990). The strong negative dependence in the vicinity of spontaneous breathing frequencies in the real part of impedance in anesthetised patients agreed with studies in awaken subjects. The authors agree that this dependence at low frequencies can hardly be attributed to regional inhomogeneities of tissues. They suggest that the mechanical behavior of the respiratory system at spontaneous breathing frequencies is largely determined by intrinsic features of tissues, such as plasto-elastic properties. They also report an average value of ≈ 9 cmH_2O/(l/s) for total resistance, mainly influenced by tissue properties at very low frequencies. The authors suggest a nonlinear plastic model should be considered to account for the mechanical behavior of the respiratory system.

A relatively good model structure, dividing the airway tissue and alveolar properties into different compartments, is the one proposed by DuBois *et al.* and schematically depicted in figure 2.4 (DuBois *et al.* 1956). This model provides the smallest total error for the following initial values: $R_{aw} = 0.01$; $L_{aw} = 0.01$; $R_t = 0.01$; $C_t = 0.01$; $L_t = 0.29$; $C_g = 0.14$; with: R_{aw} -

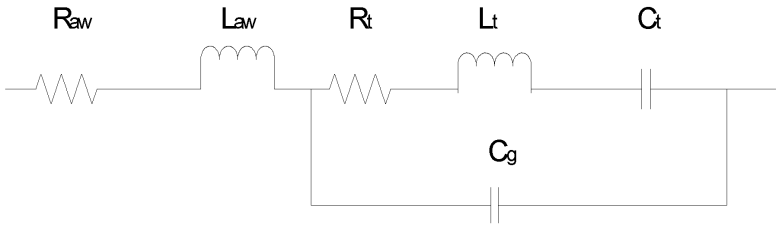

Figure 2.4: *Structure of the model from (DuBois* et al. *1956). R_{aw} - airway resistance; L_{aw} - airway inertance; R_t - tissue resistance; C_t - tissue compliance; L_t - tissue inertance; C_g - gas compression compliance.*

airway resistance; L_{aw} - airway inertance; R_t - tissue resistance; C_t - tissue compliance; L_t - tissue inertance; C_g - gas compression compliance.

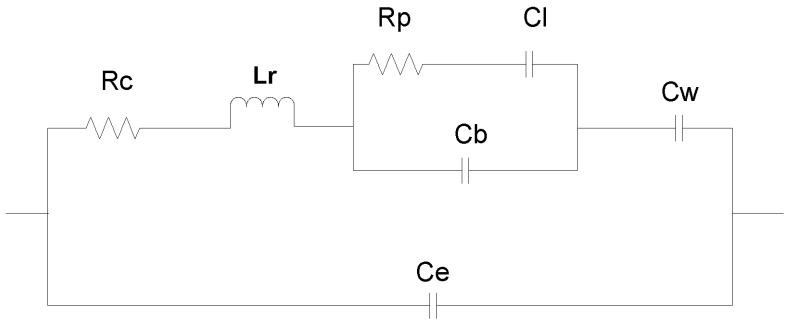

Figure 2.5: *Structure of the model from (Mead 1961). R_c - central resistance, L_r - the total inertance, R_p - peripheral resistance, C_l - lung compliance, C_b - bronchial tube compliance, C_w - wall compliance and C_e - extrathoracic compliance.*

Mechanical properties in lung and chest wall are described by the model developed originally by Mead and described later in (Van Noord 1990). Mead's model is an extended one-compartment model that does not allow the simulation of uneven alveolar ventilation (figure 2.5). Acceptable estimates were given for these initial values: $R_c = 0.01$; $L_r = 0.01$; $R_p = 0.01$; $C_l = 0.01$; $C_b = 0.01$; $C_w = 0.09$; $C_e = 0.02$, where: R_c - central resistance, L_r - the total inertance, R_p - peripheral resistance, C_l - lung compliance, C_b - bronchial tube compliance, C_w - wall compliance and C_e - extrathoracic compliance.

The Mead model (Mead 1961) (figure 2.5) allows the simulation of different influences on the respiratory mechanics (e.g. extrathoracic compliance by the mouth and the face mask, properties of the chest wall, air leaks around face mask or endotracheal tubes). The model is used to investigate different causes of airway obstructions and to assess the influence of the equipment on measurements.

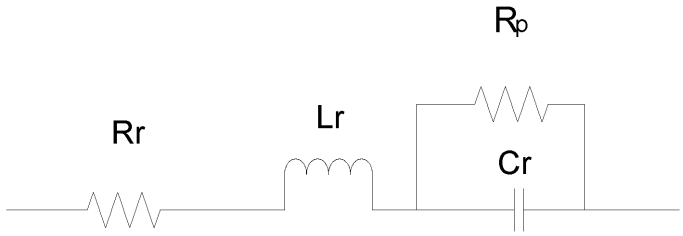

Figure 2.6: *Structure of the extended model from (Diong* et al. *2007).* R_r *- airway and lung resistance;* R_p *- peripheral resistance;* L_r *- lung inertance;* C_r *- alveolar compliance.*

Recently, an *extended RLC* model was proposed in (Diong *et al.* 2007), which can be viewed either as a simplification of the DuBois's or Mead's model, either an improvement of the simple series RLC circuit. The model allows characterization of small airways resistance (figure 2.6). For the *extended RLC* model, the corresponding initial values were set as: $R_r = 0.01$; $R_p = 0.09$; $L_r = 0.9$; $C_r = 0.31$; with: R_r - airway and lung resistance; R_p - peripheral resistance; L_r - lung inertance; C_r - alveolar compliance.

This model provides a theoretical support for the observations made in experimental studies upon the frequency-dependence of respiratory resistance at low frequencies. The added peripheral resistance R_p allows for the frequency dependence observed of the typical real impedance data, which is beyond the RLC series model's capability. The physical justification for adding this additional component is that it models the resistance presented by the respiratory system's small airways.

2.4 Proposed Parametric Models

Hitherto, integer-order parametric models for characterizing the respiratory input impedance have been broadly developed and tested in various lung

pathologies. Although they succeed to characterize in a clinically useful manner the mechanical properties of the lungs, there is a major drawback: accuracy increases with the model order and so does numerical complexity. The impedance varies significantly with frequency, requiring high order dynamical models. This problem has been tackled by introducing the concept of fractional calculus from mathematics, leading to FO models.

Two alternative parametric models are proposed: an integer-order and a fractional-order model. The first model proposed here is based on the observations from (Diong *et al.* 2007) on the influence of the upper airway shunt: RLCES (**RLC E**xtended with **S**hunt). In Mead's model, the influence of upper airway shunt is taken into account by the extrathoracic compliance C_e. The proposed model is then an extension from the Extended RLC proposed in (Diong *et al.* 2007) combined with the extrathoracic compliance from Mead (Mead 1961). The corresponding electrical scheme of the RLCES model is given in figure 2.7. The proposed parametric model is a simplification of Mead model, with similar variables: R_c - the central resistance, L_r - the total inertance, R_p - the peripheral resistance, C_b - the bronchial tube compliance and C_e - the extrathoracic compliance.

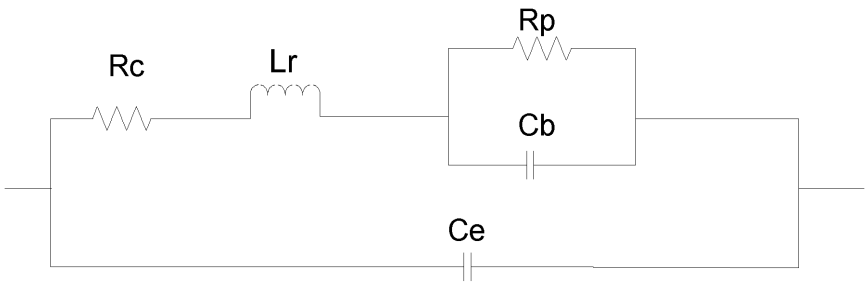

Figure 2.7: *Structure of the RLCES proposed model (Ionescu & De Keyser 2008*b*). R_c - the central resistance, L_r - the total inertance, R_p - the peripheral resistance, C_b - the bronchial tube compliance and C_e - the extrathoracic compliance.*

The second proposed model is based on the fractional order model (1.1) from chapter 1. Due to the fact that (1.1) cannot capture the real part of impedance which is increasing with frequency (Ionescu 2003, Ionescu & De Keyser 2003), we add a FO on the inertance term, therefore providing two FO in

the impedance model:

$$Z_r(s) = \frac{P(s)}{Q(s)} = R_r + L_r s^{\alpha_r} + \frac{1}{C_r s^{\beta_r}} \tag{2.4}$$

with P – pressure in cmH_2O; Q – flow in l/s; Z_r – the impedance in cmH_2O/(l/s); R_r – airway resistance in cmH_2O/(l/s), L_r – inductance in cmH_2O/(l/s^2); C_r – capacitance in l/cmH_2O; $0 \leq \alpha_r \leq 1$ and $0 \leq \beta_r \leq 1$ fractional orders and s the Laplace operator. Using the definition of complex numbers, (2.4) becomes:

$$\begin{aligned} Z_r(j\omega) = R_r + L_r\omega^{\alpha_r}\cos\left(\tfrac{\alpha_r\pi}{2}\right) + \tfrac{1}{C_r\omega^{\beta_r}}\cos\left(\tfrac{\beta_r\pi}{2}\right) + \\ j\cdot[L_r\omega^{\alpha_r}\sin\left(\tfrac{\alpha_r\pi}{2}\right) - \tfrac{1}{C_r\omega^{\beta_r}}\sin\left(\tfrac{\beta_r\pi}{2}\right)] \end{aligned} \tag{2.5}$$

It is possible to see that contrary to a series RLC system, the real part of the impedance in (2.5) depends on frequency and comprises both inductance and compliance effects. Therefore, it allows to characterize both increase and decrease with frequency in the real part of impedance, without requiring high integer order system (Ionescu & De Keyser 2004, 2006, Ionescu *et al.* 2007, Ionescu & De Keyser 2008*c*). Using the nonlinear least squares algorithm described above, the solution is given by an optimal set of $R_r, L_r, C_r, \alpha_r, \beta_r$ parameters.

2.5 Subjects

In this study, we are dealing with subjects evaluated with the FOT non-invasive lung function test. There are three averaged data sets from groups of Caucasian healthy, asthmatic and COPD patients. Table 2.1 presents the corresponding biometric and spirometric parameters.

The choice of these representative cases is motivated by the general aim of the study: to compare which model can capture with a least total error the complex respiratory input impedance of these three sets of subjects. The physiological differences between these sets of subjects are clearly visible in the complex impedance values and we expect that the parametric models proposed in this section will be able to quantify their specific properties.

2.6 Results and Discussion

We apply the input impedance identification methods described initially in (Daroczi & Hantos 1982) and revisited in (Ionescu 2003, Ionescu & De

	Healthy (7)	Asthma (5)	COPD (14)
Age (yrs)	55±3	65±2	51±6
Height (m)	1.74±0.15	1.62±0.12	1.73±0.14
Weight (kg)	82±4	78±5	71±5
VC % pred	100±3	80±8	89±7
FEV1 % pred	100±4	53±7	44±6

Table 2.1: *Biometric and spirometric parameters of the investigated (male) subjects. Values are presented as* $mean \pm SD$*; % pred: predicted according to the asymptomatic males of the present study; VC: vital capacity; FEV1: forced expiratory volume in one second.*

Keyser 2003) on the data measurements from FOT. By using (2.1), we obtain complex input impedances for each group, from which averaged sets as given in table 2.2 from 4-48 Hz frequency range.

The standard deviations on the averaged impedance data varied roughly in all three groups from a $\pm 14\%$ at 4-6 Hz, to $\pm 5\%$ at resonant frequencies (6-8Hz for healthy, 18-20Hz for asthma and COPD patients) and to $\pm 8\%$ at 40-48 Hz. For all parametric models described in section 2.4, the corresponding solutions for each subject group are given in table 2.2 (Ionescu & De Keyser 2008*b*).

The reported values are given for resistance in cmH_2O/(l/s); for inertance in cmH_2O/(l/s^2) and for compliance in l/cmH_2O. The corresponding averaged values for each model parameter and their standard deviations are reported. The results were tested using the one way analysis of variance (in Matlab, `anova1`). All reported values were statistically significant ($p < 0.001$, where p is the probability of obtaining a result at least as extreme as the one that was actually observed, assuming that the null hypothesis is true).

The error values calculated with (2.2) for each case are also reported, in terms of their averaged values and a standard deviation $> 5\%$. For those model parameters for which no standard deviation is reported, the standard deviation varied with $< 5\%$.

In the remainder of this chapter, CP4 and CP5 will denote the constant-phase model in 4 parameters from (1.1), respectively the constant-phase model in 5 parameters from (2.4).

The data from these averaged sets of complex impedance is depicted in figure 2.8.

Frequency Hz	Re Healthy	Im Healthy	Re Asthma	Im Asthma	Re COPD	Im COPD
4	2.623	-0.394	3.95	-1.75	0.1725	-0.1391
6	2.433	-0.109	3.65	-1.5	0.2047	-0.0956
8	2.421	0.136	3.3	-0.75	0.1841	-0.0742
10	2.417	0.266	3.25	-0.5	0.1699	-0.0693
12	2.467	0.427	3.1	-0.35	0.1546	-0.0609
14	2.396	0.512	2.98	-0.35	0.1440	-0.0500
16	2.36	0.671	2.8	-0.3	0.1399	-0.0358
18	2.43	0.766	2.7	-0.15	0.1365	-0.0138
20	2.417	0.812	2.6	0.10	0.1326	0.0027
22	2.465	1.011	2.65	0.5	0.1423	0.0157
24	2.515	1.213	2.58	0.6	0.1501	0.0256
26	2.398	1.357	2.55	0.7	0.1506	0.0332
28	2.491	1.394	2.53	0.75	0.1513	0.0339
30	2.643	1.62	2.3	1	0.1576	0.0386
32	2.589	1.534	2.4	1.45	0.1499	0.0470
34	2.646	2.043	2.45	1.52	0.1526	0.0487
36	2.694	1.849	2.55	1.7	0.1614	0.0532
38	2.584	2.111	2.35	2.3	0.1603	0.0642
40	2.772	2.135	2.4	2.35	0.1647	0.0751
42	2.586	2.476	2.5	2.5	0.1702	0.0855
44	2.908	2.395	2.53	2.65	0.1757	0.0960
46	3.083	2.537	2.48	2.7	0.1797	0.0966
48	2.894	2.608	2.49	3.1	0.1885	0.1002

Table 2.2: *The impedance data for the 3 typical patients (from averaged data measured with FOT) from 4-48 Hz, every 2 Hz. The real part (Re) and the imaginary part (Im) of the complex impedance are given in cmH_2O/(l/s).*

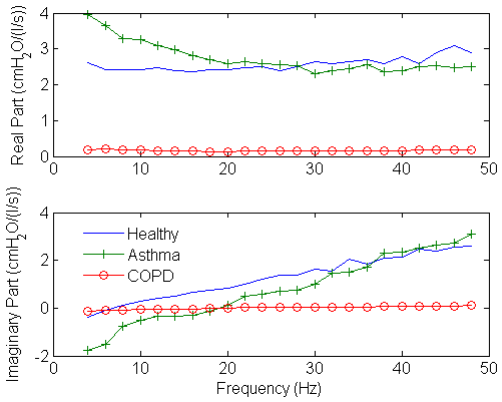

Figure 2.8: *The averaged complex impedances for healthy, asthmatic and COPD patients.*

	R_{aw}	C_s	R_{ve}	C_{ve}	E_R	E_X	E_T
Healthy	2.458±0.83	1.477e+9	0.117±0.012	2.04e-13	0.185	1.551	1.562
Asthma	1.925±0.61	0.291±0.04	0.817±0.23	6.37e-12	0.423	1.580	1.636
COPD	0.160±0.03	0.390±0.07	4.892e-4	1.43e-11	0.017	1.636	1.636

Table 2.3: *Identified values for the viscoelastic model parameters and modelling errors. Ref. figure 2.3.*

	R_{aw}	L_{aw}	R_t	C_t	L_t	C_g	E_R	E_X	E_T
Healthy	2.573±0.58	0.009±0.001	1.247±0.21	0.00064	0.019±0.008	0.033±0.012	0.183	0.121	0.219
Asthma	2.181±0.51	0.011±0.03	3.413±0.45	0.014±0.004	0.00063	0.004±0.0007	0.107	0.232	0.255
COPD	0.199±0.06	3.4e-4	0.55±0.08	0.267±0.075	0.007±0.001	0.087±0.009	0.028	0.015	0.032

Table 2.4: *Identified values for the DuBois model parameters and modelling errors. Ref. figure 2.4.*

	R_c	L_r	R_p	C_l	C_b	C_w	C_e	E_R	E_X	E_T
Healthy	2.37±0.08	0.009±0.001	0.21±0.095	13.16±2.64	0.13±0.013	0.05±0.006	1.2e-4	0.087	0.115	0.145
Asthma	1.85±0.64	0.012±0.001	2.12±0.086	21.71±1.87	0.004±0.001	0.02±0.003	1.0e-4	0.095	0.203	0.225
COPD	0.13±0.02	5e-5	0.11±0.013	1.86±0.5	0.17±0.01	0.31±0.02	4.3e-3	0.010	0.009	0.013

Table 2.5: *Identified values for the Mead model parameters and modelling errors. Ref. figure 2.5.*

	R_r	R_p	L_r	C_r	E_R	E_X	E_T
Healthy	2.57±0.04	910.57±50	0.009±0.001	0.034±0.006	0.185	0.092	0.207
Asthma	2.35±0.01	4.02±0.3	0.010±0.003	0.007±0.0005	0.114	0.247	0.272
COPD	0.19±0.02	0.68±0.07	3.77e-4	0.073±0.004	0.029	0.012	0.032

Table 2.6: *Identified values for the Extended RLC model parameters and modelling errors. Ref. figure 2.6.*

	R_c	L_r	R_p	C_b	C_e	E_R	E_X	E_T
Healthy	1.78±0.09	0.01±0.002	0.77±0.08	0.0077±0.001	2.50e-4	0.091	0.197	0.217
Asthma	2.11±0.46	0.011±0.003	3.52±0.22	0.0059±0.001	9.42e-5	0.127	0.241	0.273
COPD	0.13±0.017	4.77e-4	0.34±0.012	0.1382±0.01	0.0044±0.0003	0.011	0.010	0.014

Table 2.7: *Identified values for the RLCES model parameters and modelling errors. Ref. figure 2.7.*

	R_r	L_r	C_r	β	E_R	E_X	E_T
Healthy	2.5757	0.0089±0.0002	0.0577±0.005	1	0.1817	0.0902	0.2028
Asthma	0.6588±0.001	0.012±0.005	0.0872±0.008	0.3248±0.005	0.1345	0.2077	0.2474
COPD	0.1427	0.0004±0.0001	0.59±0.06	0.7818±0.02	0.0175	0.0102	0.0202

Table 2.8: *Identified values for the CP4 model and its modelling errors. Ref. (1.1).*

	R_r	L_r	C_r	α	β	E_R	E_X	E_T
Healthy	2.33e-14	0.088±0.0012	0.109±0.05	0.654±0.002	0.36±0.001	0.081	0.116	0.142
Asthma	0.0077±0.001	0.014±0.005	0.077±0.08	0.976±0.015	0.30±0.005	0.124	0.226	0.258
COPD	2.22e-14	0.006±0.0004	0.557±0.04	0.591±0.003	0.546±0.004	0.012	0.008	0.015

Table 2.9: *Identified values for the CP5 model and its modelling errors. Ref. (2.4)*

The performance of the novel models from section 2.4 on the impedance complex data is depicted in figures 2.9-2.10-2.11. It can be observed that both proposed models characterize sufficiently well the frequency-dependent behaviour of the impedance. It is also clear that the FO model in 4 parameters from literature, given by (1.1), is unable to capture the real part of impedance which is increasing with frequency. This model is then only valid in the low frequency range. The standard deviation intervals are not indicated in the plots for sake of clarity. Deviations are distributed as following for the RLCES and fractional-order model: $\pm 16\%$ and $\pm 10\%$ at 4-6 Hz, $\pm 3\%$ and $\pm 2\%$ at resonant frequencies, $\pm 8\%$ and $\pm 6\%$ at 40-48 Hz.

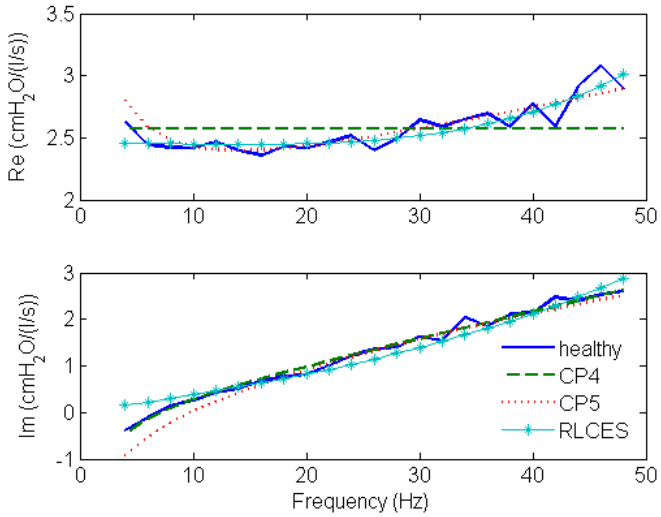

Figure 2.9: *The performance of the RLCES model (star line), the CP4 model (dashed line) and the CP5 model (dotted line), against measured data (continuous line) in healthy subjects.*

As observed from the results given in tables 2.4–2.9, the viscoelastic model has the poorest performance in terms of total error, explained by the absence of inductance in the model structure. Within the integer-order models, Mead's model has the least total error results in all subject groups. Notice that Extended RLC is a (simplified) special case of Mead's model, and therefore it will never provide better results. For the case of a healthy subject, peripheral resistance is very high (910.5778 cmH_2O/(l/s)). As reported in (Diong *et al.* 2007), in trying to minimize the error by not having the real part of the

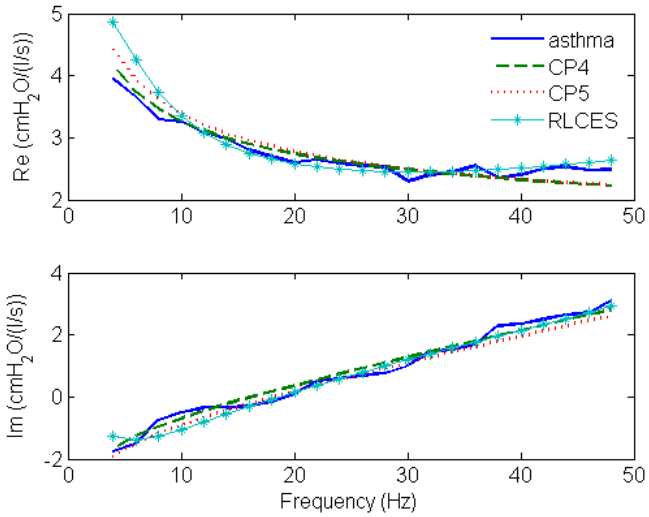

Figure 2.10: *The performance of the RLCES model (star line), the CP4 model (dashed line) and the CP5 model (dotted line), against measured data (continuous line) in asthmatic patients.*

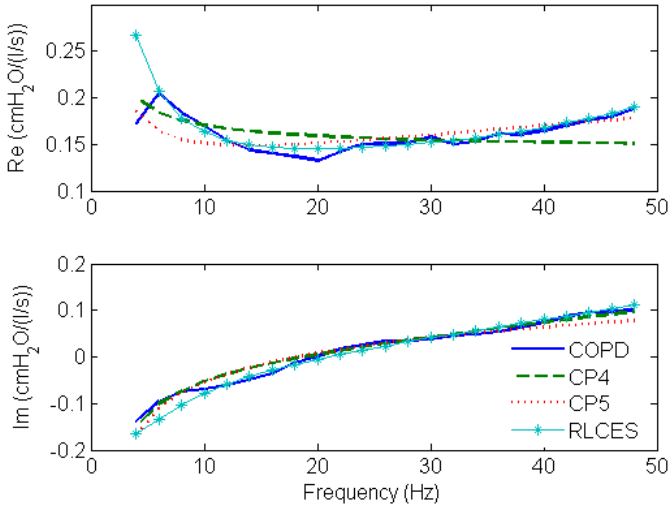

Figure 2.11: *The performance of the RLCES model (star line), the CP4 model (dashed line) and the CP5 model (dotted line), against measured data (continuous line) in COPD patients.*

impedance decreased too rapidly (with respect to frequency), R_p will tend to have larger values. Diong *et al.* suggest that it is not entirely reliable to use any individual value of the model parameter to discriminate between pathologic and healthy cases. However, the authors point to the possibility of using two-parameter combinations for discriminating between normal and ill patients.

It is also worth noticing that the estimated values of the RLCES model parameters are close to the ones estimated in the Mead model, leading to the conclusion that the absence of wall compliance does not affect significantly the total impedance of the human respiratory system.

Generally, the values for the model parameters in the three subject groups were significantly different, allowing a separation (necessary for screening or diagnosis). The airway resistance in models Viscoelastic, DuBois and RLCES were fairly close to each other, indicating good correlation between the various models for this specific parameter. The same is valid for the central resistance values in models Mead and CP5.

As referring to the specific values in each case (healthy, asthma and COPD), the resistance indicated correctly the possible variations with pathology. As expected, the viscoelastic resistance R_{ve} in Viscoelastic was significantly lower in COPD than in Healthy and Asthma groups. The peripheral resistance R_p in models Mead, Extended and RLCES had similar order of magnitude in each group, but their values did not correlate. Since the highest values are reported by the Extended model, which also has the least number of parameters of the above mentioned three model structures, we may suspect that this is due to the lumped characterization in model Extended as opposed to Mead or RLCES, where part of this resistance's effects are transmitted to other model parameters.

In DuBois, tissue compliance correlated well with physiologically expected values and pathology. Bronchial compliance C_b correlated well between models Mead and RLCES for asthma and COPD cases, but not in healthy subjects. We suspect this may be due to inaccurate partitioning of wall and lung compliance. Nevertheless, the values for C_b in asthma are very close to the reported values by Van Noord, where $C_b = 0.005$ l/cmH_2O and although the values for C_e are somewhat lower than expected, they are similar to what other authors report (Diong *et al.* 2007, Lutchen & Costa 1990, Farre *et al.* 1989). Airway inertance correlated well between model structures DuBois, Mead, Extended, RLCES, as well as in relation to expected pathology.

From the point of view of reported total errors, we may add that for all subject groups the best performance was given by Mead's model and highest errors for viscoelastic model. We may conclude that Mead's model is still the structure with least errors in parametric estimations. However, the newly proposed integer-order model RLCES gives similar total errors with less number of model parameters. This is indeed an advantage when a specific characterization is not intended, but merely a clear-cut within subject population for preliminary diagnosis. It is clear that if more specific information is required, the Mead model must be employed. Nonetheless, the model structure in Mead may not necessarily be optimal, for it over-estimates lung compliance (in healthy and asthmatic).

It is also noticeable that the total errors given by the CP5 model are comparable to the ones given by the Mead model. The main advantage of the CP5 model structure over the Mead's model structure is its reduced number of parameters to be identified. The reason for giving such good estimations is that the fractional-order captures in a more accurate and flexible way the frequency-dependence of the complex impedance. It also seems that the model from (2.4) gives most accurate estimates for the COPD case. For healthy persons, the airway resistance is very low. The reason for such low values is that part of dissipation properties are captured by the fractional-orders (Oustaloup 1995). This observation suggests eliminating the term R_r from 2.4, but this issue will be revisited later in this thesis.

Further analysis and figures describing the performance for each of the models presented in this chapter can also be found in (Ile 2007, Ionescu 2009).

2.7 Conclusions

A comparison with most representative parametric models from literature for assessing respiratory input impedance shows that FO models are more efficient than integer order models. It is also shown that the FO model in 4 parameters available from literature is limited to the low frequency range of application. Hence, the necessity for two FO terms arises and requires a physiological interpretation (i.e. CP5 model). It is therefore necessary to provide a link between the anatomy and morphology of the respiratory tract and the appearance of the fractional orders and their values. The next chapter lays the mathematical basis for attaining this objective.

Chapter 3

Mechanical Properties of the Airways

The derivation of the mechanical parameters of the airways from morphological insight is presented in this chapter. The approach consists of taking into account morphological and anatomical values such as: wall thickness, inner radius, tube length and tissue structure for each airway level and combine them into a set of equations for modelling the pressure drop, flow, wall elasticity and air velocity (axial and radial). Both elastic and viscoelastic airways are investigated, in the context of a symmetric space-filling of the lung. Effects of pulmonary disease affecting the inner radius and elastic modulus of bronchial tree are discussed. The derived mechanical parameters (resistance, inertance, compliance and conductance) are used to gather insight into the recurrence of the respiratory tree.

Part of the material presented in this chapter has been published in an extended form in:

- *Ionescu C., Segers P., De Keyser R. (2009), "Mechanical properties of the respiratory system derived from morphologic insight", IEEE Transactions on Biomedical Engineering,* ***56(4)****, 949-959;*
- *Ionescu C., Tenreiro-Machado J. (online), "Mechanical properties and impedance model for the branching network of the sapping system in the leaf of Hydrangea Macrophylla", Nonlinear Dynamics, DOI: 10.1007/s11071-009-9590-0;*
- *Ionescu C., Muntean I., Tenreiro-Machado J., De Keyser R., Abrudean M., (online) "A Theoretical Study on Modelling the Respiratory Tract*

With Ladder Networks by Means of Intrinsic Fractal Geometry", IEEE Transactions on Biomedical Engineering, Digital Object Identifier: 10.1109/TBME.2009.2030496;

- *Ionescu C., Oustaloup A., Levron F., Melchior P., Sabatier J., De Keyser R. (2009), "A model of the lungs based on fractal geometrical and structural properties", in : Proc. of the IFAC Int. Conf. on System Identification, St. Malo, France, 994-999.*

and is pending for review in the following article:

- *Ionescu C., Kosinsky W., De Keyser R., "Viscoelasticity and fractal structure in a model of human lungs", Archives of Mechanics (Elsevier).*

3.1 Introduction

Since the fractal geometry is characterized by recurrent geometry, the respiratory system is an ideal application. Lung geometry and morphology has been studied using CT scans in 3D form (Sauret *et al.* 1999). Already since Weibel, the fractal geometry present in the lung morphology has been employed in studies on airway aerodynamics (Weibel 1963). The self-similarity is related to the optimality of ventilation and asymmetry exists in the healthy lung as well. A diseased lung parenchyma contains significant heterogeneities and the optimality conditions are not anymore fulfilled (Hou *et al.* 2005).

One of the most comprehensive and earliest overviews on the mechanical properties of lungs is given by Mead, describing the initial attempts to quantify static and dynamic resistive, inertial and compliant properties of lungs. His review covers both the inspiratory and expiratory phase, at laminar and turbulent flow conditions, in terms of a single variable: air volume. Another important study has been reported in (Olson *et al.* 1970) for tube-entrance flow and pressure drop during inspiration in spontaneous ventilation. During breathing at rest, the air flow remains laminar (Hou *et al.* 2005, Olson *et al.* 1970, Pedley *et al.* 1971). A decade later, Franken *et al.* developed a model for oscillating flow of a viscous and compressible fluid in a rigid tube (Franken *et al.* 1981). It is one of the first applications of dynamic models to the conditions of the forced oscillations technique as applied for lung function testing. They modified the standard measurement device for pressure and flow at the mouth of the patient replacing it with a 2m rigid tube and based on the tube model, the flow was estimated (thus the pneumotachograph is replaced by this 2m rigid tube). They included a one dimensional model of the propagating waves and the true thermal properties of the tube wall and found that quantitative differences between models with and without thermal variations are negligible.

Based on technological and computational progress, Sauret *et al.* describes a study based on CT scans of the 3D topology and morphology of a human (cast) lung (Sauret *et al.* 1999). Mean gravity and branching angles up to level 9 bifurcations for the right and left lobe (asymmetric morphology due to heart location) were also reported, allowing detailed simulations in flow analysis studies.

There are two distinct groups of researchers, using either a symmetrical (Weibel 1963, 2005) either an asymmetrical (Horsfield *et al.* 1971, Habib *et al.* 1994) representation of the airways in the respiratory tree. We shall as-

sume the symmetric bifurcation case for finding the pressure-flow dynamics in the ducts.

3.2 Modelling Pressure-Flow Dynamics

Womersley theory has been applied to circulatory system analysis, considering the pulsatile flow in a circular pipeline for sinusoidally varying pressure-gradients (Womersley 1957). Taking into account that the breathing is periodic with a certain period (usually, for normal breathing conditions, around 4 seconds), we address the airway dynamics problem making use of this theory. For the case when sinusoidal excitation is applied to the respiratory system (Ionescu & De Keyser 2008*b*, Oostveen *et al.* 2003), this has ten times higher frequencies than the breathing, which permits analyzing oscillatory flow. To find an electrical equivalent of the respiratory duct, one needs expressions relating pressure and flow with properties of the elastic tubes, which can be done straightforward via the Womersley theory (Avolio 1980, Olufsen 2004, Segers *et al.* 1997).

The periodic breathing can be analyzed in terms of periodical functions, such as the pressure gradient:$-\frac{\partial p}{\partial z} = M_P \cos(\omega t - \Phi_P)$, where z is the axial coordinate, $\omega = 2\pi f$ is the angular frequency (rad/s), with f the frequency (Hz), M_P the modulus and Φ_P is the phase angle of the pressure gradient. Given its periodicity, it follows that also the pressure and the velocity components will be periodic, with the same angular frequency ω. The purpose is to determine the velocity in radial direction $u(r, z, t)$ with r the radial coordinate, the velocity in the axial direction $w(r, z, t)$, the pressure $p(r, z, t)$ and to calculate them using the morphological values of the lungs. In this study, we shall make use of the Womersley parameter from the Womersley theory developed for the circulatory system, with appropriate model parameters for the respiratory system, defined as the dimensionless parameter $\delta = R\sqrt{\frac{\omega\rho}{\mu}}$ (Segers *et al.* 1997, Womersley 1957), with R the airway radius. The air in the airways is treated as Newtonian, with constant viscosity $\mu = 1.8 * 10^{-5}$ kg/m-s and density $\rho = 1.075$ kg/m^3, and the derivation from the Navier-Stokes equations is done in cylinder coordinates (Welty *et al.* 1969):

$$\begin{aligned}\rho(\tfrac{\partial u}{\partial t} + u\tfrac{\partial u}{\partial r} + \tfrac{v}{r}\tfrac{\partial u}{\partial \theta} + w\tfrac{\partial u}{\partial z} - \tfrac{v^2}{r}) = -\tfrac{\partial p}{\partial r} + \rho F_r + \\ \mu[\tfrac{1}{r}\tfrac{\partial}{\partial r}(r\tfrac{\partial u}{\partial r}) - \tfrac{u}{r^2} + \tfrac{1}{r^2}\tfrac{\partial^2 u}{\partial \theta^2} - \tfrac{2}{r^2}\tfrac{\partial v}{\partial \theta} + \tfrac{\partial^2 u}{\partial z^2}]\end{aligned} \tag{3.1}$$

for the radial direction r, and:

$$\rho(\frac{\partial v}{\partial t} + u\frac{\partial v}{\partial r} + \frac{v}{r}\frac{\partial v}{\partial \theta} + w\frac{\partial v}{\partial z} + \frac{uv}{r}) = -\frac{1}{r}\frac{\partial p}{\partial \theta} + \rho F_\theta + \mu[\frac{1}{r}\frac{\partial}{\partial r}(r\frac{\partial v}{\partial r}) - \frac{v}{r^2} + \frac{1}{r^2}\frac{\partial^2 v}{\partial \theta^2} - \frac{2}{r^2}\frac{\partial u}{\partial \theta} + \frac{\partial^2 v}{\partial z^2}] \tag{3.2}$$

for the contour θ, and:

$$\rho(\frac{\partial w}{\partial t} + u\frac{\partial w}{\partial r} + \frac{v}{r}\frac{\partial w}{\partial \theta} + w\frac{\partial w}{\partial z}) = -\frac{\partial p}{\partial z} + \rho F_z + \mu[\frac{1}{r}\frac{\partial}{\partial r}(r\frac{\partial w}{\partial r}) + \frac{1}{r^2}\frac{\partial^2 w}{\partial \theta^2} + \frac{\partial^2 w}{\partial z^2}] \tag{3.3}$$

in the axial direction z. If we have the simplest form of axi-symmetrical flow in a cylindrical pipeline, the Navier Stokes equations simplify by $\frac{\partial}{\partial \theta} = \frac{\partial^2}{\partial \theta^2} = 0$ and with the contour velocity $v = 0$; consequently (3.2) can be omitted. Further on, consider no external forces F_r, F_z. Since we have very low total pressure drop variations, ≈0.1 kPa (Olson *et al.* 1970), we can divide by density ρ and introduce the dimensionless parameter $y = r/R, 0 \leq y \leq 1$ in the relation $\frac{d}{dy} = \frac{d}{dr}\frac{dr}{dy} = R\frac{d}{dr}, \frac{d}{dr} = \frac{1}{R}\frac{d}{dy}$. The simplifying assumptions can be then applied: i) the radial velocity component is small, as well as the ratio u/R and the term in the radial direction; ii) the terms $\frac{\partial^2}{\partial z^2}$ in the axial direction are negligible, leading to the following system:

$$\frac{\partial u}{\partial t} = -\frac{1}{\rho R}\frac{\partial p}{\partial y} + \frac{\mu}{\rho}[\frac{1}{yR^2}\frac{\partial u}{\partial y} + \frac{1}{R^2}\frac{\partial^2 u}{\partial y^2} - \frac{u}{R^2 y^2}] \tag{3.4}$$

$$\frac{\partial w}{\partial t} = -\frac{1}{\rho}\frac{\partial p}{\partial z} + \frac{\mu}{\rho}[\frac{1}{yR^2}\frac{\partial w}{\partial y} + \frac{1}{R^2}\frac{\partial^2 w}{\partial y^2}] \tag{3.5}$$

$$\frac{u}{Ry} + \frac{1}{R}\frac{\partial u}{\partial y} + \frac{\partial w}{\partial z} = 0 \tag{3.6}$$

Studies on the respiratory system using similar simplifying assumptions can be found in (Franken *et al.* 1981, Olson *et al.* 1970, Pedley *et al.* 1971). Given the pressure gradient is periodic, it follows that also the pressure $p(y, z, t)$ and the other velocity components $u(y, z, t), w(y, z, t)$ are periodic, as in:

$$\begin{aligned} p(y, z, t) &= A_P(y)e^{j\omega(t - z/\tilde{c})}, \\ u(y, z, t) &= A_U(y)e^{j\omega(t - z/\tilde{c})}, \\ w(y, z, t) &= A_W(y)e^{j\omega(t - z/\tilde{c})} \end{aligned} \tag{3.7}$$

where $\tilde{c}$ denotes the complex velocity of wave propagation and $j = \sqrt{-1}$. Further simplifications lead to the following system of equations:

$$\begin{gathered} u = \frac{j\omega R}{\mu\tilde{c}}\{C_1\frac{2}{\delta j^{3/2}}J_1(\delta j^{3/2}y) + \frac{A_P}{\rho\tilde{c}}y\}e^{j\omega(t-\frac{z}{\tilde{c}})} \quad \text{or} \\ u = C_1\frac{j\omega R}{\delta j^{3/2}\tilde{c}}J_1(\delta j^{3/2}y)e^{j\omega(t-\frac{z}{\tilde{c}})} + \frac{R}{2\rho\tilde{c}}M_P e^{j(\omega t-\Phi_P)} \end{gathered} \tag{3.8}$$

$$\begin{gathered} w = \{C_1 J_0(\delta j^{3/2}y) + \frac{A_P}{\rho\tilde{c}}\}e^{j\omega(t-\frac{z}{\tilde{c}})} \quad \text{or} \\ w = C_1 J_0(\delta j^{3/2}y)e^{j\omega(t-\frac{z}{\tilde{c}})} + \frac{M_P}{\omega\rho}e^{j(\omega t-\Phi_P-\frac{\pi}{2})} \end{gathered} \tag{3.9}$$

$$p(t) = A_P e^{j\omega(t-\frac{z}{\tilde{c}})} \quad \text{or} \quad -\frac{dp}{dz} = M_P e^{j(\omega t-\Phi_P)} \tag{3.10}$$

with $C_1 = -\frac{A_P}{\rho\tilde{c}}\frac{1}{J_0(\delta j^{3/2})}$, A_P the amplitude of the pressure wave, J_0 the Bessel function of the first kind and zero degree, J_1 the Bessel function of the first kind and first degree (Abramowitz & Stegun 1972), and in which:

$$-\frac{dp}{dz} = \frac{j\omega}{\tilde{c}}A_P e^{j\omega(t-\frac{z}{\tilde{c}})} = M_P e^{j(\omega t-\Phi_P)} \tag{3.11}$$

such that

$$A_P e^{j\omega(t-\frac{z}{\tilde{c}})} = \frac{\tilde{c}}{\omega}M_P e^{j(\omega t-\Phi_P-\pi/2)} \tag{3.12}$$

It is supposed that the movement of the (relatively short) elastic airway ducts is limited to the radial movement $\zeta(z,t)$ of the tube, being dependent only on the longitudinal coordinate and time. This supposition is valid for short segments ($\ll$ wavelength of the pressure wave) in which the longitudinal movement is negligible compared to the radial. The wavelength corresponding to the tracheal tube is about 2.5m long, much longer than the length of the tube itself; hence, the supposition is valid in our case (Ionescu 2008). Although the inspiratory and expiratory movements of the airways involve both radial as well as longitudinal movement, we restrict our analysis to the radial elongation only. The Poisson coefficient is denoted by ν_P and will be set to 0.45 (Lai & Hyatt 2000). The problem now contains four unknowns: $u(y,z,t)$, $w(y,z,t)$, $p(z,t)$, and $\zeta(z,t)$; therefore we need an extra equation in order to solve the system: the pipeline equation. The movement equation of the wall follows from the dynamical equilibrium of the forces applied on the wall, similar to the work reported in (Olufsen 2004). Denoting with ζ the elongation of the tube radius from R to $R+\zeta$, we have the dynamic equilibrium equation in the radial direction:

$$p(R+\zeta)d\theta dz + h\frac{E}{1-\nu_P^2}\frac{\zeta}{R}d\theta dz = h\rho_{wall}(R+\zeta)d\theta dz\frac{d^2\zeta}{dt^2} \tag{3.13}$$

where R is the initial (steady-state) radius, h is the thickness of the wall, E is the effective modulus of elasticity, ρ_{wall} is the effective density of the wall and ν_P is the Poisson coefficient. The modulus of elasticity and the wall density have to take into account that the airways are a combination of soft tissue and cartilage, the percent of which varies with the airway levels.

In this model, the effective elastic modulus and wall density, respectively, are considered in function of the airway tissue structure:

$$\begin{aligned} E &= \kappa E_c + (1-\kappa)E_s, \\ \rho_{wall} &= \kappa\rho_c + (1-\kappa)\rho_s \end{aligned} \tag{3.14}$$

taking into account at each level the fraction amount κ of corresponding cartilage tissue (index c) and soft tissue (index s) and with E_c=400kPa, E_s=60kPa, ρ_c=1140 kg/m^3, ρ_s=1060 kg/m^3.

The values of corresponding cartilage fraction are given in table 3.1. Assuming a negligible displacement ζ in comparison to R, one can simplify (3.13) with all terms in ζ/R. Dividing by $Rdzd\theta$, leads to the simplified equation of motion for the elastic airway wall:

$$p + \frac{Eh}{1-\nu_P^2}\frac{\zeta}{R^2} = \rho_{wall} h \frac{d^2\zeta}{dt^2} \tag{3.15}$$

The set of equations (3.4)-(3.6) and (3.15) form a system with four unknown parameters.

For a rigid pipeline we have that

$$\zeta = 2Re^{j\omega(t-\frac{z}{\tilde{c}})}; \tag{3.16}$$

introducing this relation in (3.15) and using (3.10) we obtain that

$$2R = \frac{A_P}{(\frac{E}{1-\nu_p^2}\frac{h}{R^2} - \rho_{wall}h\omega^2)}, \tag{3.17}$$

such that the movement of the airway wall is given as a function of the pressure

$$\zeta = \frac{A_P}{(\frac{E}{1-\nu_p^2}\frac{h}{R^2} - \rho_{wall}h\omega^2)} \cdot e^{j\omega(t-\frac{z}{\tilde{c}})}. \tag{3.18}$$

The equation for the axial velocity remains the same as in case of a rigid pipeline:

$$w(y) = \frac{M_P}{\omega\rho} M_0(y) e^{j(\omega t - \Phi_P - \pi/2 + \varepsilon_0(y))}. \tag{3.19}$$

where:

$$M_0(y)e^{j\varepsilon_0(y)} = 1 - \frac{(\delta j^{3/2} y)}{(\delta j^{3/2})} \tag{3.20}$$

Similarly, we define:

$$\begin{aligned} M_1 e^{j\varepsilon_1} &= 1 - \tfrac{2J_1(\delta j^{3/2})}{(J_0(\delta j^{3/2})\delta j^{3/2})} \\ M_2(y)e^{j\varepsilon_2(y)} &= 1 - \tfrac{2J_1(\delta j^{3/2} y)}{(J_0(\delta j^{3/2})\delta j^{3/2})} \end{aligned} \tag{3.21}$$

denoting the modulus and phase of the Bessel functions of first kind J_i and i^{th} order (Abramowitz & Stegun 1972). For an **elastic pipeline**, the *no-slip* condition is still valid ($w = 0$ for $y = \pm 1$), such that the radial velocity is:

$$\begin{aligned} u(y) = \tfrac{j\omega R}{2\rho\tilde{c}}\{y - \tfrac{2J_1(\delta j^{3/2} y)}{J_0(\delta j^{3/2} y)\delta j^{3/2}}\}A_P e^{j\omega(t-\frac{z}{\tilde{c}})} = \\ \tfrac{Ry}{2\rho\tilde{c}}\{y - \tfrac{2J_1(\delta j^{3/2} y)}{J_0(\delta j^{3/2})\delta j^{3/2}}\}M_P e^{j(\omega t - \Phi_P)} \end{aligned} \tag{3.22}$$

and using (3.21), the equivalent form of (3.22) becomes:

$$u(y) = \frac{R}{2\rho\tilde{c}} M_P M_2(y) e^{j(\omega t - \Phi_P + \varepsilon_2(y))}. \tag{3.23}$$

The flow is given by:

$$Q = \frac{\pi R^2 M_P}{\omega\rho} M_1 e^{j(\omega t - \Phi_P - \pi/2 + \varepsilon_1)} = \frac{\pi R^4 M_P}{\mu\delta^2} M_1 e^{j(\omega t - \Phi_P - \pi/2 + \varepsilon_1)}. \tag{3.24}$$

The effective pressure wave has the general form of

$$p(z,t) = A_P e^{j(\omega(t-\frac{z}{\tilde{c}}) - \phi_P)}, \tag{3.25}$$

where ϕ_P can be a phase shift for z=0 at t=0. It follows that

$$-\frac{dp}{dz} = M_P e^{j(\omega t - \Phi_P)} = \frac{A_P \omega}{\tilde{c}} e^{j(\omega(t-\frac{z}{\tilde{c}}) - \phi_P + \pi/2)}. \tag{3.26}$$

For z=0, it follows that

$$M_P e^{j(\omega t - \Phi_P)} = \frac{A_P \omega}{\acute{c}_0\sqrt{M_1}} e^{j(\omega t - \phi_P + \pi/2 - \varepsilon_1/2)}, \tag{3.27}$$

from which we have that

$$M_P = \frac{A_P \omega}{\acute{c}_0\sqrt{M_1}} \tag{3.28}$$

and

$$\Phi_P = \phi_P - \pi/2 + \varepsilon_1/2. \tag{3.29}$$

The pressure gradient is related to the characteristics of the airway duct via the Moens-Korteweg relation for the wave velocity $\acute{c}_0$, with

$$\acute{c}_0 = \sqrt{\frac{Eh}{(2\rho R(1-\nu_P^2))}}. \tag{3.30}$$

The model for wave propagation in function of the pressure p (kPa) for axial w (m/s) and radial u (m/s) velocities, for flow Q (l/s) and for the wall deformation ζ (%) at the axial distance z=0 is given by the set of equations:

$$p(t) = A_P e^{j(\omega t - \phi_P)} \tag{3.31}$$

$$u(y,t) = \frac{RA_P\omega}{2\rho\acute{c}_0^2} \cdot \frac{M_2(y)}{M_1} \cos(\omega t - \varepsilon_1 - \phi_P + \varepsilon_2(y) + \frac{\pi}{2}) \tag{3.32}$$

$$w(y,t) = \frac{R^2 A_P\omega}{\acute{c}_0\mu\sqrt{M_1}} \cdot \frac{M_0(y)}{\delta^2} \sin(\omega t - \frac{\varepsilon_1}{2} - \phi_P + \varepsilon_0(y) + \frac{\pi}{2}) \tag{3.33}$$

$$Q(t) = \frac{\pi R^4}{\mu} \frac{A_P\omega}{\acute{c}_0\sqrt{M_1}} \frac{M_1}{\delta^2} \sin(\omega t + \frac{\varepsilon_1}{2} - \phi_P + \frac{\pi}{2}) \tag{3.34}$$

$$\zeta(t) = \frac{A_P}{\frac{hE}{R^2} - \rho_{wall} h\omega^2} \cos(\omega t - \phi_P) \tag{3.35}$$

with

$$A_P = 2R(\frac{E}{1-\nu^2}\frac{h}{R^2} - \rho_{wall} h\omega^2), \tag{3.36}$$

$$\acute{c}_0 = \sqrt{\frac{Eh}{(2\rho R(1-\nu_P^2))}}, \tag{3.37}$$

One should note that the model given by (3.31)-(3.35) is a linear hydrodynamic model, adapted from Womersley (Womersley 1957) and further developed by numerous authors, such as in (Olufsen 2004, Segers *et al.* 1997). The assumption that air is incompressible and Newtonian has been previously justified and the equations are axi–symmetric for flow in a circular cylinder. The boundary condition linking the wall and pipeline equations (3.31)-(3.35) is the no-slip condition that assumes the fluid particles adherent to the inner surface of the airway and hence to the motion of the elastic wall. Due to the fact that the wall elasticity is determined by the cartilage fraction in the tissue, it is possible to consider variations in elasticity with morphology, which in turn varies with pathology.

3.3 Anatomy and morphology of the respiratory tree

There are two representative sets of airway morphological values: the symmetric case and the asymmetric case of the respiratory tree, schematically depicted in figure 3.1. The *symmetric* case assumes a dichotomously equivalent bifurcation of the airways in sub-sequent levels and is agreed by a group of authors e.g. (Weibel 2005, Mandelbrot 1983, Sauret *et al.* 1999) as in table 3.1. The *asymmetric* case is when the bifurcations are still dichotomous, but they occur in non-sequent levels, as given in table 3.2. The parameter Δ denotes the asymmetry index. In this case, a parent airway will split into two daughters: one of subsequent level $m + 1$ and one of level $m + 1 + \Delta$. This latter anatomical context is agreed by another group of authors: (Horsfield *et al.* 1971, Habib *et al.* 1994).

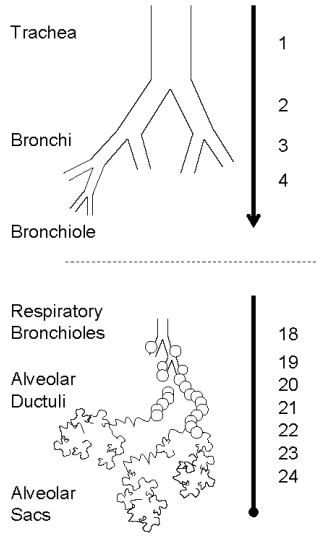

Figure 3.1: *Schematic representation of the bronchial tree: generations 1-16 transport gas and 17-24 provide gas exchange.*

Generally, it is considered that if the Reynolds number N_{RE} is smaller than 2000, then the airflow is laminar; otherwise it is turbulent (Welty *et al.* 1969). Based on the airway geometry and on an the average inspiratory flow rate of 0.5 (l/s) during tidal breathing conditions, the Reynolds number can be calculated as:

$$N_{RE} = w \cdot 2R \cdot \frac{\rho}{\mu} \tag{3.38}$$

Depth m	Length ℓ (cm)	Radius R (cm)	Wall thickness h (cm)	Cartilage fraction κ
1	10.0	0.80	0.3724	0.67
2	5.0	0.6	0.1735	0.5000
3	2.2	0.55	0.1348	0.5000
4	1.1	0.40	0.0528	0.3300
5	1.05	0.365	0.0409	0.2500
6	1.13	0.295	0.0182	0.2000
7	1.13	0.295	0.0182	0.0922
8	0.97	0.270	0.0168	0.0848
9	1.08	0.215	0.0137	0.0669
10	0.950	0.175	0.0114	0.0525
11	0.860	0.175	0.0114	0.0525
12	0.990	0.155	0.0103	0.0449
13	0.800	0.145	0.0097	0.0409
14	0.920	0.140	0.0094	0.0389
15	0.820	0.135	0.0091	0.0369
16	0.810	0.125	0.0086	0.0329
17	0.770	0.120	0.0083	0.0308
18	0.640	0.109	0.0077	0.0262
19	0.630	0.100	0.0072	0.0224
20	0.517	0.090	0.0066	0.0000
21	0.480	0.080	0.0060	0.0000
22	0.420	0.070	0.0055	0.0000
23	0.360	0.055	0.0047	0.0000
24	0.310	0.048	0.0043	0.0000

Table 3.1: *The tube parameters for the sub-glottal airways depths, whereas depth 1 denotes the trachea and depth 24 the alveoli, as used in (Hou* et al. *2005, Harper* et al. *2001, Lai & Hyatt 2000, Mauroy 2005, Weibel 1963, 2005)*

Depth m	Length ℓ (cm)	Radius R (cm)	Wall thickness h (cm)	Cartilage fraction κ	bifurcation Δ
1	10.0	0.80	0.3724	0.67	1
2	5.0	0.6	0.1735	0.5000	2
3	2.2	0.55	0.1348	0.5000	3
4	1.1	0.40	0.0528	0.3300	3
5	1.05	0.365	0.0409	0.2500	3
6	1.13	0.295	0.0244	0.2000	3
7	1.13	0.295	0.0244	0.0926	3
8	0.97	0.270	0.0205	0.0851	3
9	1.08	0.215	0.0149	0.0671	3
10	0.860	0.175	0.0126	0.0526	3
11	0.950	0.175	0.0126	0.0525	3
12	0.990	0.155	0.0118	0.0450	3
13	0.800	0.145	0.0114	0.0410	3
14	0.920	0.140	0.0112	0.0389	3
15	0.820	0.135	0.0111	0.0370	3
16	0.810	0.125	0.0107	0.0329	3
17	0.770	0.120	0.0105	0.0309	3
18	0.640	0.109	0.01	0.0262	3
19	0.630	0.100	0.0096	0.0224	3
20	0.517	0.090	0.0091	0.0000	3
21	0.480	0.080	0.0085	0.0000	3
22	0.420	0.070	0.0079	0.0000	3
23	0.360	0.055	0.0067	0.0000	2
24	0.310	0.048	0.0060	0.0000	2
25	0.250	0.038	0.0050	0.000	1
26	0.11	0.0315	0.0042	0.000	0
27	0.131	0.0265	0.0036	0.000	0
28	0.105	0.024	0.0032	0.000	0
29	0.075	0.0215	0.0029	0.000	0
30	0.059	0.04	0.0052	0.000	0
31	0.048	0.04	0.0052	0.000	0
32	0.048	0.04	0.0052	0.000	0
33	0.048	0.04	0.0052	0.000	0
34	0.048	0.04	0.0052	0.000	0
35	0.048	0.04	0.0052	0.000	0

Table 3.2: *The tube parameters for the sub-glottal airways depths, whereas depth 1 denotes the trachea and depth 35 the alveoli, as used in (Horsfield* et al. *1971, Habib* et al. *1994)*

with $\rho = 1075$ (g/m^3) the air density BTPS (Body Temperature and Pressure, Saturated) and $\mu = 0.018$ (g/m-s) the air viscosity BTPS. We have verified the values for the Reynolds number, which indeed indicated laminar flow conditions throughout the respiratory tree, varying from 1757 in the trachea to 0.1 in the alveoli (Ionescu 2008). Hence, the assumption of laminar flow conditions during tidal breathing is justified.

For deriving the parameters to be used later in an electrical equivalent model of the tree, it suffices to treat the symmetric case. The influence of asymmetry will be discussed in the next chapter.

3.4 Electrical Equivalent

By analogy to electrical networks, one can consider voltage as equivalent for respiratory pressure P and current as equivalent for air-flow Q (Kundur 1994). Electrical resistances R_e represent respiratory resistance that occur as a result of air-flow friction in the airways, electrical capacitors C_e represent volume compliance of the airways which allows them to inflate/deflate, electrical inductors L_e represent inertia of air and electrical conductances G_e represent the viscous losses. These properties are often clinically referred to as mechanical properties: resistance, compliance, inertance and conductance. The aim of this section is to derive them in function of airway morphology in case of an elastic airway wall (R_e,L_e,C_e) and in case of a viscoelastic airway wall (R_e,L_e,C_e,G_e).

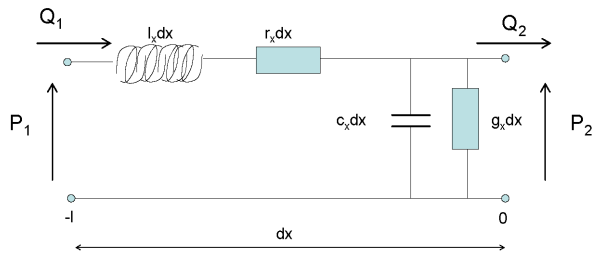

Figure 3.2: *Schematic representation of the infinitesimal distance dx over the transmission line and its parameters.*

Suppose the infinitesimal distance dx of a transmission line as depicted in figure 3.2. We have the distance-dependent parameters: l_x - induction/m; r_x - resistance/m; g_x - conductance/m; c_x - capacity/m. We consider the analogy

to voltage as being the pressure $p(x,t)$ and to current as being the air-flow $q(x,t)$ and we apply the transmission line theory. We shall make use of the complex notation:

$$\begin{aligned} p(x,t) &= P(x)e^{j(\omega t-\phi_P)} \\ q(x,t) &= Q(x)e^{j(\omega t-\phi_Q)} \end{aligned} \tag{3.39}$$

where x is the longitudinal coordinate (m), t is the time (s), ω is the angular frequency (rad/s), f is the frequency (Hz) and $j = \sqrt{-1}$. The pressure and the flow are harmonics, with the modulus dependent solely on the location within the transmission line (x). ϕ_P and ϕ_Q are the pressure and flow phase angles at t=0. The voltage difference between two points on the transmission line denoted as (x) and ($x + dx$) is due to losses over the resistance and inductance:

$$p(x+dx) - p(x) = -r_x dx \cdot q - l_x dx \frac{\partial q}{\partial t} \tag{3.40}$$

and the current difference between the same points is due to leakage losses and storage in the capacitor:

$$q(x+dx) - q(x) = -g_x dx \cdot p - c_x dx \frac{\partial p}{\partial t} \tag{3.41}$$

After division with dx, knowing that in the limit $dx \longrightarrow 0$, and introducing (3.39) in the first and second derivation gives, respectively:

$$\begin{aligned} \frac{\partial P}{\partial x} &= -(r_x + j\omega l_x)Q = -Z_l Q \\ \frac{\partial Q}{\partial x} &= -(g_x + j\omega c_x)P = -P/Z_t \\ \frac{\partial^2 P}{\partial x^2} &= -(r_x + j\omega l_x)\frac{\partial Q}{\partial x} = -Z_l \frac{\partial Q}{\partial x} \\ \frac{\partial^2 Q}{\partial x^2} &= -(g_x + j\omega c_x)\frac{\partial P}{\partial x} = -\frac{\partial P}{\partial x}/Z_t \end{aligned} \tag{3.42}$$

with

$$Z_l = -\frac{\frac{\partial P}{\partial x}}{Q} = r_x + j\omega l_x \tag{3.43}$$

the longitudinal impedance and

$$Z_t = \frac{P}{-\frac{\partial Q}{\partial x}} = \frac{1}{g_x + j\omega c_x} \tag{3.44}$$

the transversal impedance.
From (3.42) we obtain the system equations for $P(x)$ and $Q(x)$:

$$\begin{aligned} \frac{\partial^2 P}{\partial x^2} - Z_l P/Z_t = 0 \\ \frac{\partial^2 Q}{\partial x^2} - Z_l Q/Z_t = 0 \end{aligned} \tag{3.45}$$

Introducing the notation

$$\gamma = \sqrt{(r_x + j\omega l_x)(g_x + j\omega c_x)} = \sqrt{\frac{Z_l}{Z_t}}, \tag{3.46}$$

it follows that (3.45) can be re-written as

$$\begin{aligned} \frac{\partial^2 P}{\partial x^2} - \gamma^2 P = 0 \text{ and} \\ \frac{\partial^2 Q}{\partial x^2} - \gamma^2 Q = 0, \end{aligned} \tag{3.47}$$

to which the solution is given by

$$\begin{aligned} P(x) = Ae^{-\gamma x} + Be^{\gamma x} \text{and} \\ Q(x) = Ce^{-\gamma x} + De^{\gamma x} \end{aligned} \tag{3.48}$$

with complex coefficients A,B,C,D; using (3.48) in the first 2 relations from (3.42), the system can be reduced to:

$$Q(x) = \frac{1}{Z_0}(Ae^{-\gamma x} - Be^{+\gamma x}), \text{with} \tag{3.49}$$

$$Z_0 = \sqrt{\frac{r_x + j\omega l_x}{g_x + j\omega c_x}} = \sqrt{Z_l Z_t}, \tag{3.50}$$

in which Z_0 is the characteristic impedance of the transmission line cell.
Using the trigonometric relations

$$\begin{aligned} \sinh(\gamma x) = \tfrac{e^{\gamma x} - e^{-\gamma x}}{2}, \\ \cosh(\gamma x) = \tfrac{e^{\gamma x} + e^{-\gamma x}}{2} \end{aligned} \tag{3.51}$$

we can write the relationship between the input $x = -\ell$ and the output $x = 0$ as:

$$\begin{vmatrix} P_1 \\ Q_1 \end{vmatrix} = \begin{vmatrix} \cosh(\gamma\ell) & Z_0 \sinh(\gamma\ell) \\ \frac{1}{Z_0}\sinh(\gamma\ell) & \cosh(\gamma\ell) \end{vmatrix} \begin{vmatrix} P_2 \\ Q_2 \end{vmatrix} \tag{3.52}$$

with

$$Z_0 = \sqrt{\frac{r_x + j\omega l_x}{g_x + j\omega c_x}} = \sqrt{Z_l Z_t} \tag{3.53}$$

the characteristic impedance and

$$Z_l = r_x + j\omega l_x = \gamma Z_0 \tag{3.54}$$

the longitudinal impedance, respectively

$$Z_t = 1/(g_x + j\omega c_x) = Z_0/\gamma \tag{3.55}$$

the transversal impedance.

The relation for the longitudinal impedance in function of aerodynamic variables is obtained from (3.43), and gives:

$$\begin{aligned} Z_l = \frac{j\omega\rho}{\pi R^2 M_1} e^{-j\varepsilon_1} &= \frac{\mu\delta^2}{\pi R^4 M_1} e^{-j(\frac{\pi}{2}-\varepsilon_1)} \\ &= \frac{\mu\delta^2}{\pi R^4 M_1}[\sin(\varepsilon_1) + j\cos(\varepsilon_1)]; \end{aligned} \tag{3.56}$$

respectively, in terms of transmission line parameters, the longitudinal impedance is given by $Z_l = r_x + j\omega l_x$.

By equivalence of the two relations we have that the resistance per unit distance is:

$$r_x = \frac{\mu\delta^2}{\pi R^4 M_1}\sin(\varepsilon_1) \tag{3.57}$$

It follows that $\omega l_x = \frac{\mu\delta^2}{\pi R^4 M_1}\cos(\varepsilon_1)$ and recalling that $\delta = R\sqrt{\frac{\omega\rho}{\mu}}$, the inductance per unit distance is:

$$l_x = \frac{\rho}{\pi R^2}\frac{\cos(\varepsilon_1)}{M_1} \tag{3.58}$$

3.4.1 Elastic Tube walls

In case of an **elastic pipeline**, the characteristic impedance is obtained using relations (3.43), (3.44) and (3.50), leading to:

$$Z_0 = \frac{\rho}{\pi R^2}\frac{1}{1-\nu_P^2}\sqrt{\frac{Eh}{2\rho R}}\frac{1}{\sqrt{M_1}}e^{-j\frac{\varepsilon_1}{2}} \tag{3.59}$$

and for a lossless line (no air losses trough the airway walls, thus **conductance g_x is zero**), the transversal impedance is

$$Z_t = \frac{1}{j\omega c_x} = \frac{Z_0^2}{Z_l} = \frac{Eh}{(j\omega(2\pi R^3(1-\nu_P^2))}, \tag{3.60}$$

from where the capacity per unit distance can be extracted:

$$c_x = \frac{2\pi R^3(1-\nu_P^2)}{Eh} \tag{3.61}$$

Thus, from the geometrical (R, h) and mechanical (E, ν_P) characteristics of the airway tube, and from the air properties (μ, ρ) one can express the r_x, l_x and c_x parameters. In this way, the dynamic model can be expressed in an equivalent lossless transmission line by equations (3.57)-(3.61). Notice that the compliance parameter c_x in (3.61) is independent of the frequency, while both r_x (3.57) and l_x (3.58) are dependent on frequency trough the δ parameter, present also in M_1. Because we are interested only in the input impedance, we can disregard the effects introduced by the reflection coefficient. Hence, for $|\gamma| \ll 1$, one can estimate that over the length ℓ of an airway tube, we have the corresponding properties (Ionescu *et al.* 2009*f*):

$$R_e = r_x\ell = \ell\frac{\mu\delta^2}{\pi R^4}\frac{\sin(\varepsilon_1)}{M_1} \tag{3.62}$$

$$L_e = l_x\ell = \ell\frac{\rho}{\pi R^2}\frac{\cos(\varepsilon_1)}{M_1} \tag{3.63}$$

$$C_e = c_x\ell = \ell\frac{2\pi R^3(1-\nu_P^2)}{Eh} \tag{3.64}$$

3.4.2 Viscoelastic tube walls

Viscoelasticity is introduced assuming a complex function for the elastic modulus, yielding a real and an imaginary part (Bates 2007, Suki *et al.* 1994, Craiem & Armentano 2007). This can then be written as a corresponding modulus and phase:

$$E^*(j\omega) = E_S(\omega) + jE_D(\omega) = |E|\, e^{j\varphi_E} \tag{3.65}$$

The complex definition of elasticity will change the form of the wave velocity (3.37) into:

$$\acute{c}_0 = \sqrt{\frac{|E|\, he^{j\varphi_E}}{2\rho R(1-\nu_P^2)}} = \sqrt{\frac{|E|\, h}{2\rho R(1-\nu_P^2)}}e^{j\frac{\varphi_E}{2}} \tag{3.66}$$

The viscoelasticity of the wall is determined by the amount of cartilage fraction in the tissue, as the viscous component (collagen), respectively by the soft tissue fraction in the tissue as the elastic component (elastin) (Bates 2007). The equivalent of (3.65) is the ratio between stress and strain of the lung parenchymal tissue. The Young moduli is then defined as the slope of the stress-strain curve. With the model given by the above described equations, it is possible to consider variations in viscoelasticity with morphology and with pathology. This issue will be discussed in a next chapter.

In case of a **viscoelastic pipeline**, the characteristic impedance is given by

$$Z_0 = \frac{\rho}{\pi R^2}\frac{1}{1-\nu_P^2}\sqrt{\frac{|E|\,h}{2\rho R}}\frac{1}{\sqrt{M_1}}e^{-j(\frac{\varepsilon_1}{2}+\frac{\varphi_E}{2})} \tag{3.67}$$

and the transversal impedance is given by

$$Z_t = \frac{1}{g_x + j\omega c_x} = \frac{Z_0^2}{Z_l} = 1/\left(\omega\frac{2\pi R^3(1-\nu_P^2)^2}{|E|\,h}e^{j(\frac{\pi}{2}-\varphi_E)}\right), \tag{3.68}$$

from where the conductance per unit distance can be extracted:

$$g_x = \omega\frac{2\pi R^3(1-\nu_P^2)^2}{|E|\,h}\sin\varphi_E \tag{3.69}$$

and the capacitance per unit distance is given by:

$$c_x = \frac{2\pi R^3(1-\nu_P^2)^2}{|E|\,h}\cos\varphi_E \tag{3.70}$$

Thus, from the geometrical (R, h) and mechanical (E^*, ν_P) characteristics of the airway tube, and from the air properties (μ, ρ) one can express the r_x, l_x, g_x and c_x parameters. In this way, the dynamic model can be expressed in an equivalent transmission line defined by equations (3.57),(3.58),(3.69),(3.70). Similar to the elastic wall case, we can estimate that over the length ℓ of an airway tube, we have the corresponding properties:

$$R_e = r_x\ell = \ell\frac{\mu\delta^2}{\pi R^4 M_1}\sin(\varepsilon_1) \tag{3.71}$$

$$L_e = l_x\ell = \ell\frac{\rho}{\pi R^2}\frac{\cos(\varepsilon_1)}{M_1} \tag{3.72}$$

$$G_e = g_x\ell = \ell\omega\frac{2\pi R^3(1-\nu_P^2)^2}{|E|\,h}\sin\varphi_E \tag{3.73}$$

$$C_e = c_x \ell = \ell \frac{2\pi R^3 (1-\nu_P^2)^2}{|E|\, h} \cos\varphi_E \tag{3.74}$$

In the case of blood flow, leakage was interpreted as the blood lost due to vessels branching off from the parent vessel, with conductance as the electrical equivalent (Olufsen 2004). Our relation for conductance (3.73) is similar to that obtained in (Olufsen 2004).

3.4.3 Generic Recurrence in the Airways

Figure 3.3-left depicts the variation of the mechanical parameter ratios within consecutive airway levels, in a branch. The ratio for the resistance is supra-unitary, hence the resistance increases with the branch. Similarly, a sub-unitary ratio for compliance denotes a decreases in elasticity with each level. Both effects are due to a decrease in the airway cross-section. Figure 3.3-right depicts the variation of the mechanical parameter ratios with the airway level. Due to an increase in the total cross-sectional area from one level to another, the total resistance decreases (sub-unitary ratio), whereas the total compliance increases (supra-unitary ratio). Exponential changes for resistance, inertance and elastance from level 10 onwards show that mechanical properties become important towards the lower ducts (gas exchange).

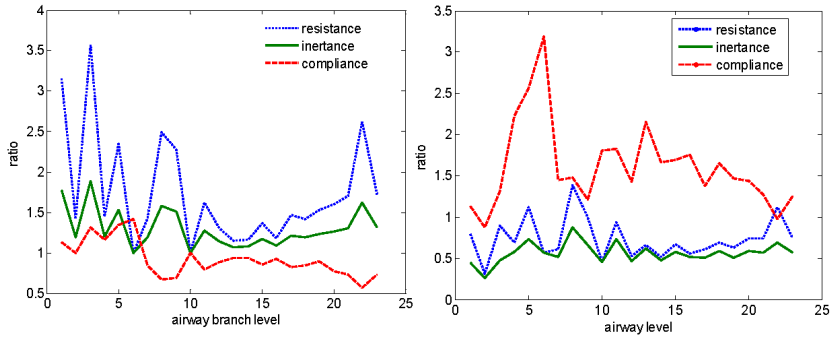

Figure 3.3: *The ratio between two consecutive branches belonging to consecutive levels (left) and between two consecutive levels (right) in the healthy lung for resistance R_e, inertance L_e and compliance C_e.*

Notice in figure 3.3 that from level 11 onward, the variances of the ratios are smaller (except the last 2 bifurcations: 22 and 23). Physiologically, level 11 corresponds to the bronchiole (Harper *et al.* 2001, Olson *et al.* 1970). We can correlate these effects to the variations in the airway radius and in the airway

cross-sectional area respectively. The radius changes from 8mm to 1.75mm, whereas the area varies from 254.5 mm^2 to 2.09mm^2 from trachea (level 1) to bronchiole (level 11). From level 11 onward, these changes are not so abrupt, thus resulting in lower variance of the mechanical parameters values as well. The nominal simulation of the respiratory tree leads to ratios as in table 3.3.

3.5 Results for Elastic Walls

The set of equations given by (3.31)-(3.35) can be used to investigate the variations in tidal breathing pressure and flow waves caused by pathology in the nominal function of the lung. Tidal breathing characterizes the inhalation and exhalation at rest (no forceful maneuvers, no exercise, etc). Two distinct scenarios will be studied: normal (healthy) and pathologic.

For a healthy subject, during tidal conditions we have a typical breathing frequency of 0.25 Hz (i.e. a breathing period of 4 seconds) and respective calculations of the parameters dependent on the tube geometry as in table 3.1 (Hou *et al.* 2005, Harper *et al.* 2001, Lai & Hyatt 2000, Mauroy 2005, Weibel 1963, 2005), with the phase shift ϕ_P=0, and a reference driving pressure A_P=0.1 kPa.

For a pathologic case, two distinct cases can be observed:

- when mucus and other particles obstruct the airway, resulting in changes in the inner radius; and
- when structural changes occur, in a more advanced level of the disease, changing the elastic modulus of the airway tissue.

Both these cases will be simulated at the alveolar level (m=24), for varying the radius values as in: R=0.048 cm; 0.024 cm; 0.012 cm for the first case and respectively varying the E-modulus values as in: E=60 kPa (compliant); 230 kPa; 400 kPa (stiff) for the second case.

Similarly, variations in pressure and flow patterns from specific diseases will have effect on the parameters from (3.57)-(3.61), affecting the total values of the input impedance. To illustrate these effects, specific morphological changes will be applied and the impedance will be evaluated over the standard clinical range of frequencies (4-48 Hz) for asthma and COPD pathologies.

Asthma is characterized by airway wall inflammation and thickening with mucus in the central and peripheral airways (levels 1-7) (Busse & Lemanske 2001, Vignola *et al.* 2004). COPD is characterized by increased resistance

of small conducting airways (levels 4-14) by airway wall thickening and mucus presence, combined with alveolar wall destruction of the emphysematous lung parenchyma (levels 18-24) (Hogg *et al.* 2004, Vignola *et al.* 2004).

3.5.1 General model performance

The pressure gradient, flow, wall displacement and radial velocity, function of the airway geometry depend on the morphological changes corresponding to each airway level. From all airway levels, results are depicted for levels 1 (trachea), 5 (bronchi) 13 (bronchiole) and 24 (alveoli) in figure 3.4. Notice that each of the parameters in model (3.31)-(3.35) are varying with the tube geometry. Figure 3.4 depicts the corresponding effects in pressure gradient, flow and wall displacement as resulted from pressure variations in percent values with respect to the initial radius of the tube. The pressure gradient is increasing with airway levels, becoming significant in the gas exchange ducts (levels 13-24), whereas the flow is decreasing from 15 l/s in the trachea to 0.00001 l/s at the alveolar level (the evaluation was made in open-system conditions, hence the values in the trachea might be over-estimated). The wall displacement is negligible in central airways, but higher than 5% in the gas exchange ducts. The pressure drop over each bifurcation is given in figure 3.4, where it can be observed that the first 5 bifurcations account for 80% of total values.

3.5.2 Effect of pathologies

The influence of disease which affects the wall structure in terms of E-moduli or the airway radius R is represented in figures 3.5 and 3.6. The results show that (as expected) higher pressure must be applied in order to obtain the same (or even less) air flow in the alveoli in case of disease. That explains why most respiratory diseases involve higher (sometimes dangerous) work of breathing, such as in COPD or lung injury patients. It can be observed that the influence of airway obstruction (changes in radius) is more drastic on the airflow than on the pressure gradient, whereas the influence of changing the wall structure (variations in tissue elasticity) affects more the pressure gradient than airflow. The analysis presented here is similar to studies in vaso-dilatation and vaso-constriction of arteries, by altering the ratio Eh/R (Olson *et al.* 1970). However, the separate study of the influence of E and R gives more insight on how each term changes respiratory pressure and flow with pathology.

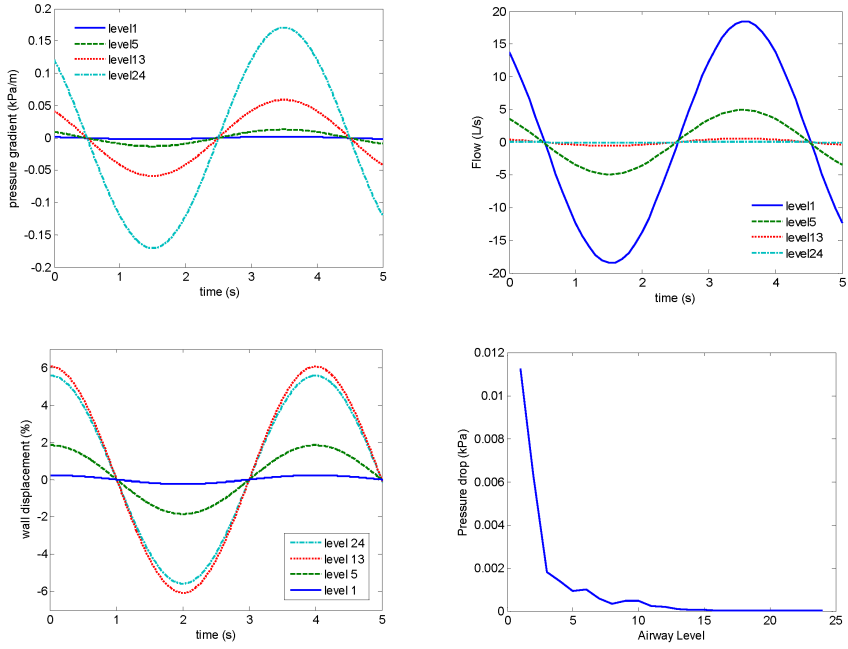

Figure 3.4: *(top-left) the pressure gradient; (top-right) the flow; (bottom-left) the wall displacement in % relative to the initial airway radius and (bottom-right) the pressure drop at each bifurcation, as function of morphology at various levels.*

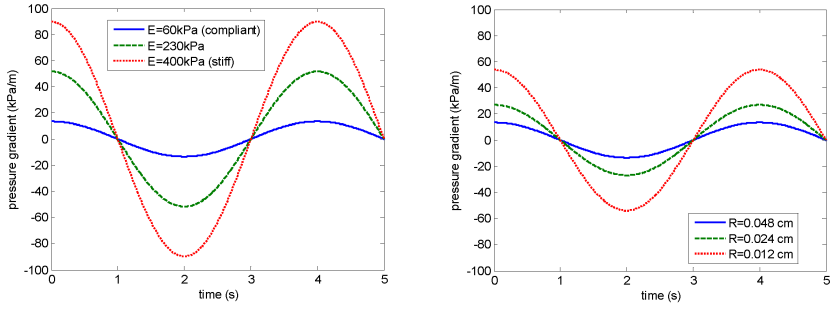

Figure 3.5: *Variations in pressure gradient at alveoli level in function of (left) changes in E and (right) changes in R.*

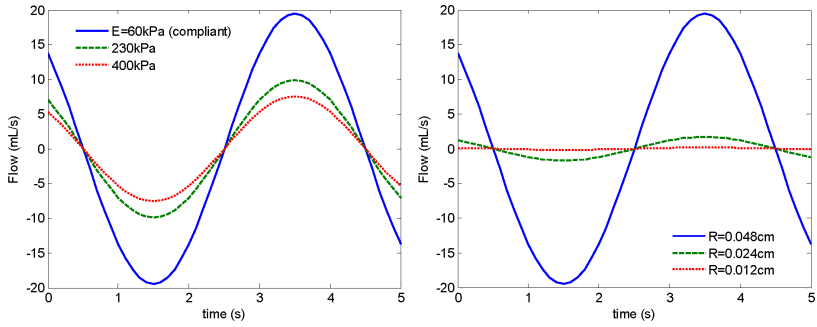

Figure 3.6: *Variations in flow at alveoli level in function of (left) changes in E and (right) changes in R.*

The results for asthma and COPD cases are presented in figure 3.7. The locations of the changes in morphology with each disease are mentioned in previous section. In asthma, airway wall inflammation and thickening with mucus is represented by altering the radius by $R - 0.5 \cdot h$ and wall thickness $1.5 \cdot h$. Altering the radius represents the presence of mucus and remodelling entails thickening of the airway walls, with increases in smooth muscle (Elizur *et al.* 2008, Vignola *et al.* 2004). In COPD, increased resistance has been represented by $R - 5 \cdot h$ in small conducting airways (levels 4-14) and by $1.5 \cdot R$ in acinar airways (levels 13-24); airway wall thickening as $6 \cdot h$ for levels 4-14, combined with alveolar wall destruction of the emphysematous lung parenchyma $h = 0.00001$ and $\kappa = 0$ (levels 18-24) (Hogg *et al.* 2004, Vignola *et al.* 2004).

One can observe the above mentioned effects of airway remodelling on the mechanical properties R_e (figure 3.7-top-left), L_e (figure 3.7-top-right) and C_e (figure 3.7-bottom-left) in healthy, asthma and COPD scenarios, for each branch. Figure 3.7-bottom-right depicts the net effect of these changes on the total input impedance values between 4-48 Hz (typical frequency range evaluated in clinical practice).

According to the specific pathology, asthma is characterized by increased resistance due to central airway collapse and increased inertance values due to increased mucus secretion (peaks at levels 6-7, where the collapse of the airways has been simulated) (Busse & Lemanske 2001). By contrast, COPD is characterized by decreased resistance at lower airway levels due to empty-spaced lung resulting from destruction of lung parenchyma and increasing

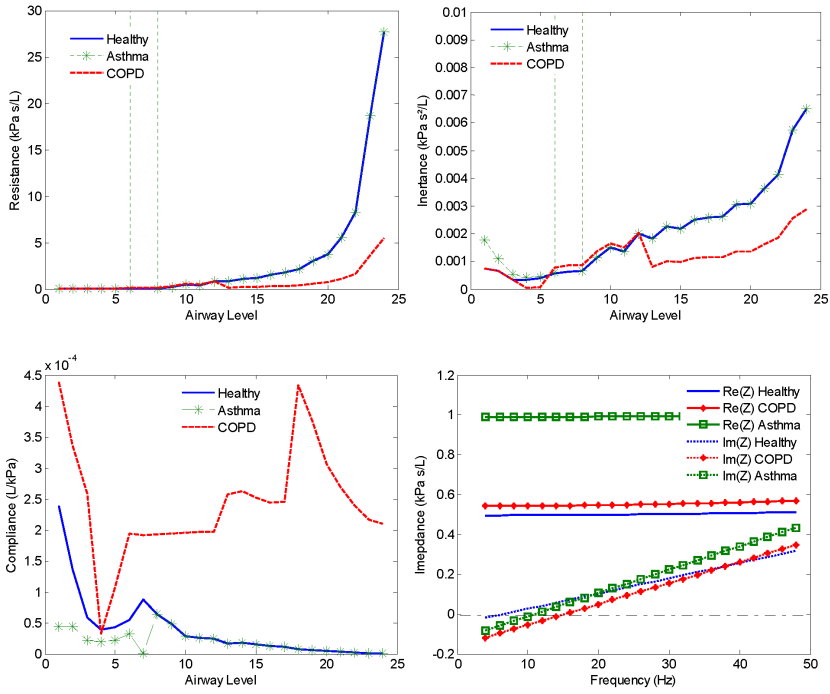

Figure 3.7: *Variations in the mechanical parameters: resistance R_e (top-left); inertance L_e (top-right); compliance C_e (bottom-left) in healthy (continuous line), asthma (star-dashed line) and COPD (dashed line) cases. The corresponding total input impedance by means of its real and imaginary parts (bottom-right).*

compliance (stiffness) due to fibrosis and rupture of elastic cross-links (Hogg *et al.* 2004). These results will be revisited in a following chapter, for a comparison against measured data.

3.6 Results for Viscoelastic Walls

Variations in pressure and flow patterns from specific diseases will have effect on the mechanical parameters (3.71)-(3.74), affecting the total values of the input impedance. To illustrate these effects, specific morphological changes will be applied and the evolution of the mechanical parameters will be evaluated for emphysema and fibrosis pathologies.

Pulmonary fibrosis involves scarring of the lung. Gradually, the air sacs of the lungs become replaced by fibrotic tissue. When the scar forms, the tissue becomes thicker causing an irreversible loss of the tissues ability to transfer oxygen into the bloodstream. Airway remodeling in fibrosis is characterized pathologically by sub-epithelial deposition of collagen in the airways, increases in airway smooth-muscle-cell mass, mucus gland hyperplasia, and mucosal neovascularization. The increased thickness is due to deposition of collagen and several other muscle-cell components. The changes in tissue are accompanied by widespread inflammation, reducing the air space or even filling it completely with inflammatory products (Elizur *et al.* 2008).

Pulmonary emphysema is characterized by loss of elasticity (increased pulmonary compliance) of the lung tissue, from destruction of structures supporting the alveoli, and destruction of capillaries feeding the alveoli. Consequently, the small airways collapse during exhalation, as alveolar collapsibility is increased, preventing the air to move into the lungs (Hogg *et al.* 2004, Vignola *et al.* 2004).

3.6.1 Effect of Pathologies

One can expect that the ratios are changing with pulmonary diseases, as suggested by both figures 3.7 and figures 3.8. In figures 3.8, the changes in fibrosis have been simulated in our model by increasing the stiffness of the smooth tissue elasticity three times, reducing the radius with 50 percent and increasing airway thickness by a factor 20, in the acinar airways (levels 13-24). In emphysema, tissue destruction at acinar level has been simulated by increased airway radius with 50 percent, an increased thickness of factor 5 and rupture of alveolar ligaments by reducing the collagen density to half.

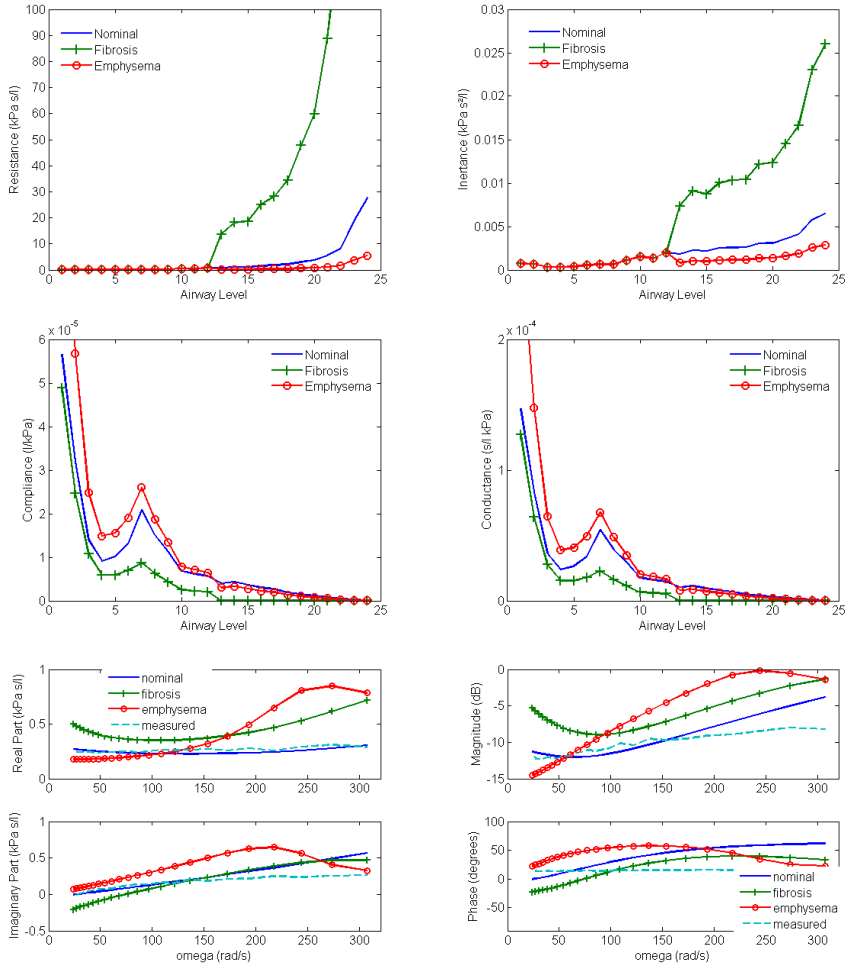

Figure 3.8: *Variations in the mechanical parameters in each airway duct: resistance (top-left); inertance (top-right); compliance (middle-left); conductance (middle-right); complex input impedance (bottom-left); and equivalent Bode plot (bottom-right) in nominal (continuous line), fibrosis (+) and emphysema (o) cases.*

	nominal	fibrosis	emphysema
ratio R	1.5207 ± 0.590 and 1.406 ± 0.336	2.738 ± 4.2877 and 1.406 ± 0.336	1.455 ± 0.684 and 1.406 ± 0.336
ratio L	1.134 ± 0.319 and 1.116 ± 0.123	1.347 ± 0.771 and 1.116 ± 0.123	1.097 ± 0.3740 and 1.116 ± 0.123
ratios C	0.871 ± 0.323 and 0.727 ± 0.123	0.752 ± 0.344 and 0.716 ± 0.120	0.814 ± 0.5297 and 0.719 ± 0.121

Table 3.3: *Ratios of the mechanical parameters between consecutive branches. Values are presented as mean $\pm$ SD for the 1..15 levels, respectively for the 16..24 levels. The ratios for G are the same as those of C.*

Further on, the results with disease are in agreement with the respective nature of airway remodelling.

In fibrosis, the mucus and fibrotic tissue appearance leads to increased overall resistance, visible in the increased values for the real part of the complex impedance, and shifting the imaginary part to the right. The latter observation is in agreement with published reports on subjects diagnosed with fibrosis (Elizur *et al.* 2008). In the Bode plot, increase in resistance is visible in the increased magnitude. The presence of the mucus will also affect viscoelasticity of the wall, therefore affecting inertance and compliance (see also ratios in table 3.3). This will then change the imaginary part, by affecting the resonance frequency (crossing from negative to positive values in imaginary part), i.e. shifting it to the right. Similarly, the phase is affected in the Bode plot.

In emphysema, due to the loss of interstitial tissue and lung parenchyma at alveolar level, increased elasticity (due to empty alveolar space) will decrease overall resistance, but the mass of air involved in the respiration will be less. This will result in low resonance frequency (short of breathing, resulting in an increased breathing frequency and work of breathing). The equivalent change in the impedance plots will be a shift upward of the imaginary part. All these changes are in good agreement with the nature of the disease and expected results from literature reports (Barnes 2000, Elizur *et al.* 2008).

3.7 Discussion

The results presented here are in agreement with previous studies and show that predominant pressure drop occurs in the upper airways (first 5 bifurcation levels) (Olson *et al.* 1970). In (Olson *et al.* 1970), airway elasticity is not

included for computational reasons and the authors claim that if included, the results will not improve too much due to numerical inaccuracies in tube elasticity or elasticity in the spur of bifurcation. Our results show that elasticity cannot be neglected, since its effects are varying significantly with airway disease. For typical flow rates during spontaneous breathing ranging 0.5-1 l/s, wall roughness is neglected since it has little effect in laminar flow conditions and for low values of the Womersley parameter. The values of the Womersley parameter δ are always less than 1, varying from 0.0471 in alveoli to 0.785 in the trachea. If one compares these values of δ for the circulatory system, where values become as high as 24, deviations from Poiseuille parabolic flow profile occur as a result (Pedley *et al.* 1971, Segers *et al.* 1997). This is not the case for the laminar flow conditions during tidal breathing (Ionescu 2008).

We use a set of simplifying assumptions which are generally accepted from previous studies (Franken *et al.* 1981, Mead 1961). **Pressure related assumptions**: the pressure at the boundaries of all parts is the same at all points of the respective boundaries. Three of the boundaries contain gas only on one side: airway opening, alveolar surface and body surface. Uniform pressure is valid if the gas is in continuity condition and no flow. These conditions are fulfilled for the body surface, during panting at the airway opening and the alveoli. The only part which is not in agreement with this hypothesis is the pleural surface, which has tissue on both sides and its pressure distribution cannot be predicted.

To summarize, the results are obtained under the following assumptions:

- laminar flow for typical Reynolds number during quiet breathing less than 2000;
- ducts are long enough (this assumption is not true, thus neglecting the entrance effects);
- the air is homogeneous and Newtonian;
- the axial velocity component is zero at the airway wall;
- linear (visco)elastic, uniform cylindrical duct (valid as approximation);
- for linearization we have assumed the following simplifications: a) $-\frac{\omega R}{c} << \delta$, for in respiration we have values between $3.5904 \cdot 10^{-5}$ and $2.1542 \cdot 10^{-6}$; b) the air velocity is small compared to the wave velocity; this is valid for most of the airways; i.e. in trachea there may be velocities as high as 10m/s, with a wave velocity of 339m/s; c) the

values for y vary between $0 \longrightarrow \pm 1$ (rigid pipe), although in reality it varies between $0 \longrightarrow \pm(1 + \zeta/R)$ (visco-elastic pipe); d) the E modulus is dependent on the airway type (cartilage fraction);

- thin-walled ducts; for the healthy respiratory system, the ratio h/R varies between 0.4625 in trachea, to 0.0896 in alveoli. When calculating the value for $\acute{c}_0$, the geometrical characteristics are introduced, modifying it accordingly.

Due to the fact that we do not seek to obtain a precise/exact value of the pressure and flow components but merely a qualitative value, we consider that a more complex formulation may be correct and more realistic, but may serve little our objectives.

The results based on the Womersley theory have been used to determine an electrical equivalent of the respiratory system and capture the mechanical properties (3.62)-(3.64). For the respiratory system, transmission line models are mostly used within high frequency ranges (above 100 Hz) for sound analysis diagnosis (Harper *et al.* 2001). However, for lower frequencies (0.1-50 Hz) the transmission line theory can be applied in a simplified form, leading to the exact solution for pressure and flow changes in normal breathing conditions. A study on the systemic circulation has been employed in (Olufsen 2004), leading to the same formula for the compliance (3.61). Similarity exists between the derivation of the input impedance in the respiratory tree in this study and modeling the smaller systemic arteries, since in both simulations the symmetric structure is employed, along with laminar flow conditions, incompressibility, Newtonian fluid and the no-slip boundary condition. The input impedance is extended to a more general tree in (Olufsen 2004), by adding the equation of crossing a bifurcation based on a law on which the geometry changes over the junction. Nevertheless, we may argue that our choice of choosing to model a completely symmetric tree still reflects its essential behavior, and can be extended with the asymmetry relations adapted from (Olufsen 2004).

It is straightforward to apply airway altering/remodeling effects in this simple model representation, but limitations should be taken into account. The major errors which may occur in this study are determined by the heterogeneity of the human lung, i.e. inter-subject variability can affect the values from table 3.1. However, these values are reported in several studies (Hou *et al.* 2005, Harper *et al.* 2001, Lai & Hyatt 2000, Mauroy 2005, Weibel 2005) and they had offered good basis for investigations, originally measured from excised

lungs (Olson *et al.* 1970, Weibel 1963) and then in plastic casts (Sauret *et al.* 1999).

Another source for errors is neglecting the effects from the branching angles. These angles influence the flow to change direction, may lead to an asymmetrical velocity profile, to develop a secondary flow in the daughter branches and the inner airway walls to be slightly stretched (Sauret *et al.* 1999). The change in cross-sectional areas which occurs from parent to daughter branches in a bifurcation causes the fluid to undergo a deceleration and may cause separation of adjoining streamlines.

Some nominal recurrence in the lungs is derived in Appendix D.

3.8 Conclusions

The novelty of the work presented in this chapter consists in that it introduces the assumption of flexible airways in a simple form, taking into account the wall tissue structure (in terms of cartilage and soft tissue percent and densities) and derives the mechanical parameters to enable changes in airway morphology with disease. The resulting models are therefore relatively simple and efficient to capture mechanical variations in lumped models (e.g. an electrical equivalent).

Here, a mathematical model for the pressure and flow variations in the respiratory tree has been developed based on similarity to the well-defined Womersley theory, which was hitherto applied only in models for the circulatory system. Due to the fact that fractal-like geometry in both circulatory and respiratory tree exists, theoretical developments for models of the circulatory system were applicable in this study as well. The mathematical model is developed for tidal breathing conditions, allowing consequent assumptions to simplify the complex modelling of aerodynamics. The influence of changes in radius and elastic modulus with disease has been assessed in terms of pressure and flow changes. The outcome of this pressure-flow dynamical model is the electrical transmission line analogue. As a result, the electrical parameters for resistance, inductance, capacitance and conductance have been determined over one airway.

In simulations for viscoelastic airways, variations in these parameters correspond to the physiological insight. Although the simplifying assumptions may introduce errors, these are not significant for our final objective.

The next step is to use the elastic and viscoelastic models of the airway ducts to model the entire respiratory structure, preserving its intrinsic geometry.

Chapter 4

The Fractal Structure of the Lungs

The construction of the electrical ladder network equivalent using the elements determined in the previous chapter is detailed here. The cases of an elastic tube wall and a viscoelastic tube wall are discussed, with supporting analytical and simulated results. A generalization of the analytical results is given, suggesting applicability to other branching systems. The estimated results are successfully validated with measured data. The chapter ends with a special analysis of the asymmetric branching and its consequences on the total input impedance values.

Part of the material presented in this chapter has been used in the following publications:

- *Ionescu C., Muntean I., Tenreiro-Machado J., De Keyser R., Abrudean M., (online) "A Theoretical Study on Modelling the Respiratory Tract With Ladder Networks by Means of Intrinsic Fractal Geometry", IEEE Transactions on Biomedical Engineering, Digital Object Identifier: 10.1109/TBME.2009.2030496;*
- *Ionescu C., Caicedo A., De Keyser R., (2007) "Total respiratory impedance analysis using ladder networks analogy for fractional-order models" in Bulletin of the Transilvania University of Brasov, Series A1,* ***14(49)****, ISSN 1223-9631, 227–234;*
- *Ionescu C., De Keyser R., (2008) "The use of non-integer order modelling in a tracheal simulation study", in Transactions on Automatic Control and Computer Science,* ***53(67)****, ISSN 1224-600X, 201–208;*

- *Muntean I., Ionescu C., Nascu I., (2009), "A simulator for the respiratory tree in healthy subjects derived from continued fractions expansion", in AIP Conference Proceedings Book vol. 1117 (Proceedings of the 1st Int. Conf. on Bio-Inspired Computational Methods Used for Difficult Problems Solving: Development of Intelligent and Complex Systems), Eds. B. Iantovics, Enachescu C., F. Filip, ISBN: 978-0-7354-0654-4, 225–231;*

- *Ionescu C., Oustaloup A., Levron F., Melchior P., Sabatier J., De Keyser R. (2009), "A model of the lungs based on fractal geometrical and structural properties", in: Proc. of the IFAC Int. Conf. on System Identification, St. Malo, France, 994-999;*

- *Ionescu C., Muntean I., De Keyser R., (2009), "The respiratory impedance in an asymmetric model of the lung structure ", in: Proc. of the Int. Symp. on Understanding Intelligent and Complex Systems, Tg Mures,Romania.*

4.1 An elastic airway wall

In this section, we make use of the formulas (3.62), (3.63) and (3.64), which are calculated with the morphologic values from table 3.1. With the resistance, inertance and capacitance values at hand, one is able to build an electrical network. Suppose the electrical network as depicted in figure 4.1, which preserves the geometry of the respiratory tree (Ionescu & De Keyser 2008*d*). In this network, Zl^*_m denotes the longitudinal impedance, whereas Zt^*_m denotes the transversal impedance of the airway tubes and m denotes the level in the respiratory tree ($m = 1..N$).

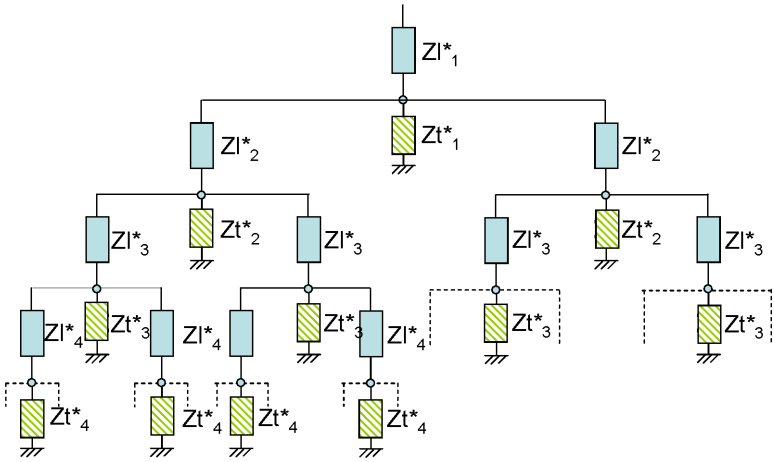

Figure 4.1: *Recursive tree representation of the respiratory tree in its electrical equivalent.*

Assuming that the flow Q is symmetric with respect to each bifurcation (divides equally trough the branches) one can define the equivalent level impedances and admittances as a function of powers 2. Hence, the total resistance per level is given by (Muntean *et al.* 2009):

$$R_{em} = R^*_{em}/2^{m-1} \tag{4.1}$$

with R^*_{em} the resistance in a single branch. Similarly, the total inertance per level is given by:

$$L_{em} = L^*_{em}/2^{m-1} \tag{4.2}$$

with L^*_{em} the inertance in a single branch; finally, the total capacitance in a level is given by:

$$C_{em} = C^*_{em} \cdot 2^{m-1} \tag{4.3}$$

with C^*_{em} the capacitance in a single branch. Using these relations, one can simplify the electrical network from figure 4.1 to an equivalent ladder network, schematically depicted in figure 4.2. In this ladder network, Zl^*_m, with $m = 1..N$ denotes the longitudinal impedance, which is defined as: $Zl^*_m(s) = R^*_{em} + L^*_{em}s$. Since both resistance and inertance in each level are divided by 2^{m-1}, then we can use the equivalent representation $Zl_m(s) = Zl^*_m/2^{m-1}$, as in figure 4.2. In the same figure, the capacitance is denoted using (4.3).

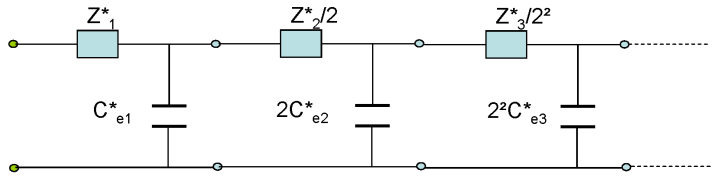

Figure 4.2: *Equivalent ladder network for the symmetric recursive tree.*

We introduce the following notations for the ratios between the levels:

$$\frac{R_{em+1}}{R_{em}} = \lambda, \quad \frac{L_{em+1}}{L_{em}} = \frac{1}{\alpha}, \quad \frac{C_{em+1}}{C_{em}} = \chi \tag{4.4}$$

with the ratios including both morphological and geometrical properties, as in figure 4.2. Hence, using the morphological values from table 3.1 in (4.1), (4.2) and (4.3), the 'nominal' ratios from (4.4) are calculated and given in table 4.1.

nominal	**levels 1..15**	**levels 16..24**
λ	0.81 ± 0.32	0.68 ± 0.16
$1/\alpha$	0.56 ± 0.17	0.56 ± 0.08
χ	1.71 ± 0.77	1.55 ± 0.29

Table 4.1: *Ratios of the mechanical parameters between consecutive levels. Values are presented as mean $\pm$ standard deviation values for the 1..15 levels, respectively for the 16..24 levels.*

The total input impedance $Z_N(s)$ of the ladder network from figure 4.2 can be written as a continuous fraction expansion (Oustaloup 1995). For sake of

mathematical clarity, we shall derive the analysis in terms of the admittance, which is the inverse of the impedance $Y_N(s) = 1/Z_N(s)$.

In this paper we make use of the theoretical basis developed in the past for similar structures, but tailored upon the conditions and the characteristics of the respiratory system.

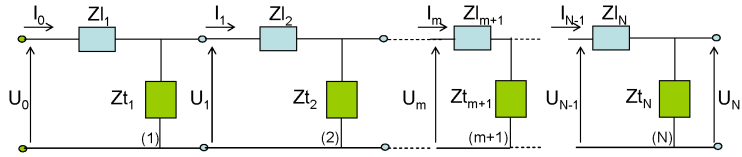

Figure 4.3: *General scheme of a ladder network in gamma-cell configuration; where N denotes the total number of cells.*

Consider the generalized case depicted in figure 4.3. The longitudinal and transversal impedances can be defined irrespective of their elements, in function of voltage and current:

$$Zl_m(s) = \frac{U_{m-1}(s) - U_m(s)}{I_{m-1}(s)} \tag{4.5}$$

and

$$Zt_m(s) = \frac{U_m(s)}{I_{m-1}(s) - I_m(s)} \tag{4.6}$$

from which we can further write:

$$U_m(s) - U_{m+1}(s) = Zl_{m+1}(s) I_m(s), \tag{4.7}$$

or, equivalently,

$$\frac{I_m(s)}{U_m(s)} = \frac{1/Zl_{m+1}(s)}{1 + \frac{U_{m+1}(s)}{I_m(s) Zl_{m+1}(s)}} \tag{4.8}$$

and

$$I_m(s) - I_{m+1}(s) = \frac{U_{m+1}(s)}{Zt_{m+1}(s)}, \tag{4.9}$$

or, equivalently

$$\frac{U_{m+1}(s)}{I_m(s)} = \frac{Zt_{m+1}(s)}{1 + Zt_{m+1}(s) \frac{I_{m+1}(s)}{U_{m+1}(s)}} \tag{4.10}$$

From (4.8)-(4.10), the total admittance of the ladder at level $m = 0$ is given by:

$$Y_1(s) = \frac{I_0(s)}{U_0(s)} = \frac{1/Zl_1(s)}{1 + \frac{U_1(s)}{I_0(s)Zl_1(s)}} \tag{4.11}$$

or, equivalently, by:

$$Y_1(s) = \frac{1/Zl_1(s)}{1 + \dfrac{Zt_1(s)/Zl_1(s)}{1 + Zt_1(s)\dfrac{I_1(s)}{U_1(s)}}} \tag{4.12}$$

If we calculate the total admittance until $m = 1$, we have that:

$$Y_2(s) = \frac{1/Zl_1(s)}{1 + \dfrac{Zt_1(s)/Zl_1(s)}{1 + \dfrac{Zt_1(s)/Zl_2(s)}{1 + \dfrac{U_2(s)}{I_1(s)Zl_2(s)}}}} \tag{4.13}$$

or, equivalently,

$$Y_2(s) = \frac{1/Zl_1(s)}{1 + \dfrac{Zt_1(s)/Zl_1(s)}{1 + \dfrac{Zt_1(s)/Zl_2(s)}{1 + \dfrac{Zt_2(s)/Zl_2(s)}{1 + Zt_2(s)\dfrac{I_2(s)}{U_2(s)}}}}} \tag{4.14}$$

From (4.12)-(4.14) one may generalize via recurrence the form of the total admittance with $m = N$ cells, for $N \to \infty$:

$$Y_N(s) = \cfrac{1/Zl_1(s)}{1 + \cfrac{Zt_1(s)/Zl_1(s)}{1 + \cfrac{Zt_1(s)/Zl_2(s)}{1 + \cfrac{Zt_2(s)/Zl_2(s)}{\cdots \cfrac{\cdots}{1 + \cfrac{Zt_{N-1}(s)/Zl_N(s)}{1 + Zt_N(s)/Zl_N(s)}}}}}} \tag{4.15}$$

which is, in fact, a continued fraction expansion (Oustaloup 1995). Re-writing (4.15) using the explicit form of the longitudinal and transversal

impedances gives:

$$Y_N(s) = \cfrac{1/(R_{e1}+L_{e1}s)}{1+\cfrac{1/[C_{e1}s(R_{e1}+L_{e1}s)]}{1+\cfrac{1/[C_{e1}s(R_{e2}+L_{e2}s)]}{1+\cfrac{1/[C_{e2}s(R_{e2}+L_{e2}s)]}{1+\cfrac{1/[C_{e2}s(R_{e3}+L_{e3}s)]}{\cdots\cfrac{\cdots}{1+\cfrac{1/[C_{e(N-1)}s(R_{eN}+L_{eN}s)]}{1+1/[C_{eN}s(R_{eN}+L_{eN}s)]}}}}}} \tag{4.16}$$

which, in terms of the recursive ratios from (4.4) can be re-written as:

$$Y_N(s) = \cfrac{1/(R_{e1}+L_{e1}s)}{1+\cfrac{1/[C_{e1}s(R_{e1}+L_{e1}s)]}{1+\cfrac{1/[C_{e1}s(\lambda R_{e1}+\frac{L_{e1}s}{\alpha})]}{1+\cfrac{1/[\chi C_{e1}s(\lambda R_{e1}+\frac{L_{e1}s}{\alpha})]}{1+\cfrac{1/[\chi C_{e1}s(\lambda^2 R_{e1}+\frac{L_{e1}s}{\alpha^2})]}{\cdots\cfrac{\cdots}{1+\cfrac{1/[\chi^{N-2}C_{e1}s(\lambda^{N-1}R_{e1}+\frac{L_{e1}s}{\alpha^{N-1}})]}{1+1/[\chi^{N-1}C_{e1}s(\lambda^{N-1}R_{e1}+\frac{L_{e1}s}{\alpha^{N-1}})]}}}}}} \tag{4.17}$$

For the set of conditions:

$$L_{e1} << R_{e1} \;\; |s| < \frac{1}{R_{e1}\cdot C_{e1}} \text{ and } |s| << \frac{R_{e1}}{L_{e1}} \tag{4.18}$$

and:

$$\alpha\cdot\chi > 1,\; \alpha\cdot\lambda > 1,\; \lambda > 1 \text{ and } \chi > 1, \tag{4.19}$$

we have that in the limit $N \to \infty$, the term $\frac{L_{e1}s}{(\alpha\lambda)^{N-1}}$ from (4.17) becomes very small compared to the term in R_{e1}. Consequently, the continued fraction expansion from (4.17) reduces to:

$$Y_N(s) \cong \cfrac{1/R_{e1}}{1+\cfrac{1/R_{e1}C_{e1}s}{1+\cfrac{1/\lambda R_{e1}C_{e1}s}{1+\cfrac{1/\chi\lambda R_{e1}C_{e1}s}{1+\cfrac{1/\chi\lambda^2 R_{e1}C_{e1}s}{\cdots\cfrac{\cdots}{1+\cfrac{1/\chi^{N-2}\lambda^{N-1}R_{e1}C_{e1}s}{1+1/\chi^{N-1}\lambda^{N-1}R_{e1}C_{e1}s}}}}}} \tag{4.20}$$

If we introduce the notations:

$$W_d(s) = \frac{1}{R_{e1}C_{e1}s},\ W_n(s) = \frac{1}{R_{e1}}, \tag{4.21}$$

then (4.20) can be reduced to an analogue representation:

$$Y_N(s) \approx \frac{W_n(s)}{1 + g(W_d(s), \lambda, \chi)} \tag{4.22}$$

in which $g(W_d(s), \lambda, \chi)$ denotes:

$$g(W_d(s), \lambda, \chi) = \frac{W_d(s)}{1 + \cfrac{W_d(s)/\lambda}{1 + \cfrac{W_d(s)/\lambda\chi}{1 + \cfrac{W_d(s)/\lambda^2\chi}{\cdots}}}} \tag{4.23}$$

Since $W_d(s)$ can be taken in front of the expansion and both λ and χ are constants, we can write that:

$$Y_N(s) \approx \frac{W_n}{K(\lambda, \chi)(W_d(s))^n} \tag{4.24}$$

with the fractional order n given by

$$n = \frac{\log(\lambda)}{\log(\lambda) + \log(\chi)} \tag{4.25}$$

or that, in our specific case:

$$Y_N(s) \cong \frac{1/R_{e1}}{K(\lambda, \chi) \cdot (1/R_{e1}C_{e1}s)^n} \tag{4.26}$$

Consequently, the impedance is given by:

$$Z_N(s) = \frac{1}{Y_N(s)} \cong \frac{K(\lambda, \chi) \cdot R_{e1}}{(R_{e1}C_{e1}s)^n} \tag{4.27}$$

The values for $K(\lambda, \chi)$ can be determined as described in (Oustaloup 1995); since we do not make use of it explicitly, its derivation will not be discussed here. Moreover, our sole purpose was to show that the continuous fraction expansion from (4.16) will lead to a compact form which contains a term in the fractional-order n. Hence, relation (4.27) shows the link between the ladder network from figure 4.2 and the appearance of a fractional order term in the form of total input impedance. In the frequency domain, the fractional order will lead to a constant-phase behaviour, i.e. a phase-locking in the frequency

range given by the convergence conditions (Oustaloup 1995). Depending on the number of cells in the ladder (N), the constant-phase behavior will emerge over a wider range of frequencies. This result is applicable to any kind of ladder network (airways, arteries, etc). However, the fractional order value and coefficients will change according to the properties (morphology, geometry) of the system.

In practice, the respiratory tract can be simulated as follows. The relations derived in chapter 3 for resistance (3.62), inertance (3.63) and compliance (3.64) are used to calculate the total level values as in (4.1), (4.2) and (4.3). Notice that the values in the trachea R_{e1}, L_{e1}, and C_{e1} need to take into account the flow and pressure effects in the upper airways (mouth, nose, larynx, pharynx). Since we do not model the upper airways, we need to take the corresponding values from literature (Peslin *et al.* 1984): $R_{UA} = 0.2$ kPa/(l/s), $L_{UA} = 0.002$ kPa/(l/s^2) and $C_{UA} = 0.25$ l/kPa. To find the level values, one can make use of the ratios from table 4.1. The last compartment needs to model the gas compression effect; hence, from literature, we introduce the series impedance consisting of (Habib *et al.* 1994): $R_{CG} = 0.05$ kPa/(l/s), $L_{CG} = 0.06$ kPa/(l/s^2) and $C_{CG} = 6$ l/kPa. This last impedance is closing the ladder network, being in parallel with the cell $N = 24$. The total admittance from (4.16) is then calculated. The equivalent total input impedance (including the upper airways and the gas compression compartment) is depicted by means of its real-imaginary parts in figure 4.4-left, respectively by its equivalent Bode plot representation in figure 4.4-right. Notice that in these figures, we show the impedance in two cases: when the airway tube is modelled by an $R - C$ element, and an $R - L - C$ element, respectively. This comparison allows capturing the effect of the inertance element, while the frequency is increasing.

In the Bode plot, a variation of the phase between 0^o and -26^o can be observed in the frequency interval $\omega \in [10^{-4}, 10^2]$ (rad/s). However, this is not the constant phase effect as expected from theory, because the fractional-order value n would have to be zero, or 0.3, respectively. If we use the analytical form of (4.25) to calculate this fractional order value, we obtain $n = 0.59$. This mismatch between simulation and theory is due to the fact that the condition of $\lambda > 1$ is not fulfilled in (4.19). We shall discuss this aspect later on.

It is also worth noticing that the extra parameter L_m has no effect in determining the value of the fractional order, which is then similar to what we expected from theoretical analysis, i.e. relation (4.20) (Ionescu *et al.* in print). On the other hand, the effect of this extra term becomes significant with increasing

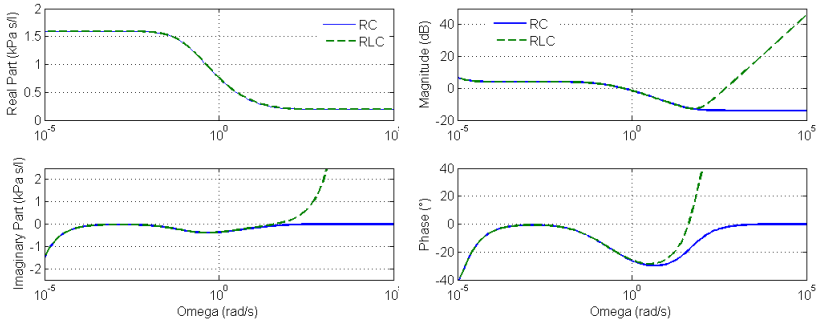

Figure 4.4: *Impedance by means of complex (left) and Bode-plot (right) representation, for the $R-C$ (continuous line) and the $R-L-C$ (dashed line) model structures.*

frequencies, namely after the frequency interval where the phase variations are observed ($\omega > 100$ rad/s).

4.2 A viscoelastic airway wall

In this section, we shall use the formulas derived in chapter 3, namely (3.71),(3.72), (3.74) and (3.73), with values from table 3.1. With these values at hand, one is able to build an electrical network as described in the previous section. The difference to the previous case (elastic) is that now the airway tube is modelled in a $R-L-C-G$ element, as described in chapter 3. This representation allows us to consider the viscoelastic wall properties, trough the elements $C-G$.

nominal	**level 1..15**	**level 16..24**
λ	0.81 ± 0.32	0.68 ± 0.16
$1/\alpha$	0.56 ± 0.17	0.56 ± 0.08
χ	1.71 ± 0.77	1.55 ± 0.29
o	1.71 ± 0.77	1.55 ± 0.29

Table 4.2: *Ratios of the mechanical parameters between consecutive levels. Values are presented as mean $\pm$ standard deviation values for the 1..15 levels, respectively for the 16..24 levels.*

For the special case of the ladder network in which $Zl_m(s) = R_{em} + L_{em}s$ and $1/Zt_m(s) = G_{em} + 1/C_{em}s$, with m denoting a level in the respiratory tree, one can analyze the properties of such a network. Next to the ratios

defined in (4.4), we add the ratio for the conductance:

$$\frac{G_{em+1}}{G_em} = \frac{1}{o} \tag{4.28}$$

where the ratio is determined similarly as for the other parameters. The nominal ratios are given in table 4.2. Notice that the ratio for C_e and G_e are similar due to the fact that the forms in (3.74) and (3.73) are the same, except for the $\sin$ and $\cos$ terms, whose effect are thus very small.

In a similar manner as for the elastic tube case, we can write that the total admittance is given by:

$$Y_N(s) = \cfrac{1/(R_{e1}+L_{e1}s)}{1+\cfrac{G_{e1}/[(G_{e1}C_{e1}s+1)(R_{e1}+L_{e1}s)]}{1+\cfrac{\frac{G_{e1}/[(G_{e1}C_{e1}s+1)(R_{e2}+L_{e2}s)]}{1+\frac{G_{e2}/[(G_{e2}C_{e2}s+1)(R_{e2}+L_{e2}s)]}{1+\frac{G_{e2}/[(G_{e2}C_{e2}s+1)(R_{e3}+L_{e3}s)]}{\cdots}}}}{\cdots\cfrac{}{1+\frac{G_{e(N-1)}/[(G_{e(N-1)}C_{e(N-1)}s+1)(R_{eN}+L_{eN}s)]}{1+G_{eN}/[(G_{eN}C_{eN}s+1)(R_{eN}+L_{eN}s)]}}}} \tag{4.29}$$

which, can be re-written in a convenient form:

$$Y_N(s) = \cfrac{1/R_{e1}(1+L_{e1}s/R_{e1})}{1+\cfrac{\frac{G_{e1}/G_{e1}C_{e1}s}{(1+1/G_{e1}C_{e1}s)R_{e1}(1+L_{e1}s/R_{e1})}}{1+\cfrac{\frac{G_{e1}/G_{e1}C_{e1}s}{(1+1/G_{e1}C_{e1}s)R_{e2}(1+L_{e2}s/R_{e2})}}{1+\cfrac{\frac{G_{e2}/G_{e2}C_{e2}s}{(1+1/G_{e2}C_{e2}s)R_{e2}(1+L_{e2}s/R_{e2})}}{1+\cfrac{\frac{G_{e2}/G_{e2}C_{e2}s}{(1+1/G_{e2}C_{e2}s)R_{e3}(1+L_{e3}s/R_{e3})}}{\cdots}}}}{\cdots\cfrac{}{1+\cfrac{\frac{G_{e(N-1)}/G_{e(N-1)}C_{e(N-1)}s}{(1+1/G_{e(N-1)}C_{e(N-1)}s)R_{eN}(1+L_{eN}s/R_{eN})}}{1+\frac{G_{eN}/G_{eN}C_{eN}s}{(1+1/G_{eN}C_{eN}s)R_{eN}(1+L_{eN}s/R_{eN})}}}} \tag{4.30}$$

We introduce the notations:

$$W_d(s) = \frac{1}{R_{e1}C_{e1}s},\ W_0(s) = \frac{1}{G_{e1}C_{e1}s} \text{ and } W_1(s) = \frac{L_{e1}s}{R_{e1}} \tag{4.31}$$

and replace for the ratios in (4.30) and we obtain that:

$$Y_N(s) = \cfrac{1/R_{e1}(1+W_1(s))}{1+\cfrac{\frac{W_d(s)/(W_0(s)+1)}{(1+W_1(s))}}{1+\cfrac{\frac{W_d(s)/\lambda(W_0(s)+1)}{(1+W_1(s)/\alpha\lambda)}}{1+\cfrac{\frac{W_d(s)/\lambda\chi(oW_0(s)/\chi+1)}{(1+W_1(s)/\alpha\lambda)}}{1+\cfrac{\frac{W_d(s)/\lambda^2\chi(oW_0(s)/\chi+1)}{(1+W_1(s)/\alpha^2\lambda^2)}}{\cdots\cfrac{\cdots}{1+\cfrac{\frac{W_d(s)/\lambda^{N-1}\chi^{N-2}(o^{N-2}W_0(s)/\chi^{N-2}+1)}{(1+W_1(s)/\alpha^{N-1}\lambda^{N-1})}}{1+\frac{W_d(s)/\lambda^{N-1}\chi^{N-1}(o^{N-1}W_0(s)/\chi^{N-1}+1)}{(1+W_1(s)/\alpha^{N-1}\lambda^{N-1})}}}}}}} \tag{4.32}$$

For the set of conditions from (4.18) and for

$$\alpha\cdot\chi>1,\ \alpha\cdot\lambda>1,\ \lambda>1 \text{ and } \chi\geq o, o>1, \tag{4.33}$$

we have that the term $\frac{o^{N-1}}{(G_{e1}C_{e1}s)\chi^{N-1}}$ from (4.32) goes to zero as frequency increases. In this case, the limit $N\to\infty$ does not play any role, since $\chi=o$; however, if $1/(G_{e1}C_{e1}s) << 1$ then we can then re-write (4.32) as:

$$Y_N(s)\cong\cfrac{1/R_{e1}(1+W_1(s))}{1+\cfrac{W_d}{1+\cfrac{W_d/\lambda}{1+\cfrac{W_d/\chi\lambda}{1+\cfrac{W_d/\chi\lambda^2}{\cdots\cfrac{\cdots}{1+\cfrac{W_d/\chi^{N-2}\lambda^{N-1}}{1+W_d/\chi^{N-1}\lambda^{N-1}}}}}}}} \tag{4.34}$$

which is similar in form to (4.22):

$$Y_N(s)\approx\frac{1/R_{e1}(1+W_1(s)))}{1+g(W_d(s),\lambda,\chi)} \tag{4.35}$$

in which

$$g(W_d(s),\lambda,\chi)=\cfrac{W_d(s)}{1+\cfrac{W_d(s)/\lambda}{1+\cfrac{W_d(s)/\lambda\chi}{1+\cfrac{W_d(s)\lambda^2\chi}{\cdots}}}} \tag{4.36}$$

which can be re-written as:

$$Y_N(s)\approx\frac{1/(R_{e1}+L_{e1}s)}{K(\lambda,\chi)(W_d(s))^n} \tag{4.37}$$

with the fractional order n given by

$$n = \frac{\log(\lambda)}{\log(\lambda) + \log(\chi)} \tag{4.38}$$

In our specific case we have that:

$$Y_N(s) \cong \frac{1/(R_{e1} + L_{e1}s)}{K(\lambda, \chi) \cdot (1/R_{e1}C_{e1}s)^n} \tag{4.39}$$

Consequently, the impedance is given by:

$$Z_N(s) = \frac{1}{Y_N(s)} \cong \frac{K(\lambda, \chi) \cdot (R_{e1} + L_{e1}s)}{(R_{e1}C_{e1}s)^n} \tag{4.40}$$

The respiratory tract is simulated in a similar manner as explained in the previous section, with the same values for the upper airways and the gas compression impedance. We have no information upon the upper airway values for G_{UA}, thus we take $G_{UA} = 1/[R_{UA} \cdot 200]$. The total impedance from (4.29) is then calculated and depicted by means of its real-imaginary parts in figure 4.5-left, respectively by its equivalent Bode plot representation in figure 4.5-right. Notice that in these figures, we show the impedance in two cases: when the airway tube is modelled by the $R - L - C$ element, and by the $R - L - C - G$ element, respectively. This comparison allows capturing the effect of the conductance element at frequencies below 0.1 rad/s.

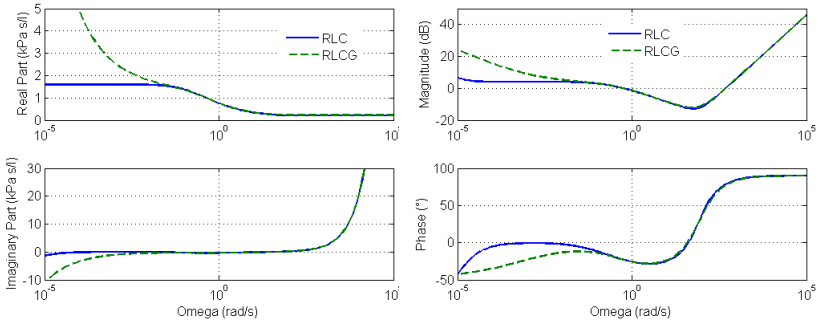

Figure 4.5: *Impedance by means of complex (left) and Bode-plot (right) representation, for the $R - L - C$ (continuous line) and the $R - L - C - G$ (dashed line) model structures.*

A similar FO behavior can be observed as in figure 4.4. This is again in accordance to the theoretical result from relations (4.34) and (4.38), which

shows that only the ratios for R_{m+1}/R_m and C_{m+1}/C_m play a role in determining the value for the fractional order at low frequencies. Another observation is that the viscoelastic effects are visible only at low frequencies, below 0.1 rad/s, which is also in agreement with rheological properties (Suki *et al.* 1994, Bates 2007, Craiem & Armentano 2007).

4.3 Model Validation

4.3.1 Measurements in the 4-48 Hz frequency interval

In order to compare the result obtained by the nominal simulator parameters with the result from measured data of healthy patients, an averaged impedance has been made from 25 healthy subjects whose biometric characteristics are given in table 4.3.

	Healthy
Age (yrs)	26 ± 3
Height (m)	1.67 ± 0.04
Weight (kg)	64 ± 3.7

Table 4.3: *Biometric parameters of the healthy subjects. Values are presented as mean $\pm$ standard deviation values, as from (Ionescu & De Keyser 2009*b*)*

These subjects have been tested for their lung function using the forced oscillation technique, as described in chapter 2. From the non-invasive measurement of the air-pressure and air-flow at the mouth, the complex impedance is obtained. The range of frequencies where the data is measured is between 25 rad/s and 300 rad/s (i.e. from 4 to 48 Hz). The impedance data from the healthy subjects with the corresponding mean and standard deviation values is given in figure 4.6.

4.3.2 Results for the 4-48 Hz frequency interval

From the measured healthy subjects, we obtain the averaged impedance and the standard deviation values which offer a lower and upper bound, as depicted in figure 4.6. The RLC-ladder model for the respiratory tree calculated with parameters from table 3.1 and (3.62)-(3.64), neglects the impedance introduced by the upper airways segment. In order to make the comparison with

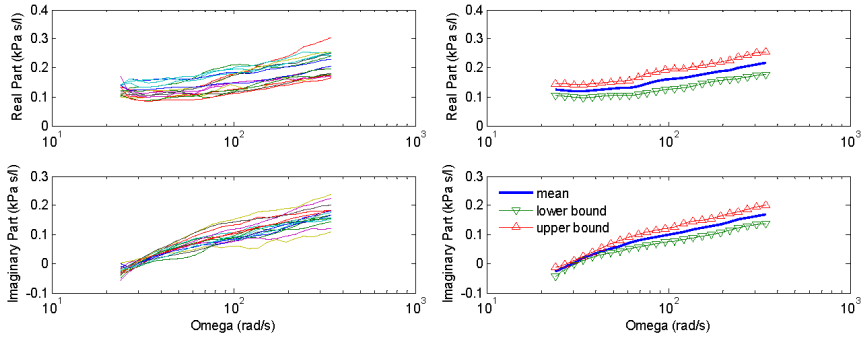

Figure 4.6: *Measured impedance values from healthy subjects (left) and the corresponding mean with standard deviation values (right).*

the measured data, one has to add this extra impedance to obtain the total estimated input impedance. By adding the values of upper airway impedance parameters: $R_{UA} = 0.35$ kPa/(l/s), $L_{UA} = 0.00045$ kPa/(l/s^2), $C_{UA} = 0.85$ l/kPa, one obtains satisfactory values in the clinical range of frequencies, as depicted in figure 4.7. One should keep in mind that no study has been reported in literature upon the variations and confidence intervals of the upper airway parameters values. These values represent a tuning parameter of our ladder network model, and in this particular case they have been tuned for the averaged values of impedance given in figure 4.7.

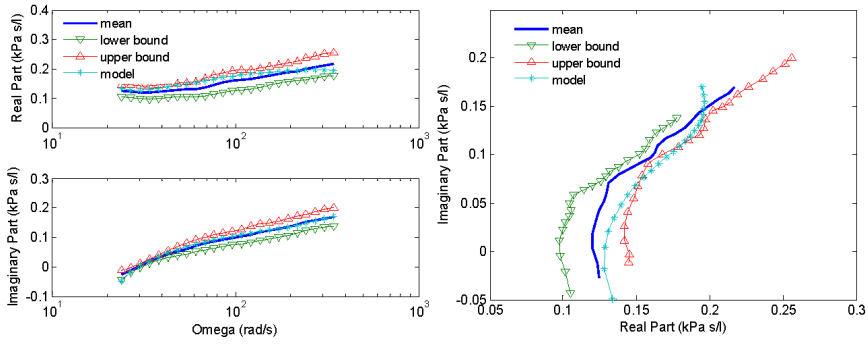

Figure 4.7: *Comparison of the RLC-ladder model performance, within the measured frequency range, against data from healthy subjects (left) and equivalent polar plot representation (right).*

Since figure 4.5 shows the same result in the 25-300 rad/s frequency range for both elastic and viscoelastic airway wall models, it is clear that the same

result is obtained for the $R-L-C-G$ ladder network model as in figure 4.7.

4.3.3 Model Analysis

In this study, we investigate three cases: the nominal, the pathologic case and the extended case. The nominal case is denoted by the ladder network model in which the ratios from table 4.1 are used. In the **pathologic case**, due to the fact that airway morphology is affected by disease, changes occur in the mechanical parameters such that the overall resistance increases and the compliance decreases (e.g. in chronic obstructive pulmonary disease), resulting in the ratios from table 4.4.

pathologic	**levels 1..15**	**levels 16..24**
λ	1.12 ± 0.22	1.16 ± 0.06
$1/\alpha$	0.54 ± 0.11	0.65 ± 0.08
χ	1.22 ± 0.27	1.22 ± 0.20

Table 4.4: *Ratios of the mechanical parameters between consecutive levels in pathology. Values are presented as mean $\pm$ standard deviation values for the 1..15 levels, respectively for the 16..24 levels.*

From this table, we can observe that all conditions from (4.19) are now fulfilled; including $\lambda > 1$. The extended case consists of increasing the number of cells in the ladder network, while keeping constant the ratios from table 4.4.

The simulated total input impedance is depicted by means of its equivalent Bode plot representation in figure 4.8-left in the nominal case, in the pathologic case and in figure 4.8-right the extended case (varying the number of cells in the ladder network). From the Bode plot, it is clear that the fractional order behaviour (phase locking) depends on the ratios between the ladder network parameters, since its value varies from one scenario to the other.

As mentioned previously, the nominal case does not fulfill the condition $\lambda > 1$, hence the constant-phase behaviour does not appear as expected from theory. In the **pathologic case**, one may observe that in the frequency interval $\omega \in [10^{-4}, 10^{-1}]$ (rad/s) the constant phase effect is visible. The magnitude decreases with 45 dB over four decades, which results in a change of about -11 dB/dec. The phase exhibits a phase-locking within this frequency range, around the value of -48^o. From $-n \cdot 20$ dB/dec=11 dB/dec we have that $n \cong 0.55$ and from $-n \cdot 90^o = 48^o$, it follows that $n \cong 0.53$. If one calcu-

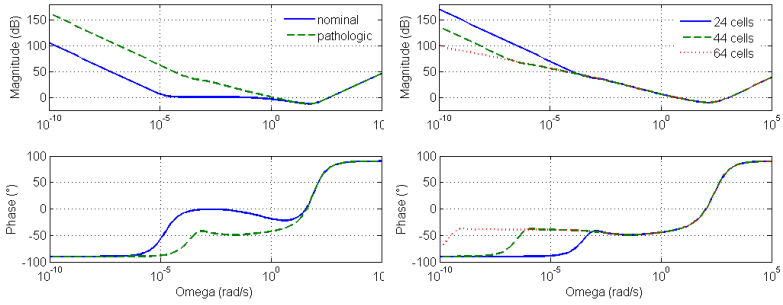

Figure 4.8: *(left): Impedance by means of Bode-plot representation, for the nominal and the pathologic scenarios; (right): for the pathologic case, but with increasing number of cells in the ladder network (the extended scenario).*

lates the fractional order value from (4.25) with averaged ratio values from table 4.4, one comes up with $n = 0.59$, which corresponds closely to the value observed in figure 4.8. This result proves that the formula for n is accurate if the convergence conditions are fulfilled.

In the **extended case**, figure 4.8-right shows the effect of increasing the number of cells, while keeping the same ratios as in table 4.4. Indeed, since the ratios are close to 1, the convergence using relation (4.25) is somewhat difficult. Therefore, increasing the number of cells will help convergence in the limit; recall here that the formula (4.25) was derived considering $N \to \infty$. Increasing the number of cells in the ladder network leads indeed to a constant phase behavior corresponding to a phase value of about -39^o, which is close to the calculated value using (4.25), i.e. $n = 0.40$.

Our findings justify the use of a FO parametric model to characterize the respiratory input impedance (Ionescu & De Keyser 2008*b*). Hence, we established that the origins of the FO behaviour are not only the viscoelastic properties of the lung tissue, typically visible at low frequencies, but also the fractal structure of the respiratory tree. It is interesting to note that both viscoelasticity and diffusion appear at low frequencies, but the diffusion is not tackled in this thesis. The proposed model allows variations in the parameters by altering the elastic modulus E and cartilage fraction κ, as well as variations in the airway geometry by altering the airway radius R, length ℓ and thickness h. Although preserving its fractal structure, these alterations can be correlated to airway remodeling in pathology, leading to different values in the ratios, e.g. those given in (4.4). The results depicted in figure 4.8

indicate that viscoelastic and diffusion phenomena are not the only origin of the phase constancy (non-integer order) models for the lungs, but also the intrinsic recurrent geometry has a similar contribution. Although simple, the nominal case of our model proves to be reasonably close to the data measured from the healthy subjects, showing that it is able to capture the intrinsic properties of the respiratory tree.

4.3.4 Model Validation at Low Frequencies

It is difficult to measure the respiratory impedance at frequencies below the breathing frequency ($\approx$ 0.15 Hz-0.3 Hz) due to high interference between the excitation signal and the breathing signal. For the identification of the respiratory impedance, the breathing signal is considered as pure noise (Ionescu & De Keyser 2003). Hence, there are only a few papers in the literature discussing oscillatory impedance at low frequencies. For example, Hantos *et al.* gives the input impedance measurement in five healthy subjects from 0.25 - 5 Hz frequency interval (Hantos *et al.* 1986). Although they discuss the results in terms of the complex impedance, we can approximate the equivalent magnitude-phase (Bode) plot (see figure 4.9). From figure 4.10 we find that the phase varies from -60^o to -20^o. Hence, a change of about 40^o per decade, resulting in a variation of the fractional order between $n = 0.66$ and $n = 0.22$. The authors discuss that in the respective range of frequencies, the compliance plays an important role, again in agreement with our findings.

From this, we conclude that our model underestimates the resistance and overestimates the compliance parameters. Hence, we identify the ratios for λ and for χ based on data from (Hantos *et al.* 1986), along with the upper airway values for R_{UA} and C_{UA}. The identified values are: $\lambda = 1.18$, $\chi = 1.04$, $R_{UA} = 0.0155$ and $C_{UA} = 0.0191$.

In another study, Babik *et al.* investigate the effect of cardiopulmonary bypass on the respiratory mechanics at low frequency (Babik *et al.* 2003). They measure the impedance via an endotracheal tube, in the 0.2 - 2 Hz frequency range. They find higher values for the resistance and lower values for the compliance and inertance than in (Hantos *et al.* 1986), as shown in figure 4.9. This suggests that in anaesthesia, constriction is present, causing partial closure of airways and resulting in increased tissue hysteresivity (non-homogeneous effects). This effect is close to that observed in COPD lungs, namely a pronounced phase constancy to lower values, as in figure 4.10. From figure 4.10, we find that the phase varies from -74^o to -66^o, resulting in an averaged FO value of $n = 0.77$ (Babik *et al.* 2003).

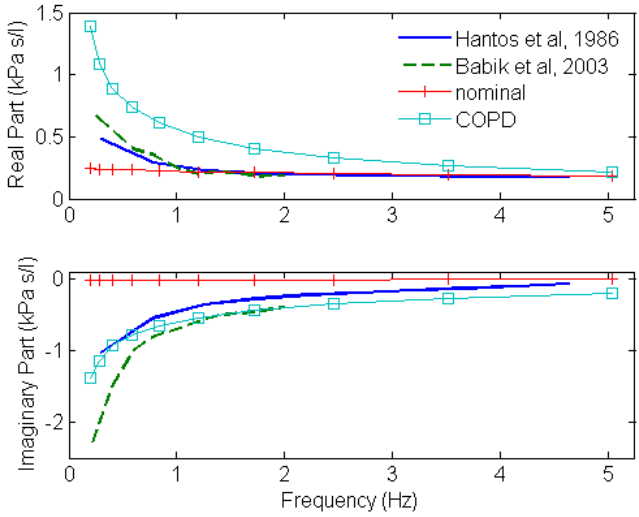

Figure 4.9: *Complex Impedance: validation with data from literature at low frequencies (Hantos* et al. *1986), (Babik* et al. *2003), for the nominal (+) and copd (o) cases.*

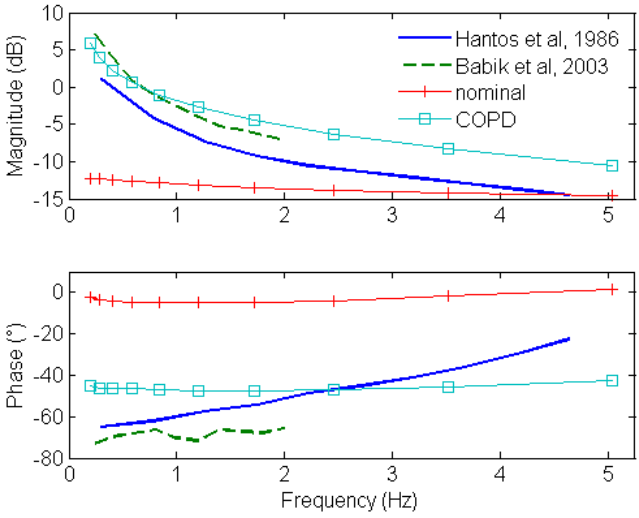

Figure 4.10: *Bode plot: validation with data from literature at low frequencies (Hantos* et al. *1986), (Babik* et al. *2003), for the nominal (+) and copd (o) cases.*

The identified values based on data from (Babik *et al.* 2003) are: $\lambda = 1.35$, $\chi = 1.02$, $R_{UA} = 0.0095$ and $C_{UA} = 0.0148$. Notice that the ladder network model identified lower values in upper airway resistance in anesthetized patients (Babik *et al.* 2003) than in healthy subjects measured during tidal breathing (Hantos *et al.* 1986). This is not surprising, since the measurement in anesthetized subjects is done by skipping the upper airways and measuring directly in the trachea (intubated patients). Typically, most of these patients are under artificial ventilation during surgery. Since both sets of data come from subjects with healthy lung parenchyma, the identified values are similar for the ratios. We conclude therefore that the results obtained with our model are reasonable and correspond to practical insight.

4.4 Influence of Asymmetric Space Filling

In his recent publication, Weibel discusses the reduction of diameter and length by a constant factor for both blood vessels and airways (Weibel 2005). He recognizes the theoretical contributions of Murray (Murray 1926, Bennet *et al.* 2009), i.e. that the dissipation of energy due to flow of blood or air in a branched tube system can be minimized if the diameter of the two daughter-branches are related to the diameter of the parent as in $d_{parent}^3 = d_1^3 + d_2^3$. In the context of fractal geometry, the reduction factor depends on the fractal dimension fD of the branching tree such that the correct formula is: $d_1 = d_{parent} \cdot 2^{-1/fD}$. In the case of Hess-Murray law, $fD = 3$ because the tree is considered to be space-filling (Elzbieta *et al.* 2005). In his investigations, Weibel found that the slope of the conducting airway diameters against the generations was given by $d(m) = d_0 \cdot 2^{-m/3}$, with d_0 the tracheal diameter and m the airway generation. He then concludes that the conducting airways of the human lung are designed as a self-similar and space-filling fractal tree, with a homothety factor of $2^{-1/3} = 0.79$ (similitude ratio). However, as discussed in chapter 3 and in the beginning of chapter 4, this average has a significant variance in the first generations. Hence, the average value changes in the diffusion zone (airways from 16th generation onward). These observations and the fact that Weibel himself discusses that a small change in the homothety factor results in a dramatic increase in peripheral bronchiolar resistance, suggests that the lung must be capable to adjust itself to the optimality conditions. Indeed, a closer analysis reveals that the homothety factor is about 0.79 in the 6th generation, but it increases slowly to about 0.9 in the 16th generation, with an average of 0.85 for the small airways (Weibel 2005). The physiological implications of this observation are:

- the flow resistance decreases in the small airways and
- a small reduction in the homothety factor does not affect significantly the lung function.

In the context of the above observations, one may explore the possibility of the respiratory system as a multi-fractal structure. A self-similar multi-fractal spatial distribution forms the basis for breaking the symmetry of bifurcation design within a tree. In their study, Bennet *et al.* discuss the implications of self-affine scaling (Bennet *et al.* 2009). It turns out that the fractal dimension changes when calculated from different reference points. Therefore, the slope determining the homothety factor changes when viewed at a fine or coarse grained diameter scale. This latter observation is of interest in the context of this thesis, since it supports the idea of a multi-fractal structure. For example, the average of the radius ratio changes from $2^{-0.17} = 0.88$ from (D.1) to 0.89 when only the first 16 generations are taken into account, respectively to 0.87 for the alveoli (generations 17-24). This implies that the homothety factor changes, depending on the spatial location within the tree. On the other hand, if we analyze the radius ratio from generations 1 to 24 in steps of 4, we obtain an average of 0.85, whereas if we use steps of 2, we obtain an average homothety factor of 0.86. These changes might not seem significant, but one should recall that they are originated by the symmetric geometry of the respiratory tree. However, when asymmetry is considered, one deals with several homothety factors, i.e. as schematically drawn in figure 4.11.

It has been demonstrated by a systematic analysis that the airway tree in different species shows a common fractal structure, in spite of some gross differences in airway morphology (Weibel 2005). Nevertheless, we propose to investigate the case of asymmetric branching in the human lungs. The Horsfield representation will be used, as from (Horsfield *et al.* 1971), with the values listed in Table 3.2. In this scenario, an airway of level m bifurcates into two daughters: one of order $m + 1$ and one of order $m + 1 + \Delta$, with Δ the asymmetry index. As a result of the asymmetry, the electrical network becomes as in figure 4.11. Figure 4.12 shows the number of branches that are in one generation, for the symmetric and asymmetric lung structure. Notice the different slope which characterizes the space-filling distribution; the top-figure shows that the slope is lower in the asymmetric tree section than in the symmetric tree section (Ionescu *et al.* 2009*d*).

Since the symmetry is lost, one cannot simplify the electrical network to its ladder network equivalent as in figure 4.2. Therefore, one must calculate explicitly the impedance from level 36 to level 1. To avoid complex numer-

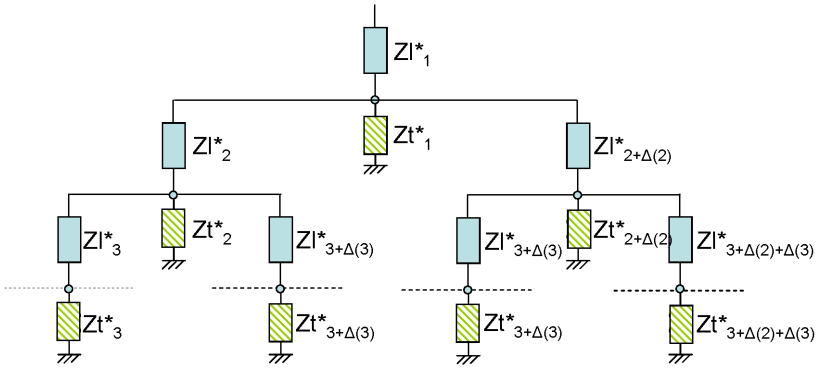

Figure 4.11: *Asymmetric representation for the first four generations, in its electrical equivalent.*

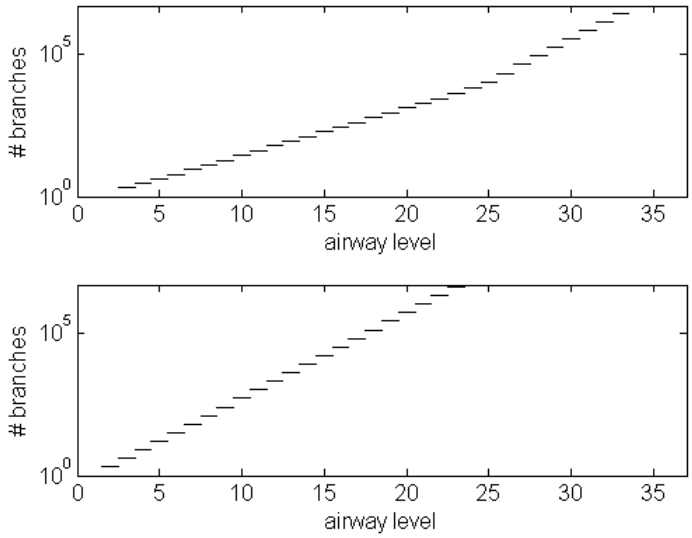

Figure 4.12: *Number of branches for each generation, in the asymmetric (top) and symmetric (bottom) generation. Notice that the Y-axis is logarithmic.*

ical formulations, the impedance along the longest path was calculated, as in (Habib *et al.* 1994). One should notice that from level 26 onward, the asymmetry index is zero, therefore symmetric bifurcation occurs (recall here Table 3.2). The effect of this change in the asymmetry index is visible in figure 4.12, i.e. a change in the slope. The initial values in the trachea are imposed similarly as in the symmetric case (Peslin *et al.* 1984). Figure 4.13 shows the total impedance by means of its complex representation (left) and its Bode plot (right), for the symmetric and the asymmetric tree, whereas the airway tubes are modelled by an $R-L-C$ element in both representations.

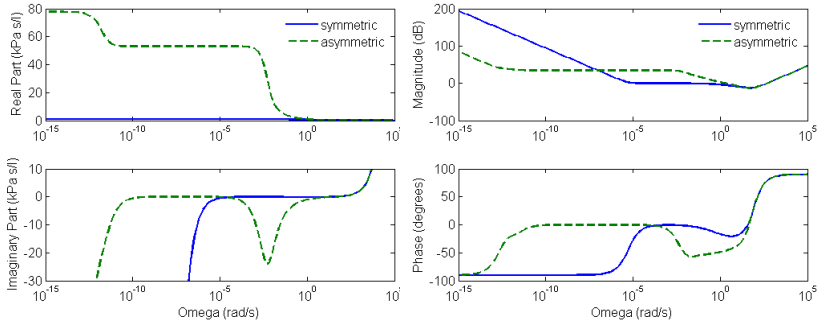

Figure 4.13: *Impedance by means of complex (left) and Bode-plot (right) representation, symmetric (continuous line) and the asymmetric (dashed line) tree.*

It is significant to observe that in the frequency interval of clinical interest, $\omega \in [25, 300]$ rad/s, the two impedances tend to behave similarly. A detail of figure 4.13 can be viewed in figure 4.14. For the asymmetric case, we have a decrease of about -10dB/dec and a phase of approximately -50^o, resulting in a fractional order of $n \cong 0.5$. The constant-phase behavior is emphasized at frequencies below those evaluated standardly in clinical practice, i.e. below 5 Hz. However, in the standard clinical range of frequencies for the forced oscillation technique, namely 4-48 Hz, both models give similar results, as depicted in figure 4.15 below.

4.5 Conclusions

In this Chapter, it has been shown that the structure of the respiratory tree leads to an impedance exhibiting fractional-order behavior. The conclusions

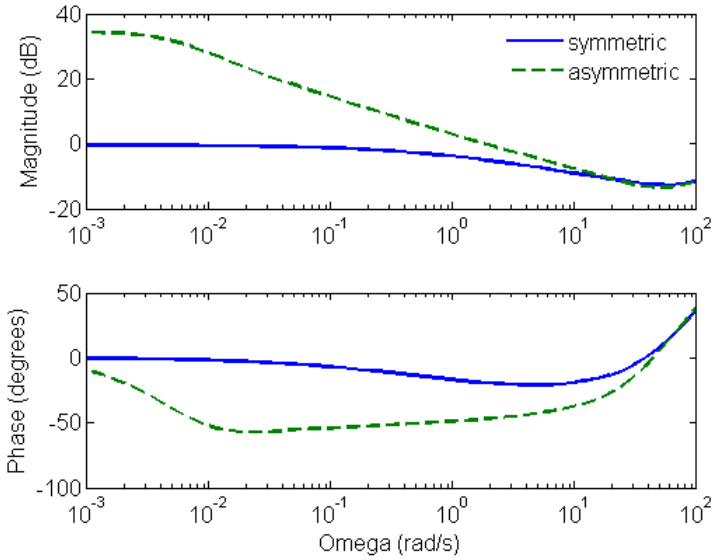

Figure 4.14: *Detailed view of the impedance by means of the Bode-plot representation, for the symmetric (continuous line) and the asymmetric (dashed line) tree.*

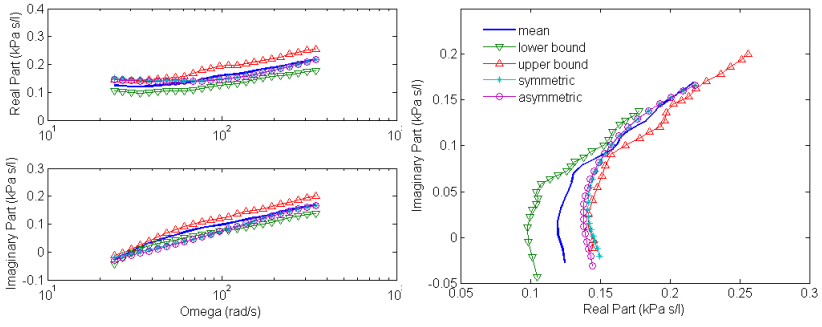

Figure 4.15: *The estimated impedance within the measured frequency range for the symmetric (*) and the asymmetric (o) case, against averaged data from healthy subjects (left) and equivalent polar plot representation (right).*

of the investigations can be classified in two groups, namely, for the symmetric and for the asymmetric tree.

For the symmetric tree representation, we have established the following:

- a recurrent relation can be obtained between the model parameters of each airway generation;
- the recurrence leads to a homothety factor, which is different for the conductive (levels 1..15) and diffusive (levels 16..24) zones;
- if symmetry exists, then the total input impedance can be calculated in a simplified, recurrent manner;
- the impedance exhibits a fractional order behavior leading to a fractional-order value for the symmetric case, if the convergence conditions are fulfilled; otherwise the constant-phase behaviour is missing;
- the ratios for inertance $1/\alpha$ and for the conductance o elements do not play a role in determining the value of the fractional order, the latter being determined solely by the ratios of the resistance λ and of the capacitance χ elements.

For the asymmetric tree representation, the following remarks can be summarized:

- the impedance exhibits a fractional order behaviour in the nominal case, without fulfilling the theoretical conditions for convergence; in this case it is difficult to calculate analytically the value of the fractional order;
- the fractional order behavior is still present, although the fractal structure and dimension is not uniquely characterised;
- the fractional order value is changing if the degree of asymmetry is changed (this observation is significant for the case of diseased lungs).

The novelty of the results presented in this chapter consists in that of showing that a fractional order behavior is present in the respiratory impedance, justifying the use of fractional order model parameters from the intrinsic geometry of the lungs. We have also discussed the existence of the fractional order behavior even in the asymmetric tree representation. A link has been established and validated between the recurrent ratios in the symmetric tree

and the value of the fractional order. For the asymmetric tree, this link has not been established, but it was shown that the fractional order value depends on the multi-fractal structure of the lungs, hence related to the changes in the homothety factor. In doing so, it is clear that changes in the respiratory tree with disease will lead to different fractional order values.

Since the results in this chapter are based on the geometrical structure coupled with elastic and viscoelastic properties, it is interesting to discuss our modelling approach in a mechanical analogue.

Chapter 5

Viscoelasticity of the Lung Parenchyma

This chapter provides an equivalent mechanical representation for the elastic and viscoelastic models developed previously (and presented via an electrical analogue) in chapter 4. Assuming a dichotomously branching tree, each airway tube is modeled by a combination of Maxwell and Kelvin-Voigt elements calculated from morphological values. This will allow comparison to models reported in literature and provide the link between the appearance of the FO behaviour and both intrinsic fractal geometry, as well as the rheological properties of the lung parenchyma.

The material presented in this chapter has been in part published in:

- *De Geeter N., Ionescu C., De Keyser R. (2009), A mechanical model of soft biological tissue - an application to lung parenchyma, in : IEEE Proc. of the Eng Med Biol Comp, Minneapolis, USA, 2863–2866.*

5.1 Basic elements

When a force F is applied on an object with initial length ℓ and cross-sectional area A, a mechanical stress σ results. Consequently, a deformation occurs $\Delta\ell$ which is defined as the strain ϵ:

$$\sigma = \frac{F}{A} \; ; \; \epsilon = \frac{\Delta\ell}{\ell} \tag{5.1}$$

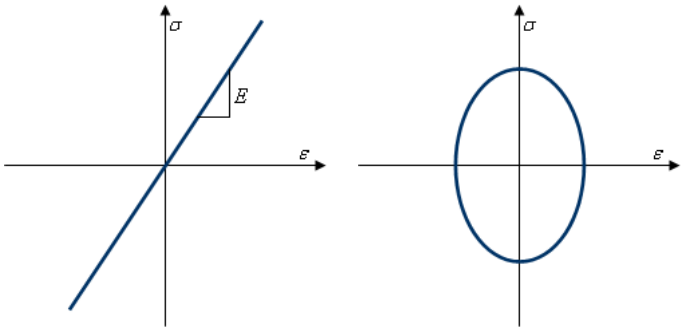

Figure 5.1: *The stress-strain curves for a spring (left) and for a damper (right).*

The following relations can be defined between the stress and the strain, in which E is the elasticity modulus and η the viscosity coefficient (Craiem & Armentano 2007):

For a spring:

$$\sigma(t) = E \cdot \epsilon(t) \tag{5.2}$$

denoting the Hooke's Law and the linear elastic behaviour of materials. Supposing a sinusoidal strain applied to the material: $\epsilon(t) = \epsilon_0 \cdot sin(\omega t)$, then the stress is in phase with the strain and its amplitude is given by $E \cdot \epsilon_0$. Observing the corresponding stress-strain curve from figure 5.1-left, the load and unload are following the same path; therefore no loss of energy occurs. Hence, we conclude that elastic materials do not show energy-dissipation phenomena.

For a damper:

$$\sigma(t) = \mu \cdot \frac{d}{dt}\epsilon(t) \tag{5.3}$$

denoting Newton's Law and describing the viscous behaviour of a linear flow. Applying a similar strain as above, the stress will lead the strain by 90^o with an amplitude equal to $\mu \cdot \omega \cdot \epsilon_0$. The amplitude is therefore frequency-dependent. When both signals are opposite in phase, as depicted in figure

5.1-right, we see that all the energy is used (equal hysteresis on both sides). Therefore, we conclude that viscous materials show energy-dissipation phenomena.

For a spring-pot of order n (with $0 \leq n \leq 1$) we have that:

$$\sigma(t) = \eta \cdot \frac{d^n}{dt^n}\epsilon(t) \tag{5.4}$$

and it denotes an element characterizing the combined effect of elastic and viscous behavior in a material. Notice that for $n = 0$ we have a pure elastic element (spring), whereas for $n = 1$ we have a pure viscous element (dashpot).

When the material undergoes a dynamical excitation, the stress will lead the strain in phase with an angle φ between 0 en $\pi/2$ radians. The amplitude of the stress is $E_d \cdot \epsilon$, from:

$$\sigma(t) = E_d(\omega) \cdot \epsilon \cdot \sin\left(\omega t + \varphi(\omega)\right) \tag{5.5}$$

The plot of the stress and strain below shows that part of the energy is stored and part is dissipated, resulting in a hysteresis.

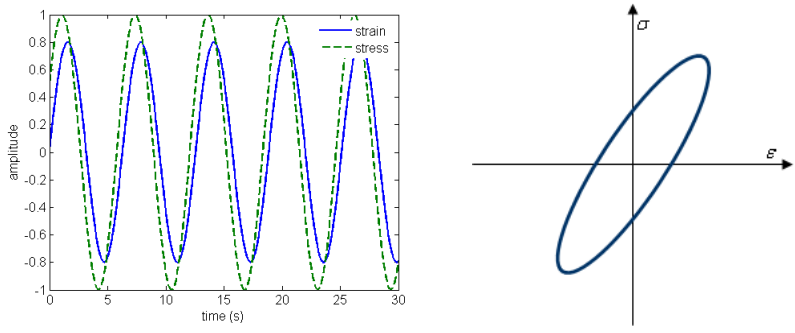

Figure 5.2: *The stress-strain curve of a viscoelastic material.*

The most simple combination of the basic elements presented above is a series spring-dashpot, referred to as the **Maxwell-element** and depicted in figure 5.3.

For a constant strain variation we have that:

$$\sigma(t) = E \cdot \epsilon \cdot e^{\left(-\frac{t}{\tau}\right)} \tag{5.6}$$

with $\tau = \frac{\eta}{E}$, the relaxation-time. At time $t = 0$ the spring will be fully taut, whereas the damper will remain unchanged. Within some time, the damper

will start to take over the stress from the spring and relax it. Hence, the Maxwell-element can characterize stress relaxation.

For a constant stress variation (step inputs) we have that:

$$\epsilon(t) = \sigma \left(\frac{1}{E} + \frac{t}{\eta} \right) \tag{5.7}$$

which shows a spontaneous elastic strain with the stress. When the stress variation stops, the spring returns to its initial position, while the damper remains in an irreversible state.

A second possible combination is the parallel spring-dashpot, referred to as the **Kelvin-Voigt** element (see figure 5.3). In this model, we cannot account for a constant strain, given the force on the damper must be infinitely big; hence, this model does not show stress-relaxation.

Assuming a constant stress input, we have that:

$$\epsilon(t) = \frac{\sigma}{E} \left(1 - e^{\left(-\frac{t}{\tau}\right)} \right) \tag{5.8}$$

with $\tau = \frac{\eta}{E}$, the relaxation-time. At the time instant $t = 0$, the damper begins to change slowly, while the spring reached asymptotically its taut-value. Hence, the Kelvin-Voigt element describes good the creep phenomena in viscoelastic materials.

Finally, both the Maxwell-element, as well as the Kelvin-Voigt element, do not fully characterize the true viscoelastic behaviour. Hence, combining both elements seems to be a good solution to overcome their individual limitation: N parallel Maxwell-elements, all in parallel with an extra spring, as shown in figure 5.3.

5.2 Viscoelasticity in the lungs

During quiet breathing, energy is used to overcome elastic and resistive forces. The classic equation of motion describes the relationship among pressure, volume and flow as:

$$P(t) = E_r \cdot V(t) + R_r \cdot Q(t) + P_0 \tag{5.9}$$

where at any instant t, P is the applied pressure, E_r is the elastance, V is the volume, R_r is the resistance, Q is the flow and P_0 is the pressure corresponding to transpulmonary pressure at end-expiration. The representative model

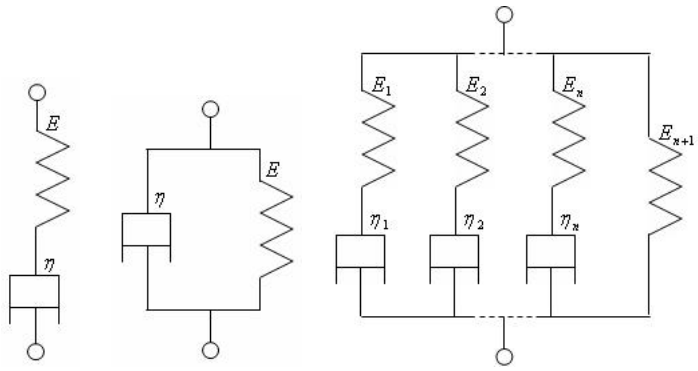

Figure 5.3: *From left to right: the Maxwell- and the Kelvin-Voigt-element, followed by a combination of the two.*

for this equation is the resistive-elastic model, characterized by a single resistive compartment connected to a single elastic compartment, and represented by a dashpot in parallel with a spring (Kelvin-Voigt element). To increase volume in this resistive-elastic model, part of the applied energy would be dissipated by the dashpot (resistance), whereas another fraction of the total energy would be stored in the spring (elastance), providing the driving pressure for expiration. This model does not account for the stress relaxation observed in the lung parenchyma, but it is widely used in practice.

Recoil pressures at same lung volumes are always less during deflation than inflation (hysteresis), hence the mechanical energy (work of breathing) follows the same property. The area within the pressure-volume loops represents the lost energy per breathing cycle. During quiet breathing, this area is nearly independent of frequency. Thus, under constant amplitude cycling, energy dissipation is nearly independent of frequency. However, the dissipation is proportional to the product of resistance and frequency, hence, implying that the resistance is inversely proportional to the frequency.

Close to the hysteresis observed during volume cycling of the lung, are the phenomena of stress adaptation and creep. In this line, soft biological tissues are known to be highly viscoelastic in nature. In contrast to perfect elastic materials, the viscoelastic materials do not maintain a constant stress under constant deformation; the stress slowly relaxes - stress relaxation. On the other hand, under constant deformation, the material undergoes a continuous deformation in time - creep. The linear viscoelastic model predicts dynamic elastance and its frequency dependence quite well, but it cannot account for

about one third of the energy loss (hysteresis), suggesting that additional plastoelastic elements are necessary in the model.

During cycling loading, the stress that develops in the viscoelastic body displays:

- a component in phase with strain, which is the elastic stress contributing to the storage modulus E_S (elastance); and
- a component out of phase with strain, corresponding to the viscous dissipation and contributing to the loss of modulus E_D (damping).

The viscoelastic properties of lung tissue cause the effective tissue resistance to be very high at very low frequencies, but then to decrease asymptotically towards zero, at higher frequencies. Consequently, the tissue resistance has the main contribution in the total lung resistance. At breathing frequencies in the range of 0.2 - 0.4 Hz, tissue resistance can account for $\approx 40\%$ of lung resistance.

The constant-phase model by Hantos *et al.* (Hantos *et al.* 1992*b*) from (1.1) describing the viscoelastic properties of lung tissues, has been considered superior to the classic spring and dashpot representation, since it contains a combined element. Although the electrical analogue of viscoelastic processes as well as the phenomenological and mechanical approaches yield good quantitative correspondence with data, they lack anatomic and mechanistic specificity.

Later models tried to deal with dynamic tissue behavior on a mechanistic basis. Some mechanisms have been proposed as contributors to the constant-phase tissue viscoelasticity, such as the structural disposition of fibers and their instantaneous configuration during motion, since elastic fibers dissipate energy as they slip with respect to each other. Additionally, lung tissue might exhibit molecular mechanisms similar to those proposed for polymer rheology. Maksym & Bates (Maksym & Bates 1997) suggested a role for the relative stress-bearing contributions of collagen and elastin fibers based on the differential elastic properties of these two types of fibers, in which collagen fibers were progressively recruited with strain. Bates (Bates 2007) also proposed that the nonlinear elastic properties and linear elastic behaviour of lung tissues arise from different physical processes, whereas elastic recoil is linked to geometry as fibers rearrange themselves; stress adaptation would reflect a process of diffusion due to the thermal motion of the fibers with respect to each other and to the ground substance.

However, viscoelasticity of lung parenchyma determines the mechanical properties of the overall lung function. Since the system acts as a whole, it is important to characterize the mechanical properties as they propagate within consequent levels. Several research groups investigated the viscoelasticity of the lung parenchyma in animal and human studies (ex-vivo) (Maksym & Bates 1997, Suki *et al.* 1994), but their investigations neglect the interconnection to the rest of the respiratory system.

5.3 Equivalent mechanical model

In this chapter we treat the *symmetric* structure of the respiratory tree (Mandelbrot 1983, Sauret *et al.* 1999, Weibel 1963, 2005), with morphological values given as in table 3.1. For the purpose of this study, we investigate the airways within the respiratory zone, corresponding to levels 16-24, as schematically depicted in figure 5.4 (Hou *et al.* 2005, Weibel 2005). In this figure, A_m denotes the cross sectional area, ℓ_m denotes the length, R_{em} the resistance and C_{em} the capacitance of one airway tube from level m, respectively.

In the respiratory zone, the oxygen and carbon dioxide exchange takes place between the air in the lung and the blood in the small-diameter blood vessels that surround the alveoli. The gas compression impedance is modelled by a series $R_{CG} - L_{CG} - C_{CG}$ impedance, as described in chapter 4.

For the case of elastic tube walls, we have no viscous losses, thus no conductance G_e element, as defined in section 3.4.1. Using (3.62)-(3.64), the equations for the electrical model are given by:

$$\begin{aligned} e_0 &= R_{e1} i_1 + e_1;\ \ e_1 = \tfrac{R_{e2}}{2} i_2 + e_2 \\ i_1 &= i_2 + C_{e1} \dot{e}_1;\ \ i_2 = 2 C_{e2} \dot{e}_2 \end{aligned} \tag{5.10}$$

with e the voltage and i the current represented as in figure 5.5. The electromechanical analogy is given in table 5.1.

Using the electromechanical analogy from table 5.1, we can derive an equivalent mechanical model. This can be done starting from the electrical model equations (5.10). The electrical element ($R_e C_e$ series) corresponds to the mechanical Kelvin-Voigt element (spring in parallel with dashpot):

$$\begin{aligned} F_0 &= B_1 v_1 + F_1;\ F_1 = \tfrac{B_2}{2} v_2 + F_2 \\ v_1 &= v_2 + \tfrac{1}{K_1} \dot{F}_1;\ v_2 = \tfrac{2}{K_2} \dot{F}_2 \end{aligned} \tag{5.11}$$

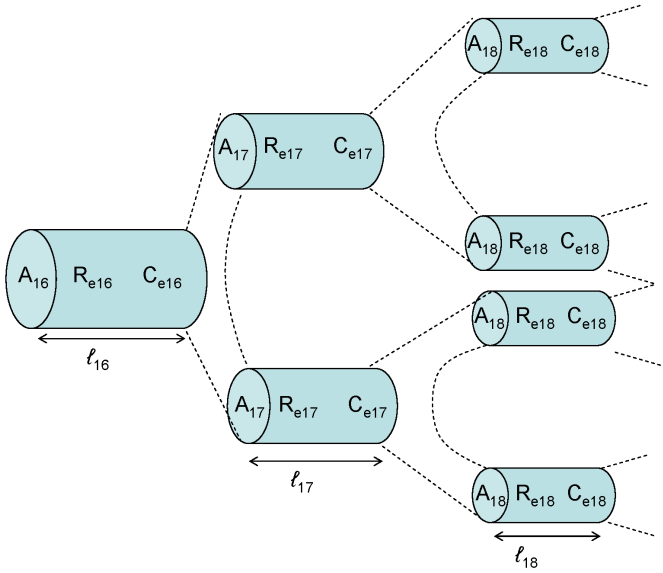

Figure 5.4: *A schematic representation of the electrical model for the lung parenchymal tissue as an interconnected system (starting from level 16).*

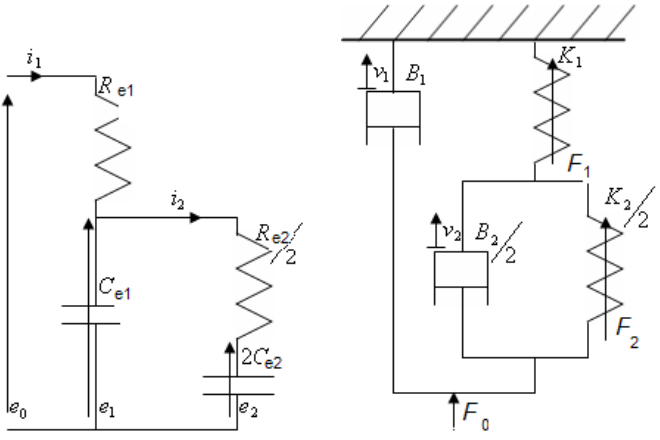

Figure 5.5: *An illustrating example of the first two levels in the electrical and the mechanical networks.*

Table 5.1: *The electromechanical analogy.*

Electrical	**Mechanical**
Voltage e $[V]$	Force F $[N]$
Current i $[A]$	Velocity v $[m/s]$
Resistance R_e $[\Omega]$	Damping constant B $[Ns/m]$
Capacitance C_e $[F]$	Spring constant $1/K$ $[m/N]$
Inductance L_e $[H]$	Mass M $[kg]$

The values of resistors and capacitors are calculated with the model from figure 5.5 and relations (3.62)-(3.64): $R_{e16} = 1.57$ kPa/(l/s) and $C_{e16} = 3.06 \cdot 10^{-6}$ l/kPa. From these values one can calculate the equivalent B_m^* and K_m^* values, taking into account that $R_{em} = R_{em}^*/2^{m-1}$ and $C_{em} = 2^{m-1}C_{em}^*$ respectively, from (4.1) and (4.3). The superscript $*$ denotes a single branch in the respiratory level represented by the subscript m.

$$\begin{aligned} B_m^* &= \tfrac{F_m}{v_m} = \tfrac{P_m}{Q_m} A_m^2 = R_{em}^* A_m^2 \\ K_m^* &= \tfrac{F_m}{x_m} = \tfrac{P_m}{V_m} A_m^2 = \tfrac{A_m^2}{C_{em}^*} \end{aligned} \tag{5.12}$$

with P the pressure, Q the flow, V the volume, $A_m = \pi R_m^2$ the area, R_m the radius of a tube at level m and x the axial displacement.

Figure 5.6-left depicts the evolution of the parameters in a single tube at a certain level m, whereas figure 5.6-right depicts their evolution in the entire level. One may observe that the evolution in a single tube, in consecutive levels is quasi-linear for both parameters (figure 5.6-left). However, since the total parameter values from figure 5.6-right depend on the total number of tubes within each level, they change as an exponential decaying function. When represented on a logarithmic scale, one can observe a quasi-linear behavior, as in figure 5.6-right.

In a similar manner as the electrical impedance, one may obtain $H(s)$, which defines the relation from velocity (input) to force (output) $F(s)/v(s)$, with s the Laplace operator. The transfer function of a cell in the ladder network consisting of one damper and one spring, is:

$$H(s) = B + \frac{K}{s} \tag{5.13}$$

which can be evaluated over a range of frequencies, e.g. $\omega \in [10^{-5}, 10^5]$, with the result depicted in figure 5.7. In this figure '24' denotes that the $H(s)$ is calculated at level 24; '23' denotes that $H(s)$ is calculated at level 23, etc.

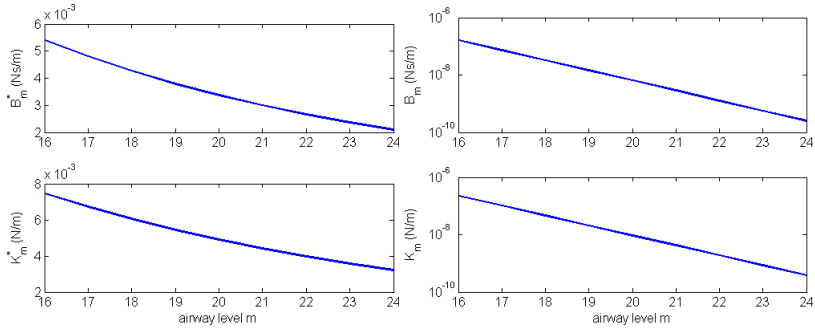

Figure 5.6: *Parameter evolution in singular tubes (left) and in the entire level (right), for levels 16–24.*

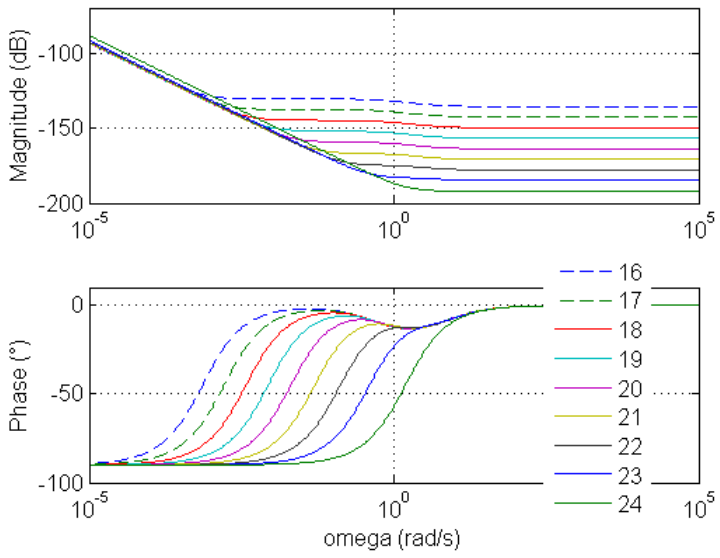

Figure 5.7: *The corresponding frequency response of the transfer function for the network of spring-dashpot elements in levels 16–24.*

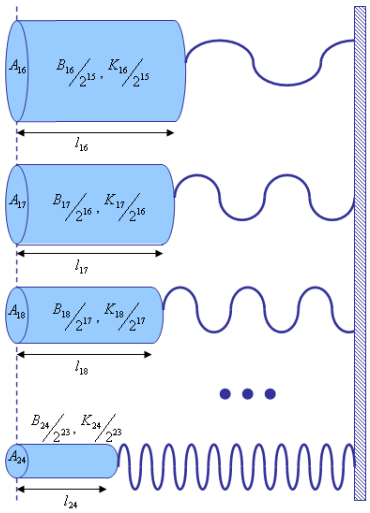

Figure 5.8: *A schematic representation of the mechanical model for the lung parenchymal tissue (levels 16–24).*

Due to the fact that the network is dichotomous and symmetric, we can obtain the total mechanical impedance using the network structure as in figure 5.5, with B_m and K_m calculated with (5.12). Since the Kelvin-Voigt elements corresponding to one level are in parallel, their transfer function H_m will be in series with the spring in the level $m-1$. The next corresponding transfer function is in parallel with the damper in the level $m-1$, as depicted schematically by figure 5.9. In this manner, the total transfer function $H(s)$ can be determined, starting at level 24 (De Geeter *et al.* 2009).

The lung parenchyma consists of interwoven collagen (infinitely stiff) and elastin (elastic) fibers. Each level in the respiratory tree has a specific balance between these two components. In our model we take this balance into account in (3.14), in function of the cartilage percent (table 3.1). Following this reasoning, a similar representation of the mechanical model is given in figure 5.8. Here, the cylinders represent the collagen fibers within one level, which are interconnected with elastin fibers, represented by inextensible unstressed strings. This representation varies from that of Bates in that it represents the total collagen-elastin distribution in a level and not in a single tissue strip (Bates 2007).

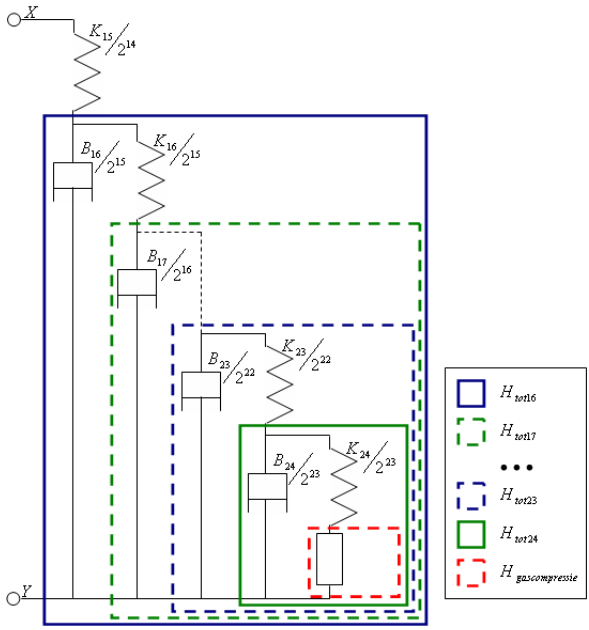

Figure 5.9: *A schematic representation of how the mechanical impedance $H(s)$ is calculated from level 24 by adding levels up to level 16 (De Geeter* et al. *2009).*

5.4 Stress-Strain curves

5.4.1 Stepwise variations of strain

The elastic modulus is defined as the ratio between stress and strain properties. The Kelvin-Voigt body is the simplest viscoelastic model that can store and dissipate energy, consisting of a perfectly elastic element (i.e. spring) arranged in parallel with a purely viscous element (i.e. dashpot). The corresponding equation is given by:

$$\sigma(t) = \frac{K\ell}{A}\epsilon(t) + \frac{B\ell}{A}\frac{d\epsilon(t)}{dt} \tag{5.14}$$

with σ the stress, ϵ the strain, ℓ the length, A the area and K, B the constants of the spring and dashpot, respectively (Craiem & Armentano 2007). The stress can be defined as pressure, whereas the latter is given by force distribution over the area. The strain ϵ is defined as the ratio of the change in length over the initial length: $\Delta\ell/\ell$. Starting with an unstressed tissue, we apply a strain that increases in steps of 10% until it reaches 100%. The new length can be calculated as:

$$\ell_{new} = (1 + \epsilon)\ell_{old} \tag{5.15}$$

with the subscript old denoting the characteristics before applying the strain step. Assuming a constant tissue volume V_t, the radius will decrease:

$$R_{new} = \frac{V_t}{2\pi\ell_{new}h} = \frac{R_{old} \cdot \ell_{old}}{\ell_{new}} \tag{5.16}$$

with R_{new} and R_{old} the new and old airway radius, respectively. We neglect the changes in the thickness h of the tube wall with changes in the strain. Applying a typical value for the oscillatory flow $Q = 0.5$ l/s at the oscillatory frequency of 5 Hz, the velocity v can be calculated as:

$$v_{new} = \frac{5 \cdot 10^{-4}}{A_{new}} \tag{5.17}$$

Since the B's and K's are time-invariant material properties, the transfer function $H(s)$ from (5.13) will be independent of the strain. The elongation $\Delta\ell$ of the airway tube will have an effect on the pipeline equation (3.13) which can be expressed as:

$$p + \frac{h}{R\left(1 - \nu_p^2\right)}\left(\frac{K\ell}{A}\epsilon + \frac{B\ell}{A}\frac{d\epsilon}{dt}\right) = 0 \tag{5.18}$$

with ν_p the Poisson coefficient. The new values for the pressure and the stress are given by:

$$P_{new} = \frac{F_{new}}{A_{new}} = \frac{v_{new} H}{\pi R_{new}^2} \tag{5.19}$$

$$\sigma_{new} = -P_{new} \frac{R_{new}\left(1-\nu_p^2\right)}{h} \tag{5.20}$$

Hence, in this representation, the stress and strain properties can be evaluated using (5.15)-(5.20), leading to the stress-strain curves depicted in figure 5.10. The strain is increased in steps of 10% from 10 to 100%. Starting from level 24, one can then calculate the stress-strain curve at the input of each level. This then will give rheological information in the context that all parenchymal levels are interconnected.

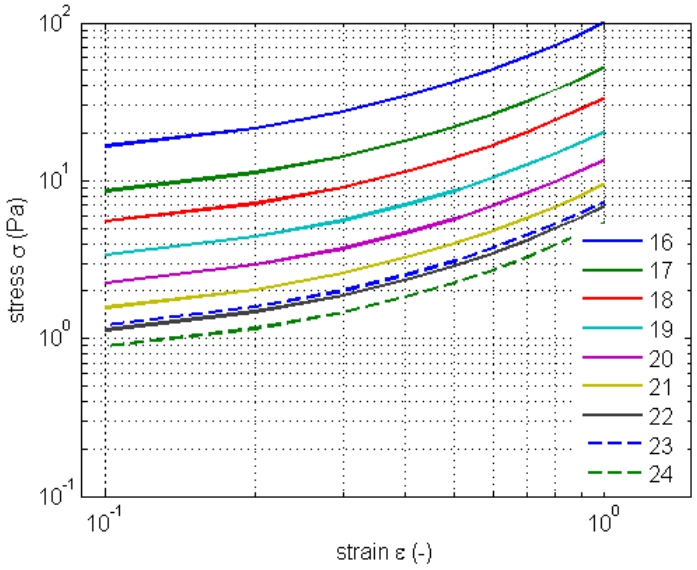

Figure 5.10: *The stress-strain curves for a ladder network model of the level 24, building up additional cells, until level 16.*

As expected, the stress increases with the degree of elongation applied to the entire structure. The more levels we have in our structure, the higher the values of the stress-strain curve, due to higher amount of cartilage tissue (collagen). The latter observation has been illustrated in figure 5.8. The obtained results are qualitatively similar to those reported in literature (Maksym & Bates 1997, Suki *et al.* 1994). Quantitatively, it is not possible to make an

evaluation of our model, since the values reported hitherto in the literature are based on excised tissue strips.

5.4.2 Sinusoidal variations of strain

In the previous section, a stepwise strain excitation was applied in steps of 10% until 100%. Similarly to the calculus presented previously, the new fractal-mechanical model can be excited by a dynamic strain excitation; i.e. a sinusoidal excitation, which is closer to the breathing phenomena. It is noteworth to realize that since our model consists of a combination of springs and dampers, the stress-strain curve will be a result of the two individual curves from figure 5.1. Moreover, since we only characterise the respiratory zone by the viscoelastic lung parenchyma, we also expect a stress-strain curve as in 5.2.

Applying a sinusoidal strain on the lung model with amplitude ϵ_0 and frequency $\omega = 2\pi f$ it follows that:

$$\epsilon(t) = \epsilon_0 \cdot \sin(\omega t) \tag{5.21}$$

which results in a sinusoidal stress response, as in (5.5).

Using $\sin(\alpha + \beta) = \cos(\alpha)\sin(\beta) + \sin(\alpha)\cos(\beta)$ yields:

$$\begin{aligned} \sigma(t) = \quad & E_d \cdot \epsilon_0 \cdot \sin(\omega t + \varphi_d) = \\ & \epsilon_0 \cdot [E_d \cos(\varphi_d)\sin(\omega t) + E_d \sin(\varphi_d)\cos(\omega t)] \end{aligned} \tag{5.22}$$

with E_d the dynamic modulus and φ_d the corresponding angle. Introducing the storage modulus $E_S = E_d \cos(\varphi_d)$ and the loss modulus $E_D = E_d \sin(\varphi_d)$, one may calculate the dissipated energy W in one cycle:

$$\begin{aligned} W = \quad & \int \sigma d\epsilon \\ = \quad & \int_0^T \epsilon_0 \cdot [E_d \cos(\varphi_d)\sin(\omega t) + E_d \sin(\varphi_d)\cos(\omega t)]\, \epsilon_0 \sin(\omega t) dt \\ = \quad & \pi \epsilon_0^2 E_d \sin(\varphi_d) \end{aligned} \tag{5.23}$$

with $T = 1/f$ the corresponding period and f the frequency in Hz. The used energy is therefore directly proportional to the loss modulus. The storage modulus is a measure for the necessary power to overcome elastic forces and to release them when the excitation ceases.

Viscoelastic properties can be analyzed by means of a frequency dependent complex elastic modulus E^* (Craiem & Armentano 2007):

$$E^*(j\omega) = \frac{\sigma(j\omega)}{\epsilon(j\omega)} = E_S(\omega) + jE_D(\omega) \tag{5.24}$$

whereas the parameters are related to the viscous behaviour of the material. In the Kelvin-Voigt model, the relation between stress and strain is given by:

$$\sigma(t) = E\epsilon(t) + \eta\frac{d\epsilon(t)}{dt} \tag{5.25}$$

Applying the Fourier transform leads to:

$$E^*(j\omega) = E + \eta(j\omega) \tag{5.26}$$

For a viscoelastic material the mechanical impedance $H(s)$ of this material is given by:

$$H(s) = \frac{K}{s} + B \tag{5.27}$$

which leads to the following relation for the complex modulus:

$$E^*(s) = \frac{\ell}{A} \cdot s \cdot H(s) \tag{5.28}$$

Applying the Laplace transform on the sinusoidal strain $\epsilon(t) = \epsilon_0 \cdot \sin(\omega t)$ we have that:

$$\epsilon(s) = \epsilon_0 \frac{\omega}{s^2 + \omega^2} \tag{5.29}$$

and the stress can be calculated as:

$$\begin{array}{ll} \sigma(s) & = E^*(s)\epsilon(s) \\ \sigma(t) & = L^{-1}\left\{\sigma(s)\right\} \end{array} \tag{5.30}$$

The results for a sinusoidal strain of $\omega = 2\pi 0.25$ (rad/s) and of $\omega = 2\pi 4$ (rad/s) are given in figure 5.11.

As expected, the energy is dissipated and the ellipse curve is deformed to a hysteresis curve (Hildebrandt 1970). There is also a slope on this hysteresis loop, which points to the fact that both energy storage and dissipation occurs during the test. As the frequency increases, the loop becomes closer to the ellipse form, suggesting that viscous behaviour becomes negligible.

The evolution with frequency of the complex modulus from (5.28) is depicted in figure 5.12 below. It is clear that the real part varies with frequency, hence if one would identify a lumped model in a limited frequency range, would need a fractional-order model (Ionescu & De Keyser 2003), as explained by means of (2.5). Notice that in our model representation, the ladder network leads to a similar effect of constant-phase behaviour as that of the electrical ladder network in the previous chapter. This effect is visible in figure 5.12-right, below $\omega < 10^{0.3}$ (rad/s) frequency range.

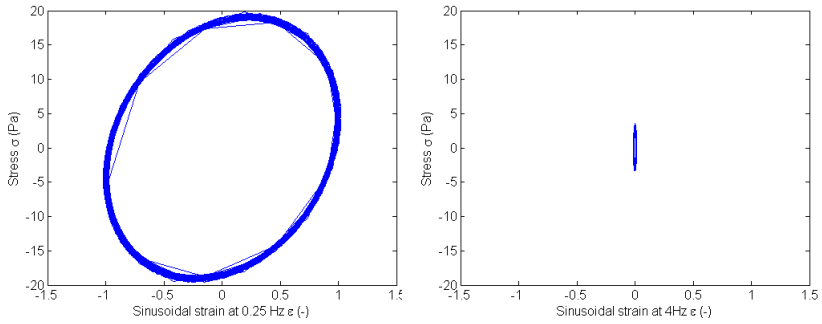

Figure 5.11: *The stress-strain curve for sinusoidal strain at* $\epsilon(t) = \epsilon_0 \cdot \sin(2\pi 0.25t)$ *and at* $\epsilon(t) = \epsilon_0 \cdot \sin(2\pi 4t)$.

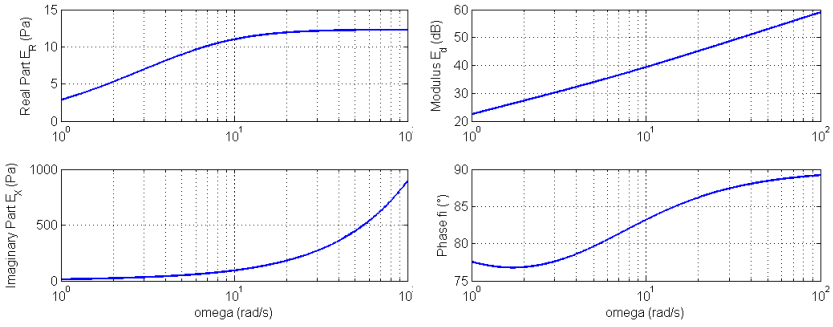

Figure 5.12: *The frequency response of the elastic modulus in its complex representation (left) and in its equivalent Bode plot (right).*

In a similar study, Craiem & Armentano acknowledge the necessity of a fractional order to characterize viscoelasticity in the arterial wall of the circulatory system in a sheep (Craiem & Armentano 2007).

Compared to the values in literature, one may say that our results are within reasonable values. For example, in (Yuan *et al.* 2000) the authors obtain values of 2-8 kPa for the storage modulus, respectively values of 0.2-1 kPa for the loss modulus in guinea pigs lung tissue strips. It is difficult to compare our results to those from (Yuan *et al.* 2000), because they come from animal studies and in general, most of the authors provide values from tissue strips instead of an interconnected system of lung parenchymal airways.

5.5 Conclusions

Biological tissue is essentially viscoelastic, and following a stress-strain analysis, a hysteresis loop is evident. In this chapter, a link between our ladder network model of the respiratory tree and viscoelastic properties in the lung parenchyma has been presented by building a mechanical analogue for the respiratory zone (levels 16-24).

Our findings show that the proposed model is able to reproduce well the results expected from theoretical background, both qualitatively, as well as quantitatively. Furthermore, we introduce a method to calculate the stress-strain relationship from intrinsic geometrical and material properties of the airways and assess stress-strain properties of the lung parenchyma with respect to the airways as an interconnected tree.

We also prove the necessity of using fractional order models when characterizing the storage modulus, which varies with frequency. In this chapter we show that the respiratory system requires a combination of spring and dashpot elements in its model structure, to characterize viscoelasticity from its intrinsic geometry and morphology.

Chapter 6

Clinical Applications

This chapter starts by presenting an analysis of the modelling performance of several candidate fractional-order models on the respiratory impedance. The models are presented on an evolutionary basis from the most simple to the most complex representation. The model delivering the least modelling errors and having the least number of parameters will be selected as the best candidate to model the input impedance in the 4-48 Hz frequency interval.

Once the best model is selected, we investigate the ability of the selected FO model, in classifying between healthy and pathologic patient data. The investigated groups are: healthy vs Chronic Obstructive Pulmonary Disease; healthy vs kyphoscoliosis; healthy vs asthma in children; healthy vs cystic fibrosis in children.

Extended parts of the material presented in this chapter has been published in:

- *Ionescu C., De Keyser R. (2009), "Relations between Fractional Order Model Parameters and Lung Pathology in Chronic Obstructive Pulmonary Disease", IEEE Transactions on Biomedical Engineering,* ***56(4)****, 978-987;*

- *Ionescu C., Derom E., De Keyser R. (2009), "Assessment of respiratory mechanical properties with constant-phase models in healthy and COPD lungs", Computer Methods and Programs in Biomedicine, DOI: 10.1016/j.cmpb.2009.06.006;*

- *Ionescu C., Desager K., De Keyser R. (2009), "Estimating respiratory mechanics with constant-phase models in healthy lungs from forced*

oscillations measurements", Studia Universitatis Vasile Goldis, Life Science Series, ***19(1)****, 123-132;*

- *Ionescu C., De Keyser R. (2008), "Model-free Adaptive Control in Frequency Domain: Application to Mechanical Ventilation", chapter in book: Frontiers in Adaptive Control, ed. S. Cong, www.intechweb.org/books.php (open access), In-Tech, 253-270,*
- *Ionescu C., De Keyser R. (2008), "Time domain validation of a fractional order model for human respiratory system", in Proc. of the 14th IEEE Mediterranean Electrochemical Conf (MELECON08), Ajaccio, Corsica, 89–95;*
- *Ionescu C., De Keyser R., Desager K., Derom E. (2009), "Fractional order models for the input impedance of the respiratory system", chapter in book: Recent Advances in Biomedical Engineering, www.intechweb.org/books.php (open access), In-Tech, 1–20;*
- *De Keyser R., Ionescu C., Lazar C., (2009) "Frequency-Response based CACSD for Fractional Order Systems", chapter in book: New Trends in Nanotechnology and Fractional Calculus Applications, Baleanu et al (Eds), Springer, 415–423.*

and is pending review in the following papers:

- *Ionescu C., Desager K., De Keyser R. "Fractional order model parameters for the input impedance in healthy and in asthmatic children", Computer Methods and Programs in Biomedicine.*

6.1 Introduction

This chapter is dedicated to selecting the best candidate model to characterize the impedance and further validation in clinical studies.

An analysis of the modelling performance of several candidate fractional-order models on the respiratory impedance is necessary, in order to decide which model is most suitable in the frequency range of interest. The models are presented on an evolutionary basis from the most simple to the most complex representation. The model delivering the least modelling errors and having the least number of parameters will be selected as the best candidate to model the input impedance in the 4-48 Hz frequency interval.

Once the best model is selected, the ability of the selected FO model in classifying between healthy and pathologic patient data needs to be assessed. The investigated clinical groups are: healthy vs Chronic Obstructive Pulmonary Disease; healthy vs kyphoscoliosis; healthy vs asthma in children; healthy vs cystic fibrosis in children. All these measurements have been performed by myself, with the same forced oscillation lung function testing device, available in our laboratory. The spirometric and plethysmographic tests have been done according to the standard procedures, to avoid biased protocols. For the tests in the hospitals, professional technical assistance was provided and supervised by myself.

6.2 Which Fractional-order Model?

It is interesting to compare the models existing in literature with some similar candidate models, in the 4-48 Hz frequency range. This frequency range is commonly evaluated in clinical trials using the forced oscillation lung function test (Oostveen *et al.* 2003). We therefore propose the following FO models, in order of complexity (Ionescu *et al.* 2009*c*, *a*).

6.2.1 Candidate Models

The first model, from here-on referred to as FO1, is:

$$Z_{FO1}(s) = R_r + \frac{1}{C_r s^{\beta_r}} \tag{6.1}$$

with R_r the resistance (kPa/(l/s)), C_r the capacitance (l/kPa) and $0 \leq \beta_r \leq 1$. This model was initially developed for frequencies below 5 Hz, whereas the

effect of the inductance is negligible (Hantos *et al.* 1992*b*). Therefore, when evaluating such model in the 4-48Hz frequency interval, one may expect inferior performance results.

The second model proposed here, referred to as FO2, is obtained from (6.1) by adding the inductance term (Hantos *et al.* 1992*a*):

$$Z_{FO2}(s) = R_r + L_r s + \frac{1}{C_r s^{\beta_r}} \tag{6.2}$$

As described in chapter 2, experimental results show that in several patients, the real part of the complex impedance may increase with frequency. Splitting (6.2) in its real and imaginary parts yields:

$$\begin{aligned} Z_r(j\omega) = R_r + \tfrac{1}{C_r\omega^{\beta_r}} \cos\left(\tfrac{\beta_r\pi}{2}\right) + \\ j \cdot [L_r\omega \sin\left(\tfrac{\pi}{2}\right) - \tfrac{1}{C_r\omega^{\beta_r}} \sin\left(\tfrac{\beta_r\pi}{2}\right)] \end{aligned} \tag{6.3}$$

Hence, it can be observed that when frequency increases, the real part of the term in C_r decreases, therefore unable to characterize correctly the impedance. However, if the model is evaluated in a frequency range in which the real part of the impedance is decreasing with frequency, the model performs well.

The third model (FO3) proposed for evaluation has an extra FO term in the inductance:

$$Z_{FO3}(s) = R_r + L_r s^{\alpha_r} + \frac{1}{C_r s^{\beta_r}} \tag{6.4}$$

which is in fact (2.4). This model will tackle the limitation from FO2 and will be able to capture both increasing, as well as decreasing variations with frequency in the real part of the impedance.

The last model proposed for evaluation in this chapter is based on the work of this thesis, i.e. the FO4 model:

$$Z_{FO4}(s) = L_r s^{\alpha_r} + \frac{1}{C_r s^{\beta_r}} \tag{6.5}$$

which does not contain the resistance term R_r. Indeed, the theory of fractional order appearance in ladder networks shows that the effects of R_r are indirectly captured in the values of the FO terms and FO coefficients (Oustaloup 1995, Ionescu *et al.* 2009*e*). Hence, if it turns out that the R_r term in FO3 will not give significant values, then FO4 will have less model parameters to be interpreted by the clinicians.

6.2.2 Subjects

The first group evaluated here consists of male volunteers without a history of respiratory disease, whose lung function tests were performed in our laboratory and Table 6.1 presents their biometric parameters, whereas a detailed analysis on their respiratory impedance parameters will be discussed later in this chapter.

A second group consists of former coal miners from the Petrosani area, kept under observation at the 'Leon Danielo' Hospital in Cluj-Napoca, Romania, and diagnosed with COPD (Chronic Obstructive Pulmonary Disease). Table 6.1 presents the corresponding biometric and spirometric parameters.

	Healthy (17)	COPD (17)
Age (yrs)	26 ± 3	51 ± 11
Height (m)	1.67 ± 0.04	1.74 ± 0.09
Weight (kg)	64 ± 3.7	76 ± 8
VC % pred	-	89 ± 7
FEV_1 % pred	-	44 ± 6

Table 6.1: *Biometric and spirometric parameters of the investigated subjects. Values are presented as mean $\pm$ standard deviations; % pred: predicted according to the asymptomatic males of the study; VC: vital capacity; FEV_1: forced expiratory volume in one second.*

The measurements of the input impedance values for these two groups of volunteers have been performed according to the forced oscillation lung function test described in section 2.1 and the model from (2.1). The modelling errors have been calculated according to (2.2).

6.2.3 Results

The complex impedance values for the healthy and COPD patients have been obtained using (2.1) and they are depicted in figure 6.1 below. It can be observed that the healthy group has a resonant frequency (zero crossing in the imaginary part) around 8 Hz, whereas the COPD group around 16 Hz. The real part denotes mainly the mechanical resistance of the lung tissue, which is generally increased in the COPD group, resulting in higher work of breathing. Also, the resistance at low frequencies is much increased in the COPD group, suggesting increased damping of the lung parenchyma (Hogg *et al.* 2004).

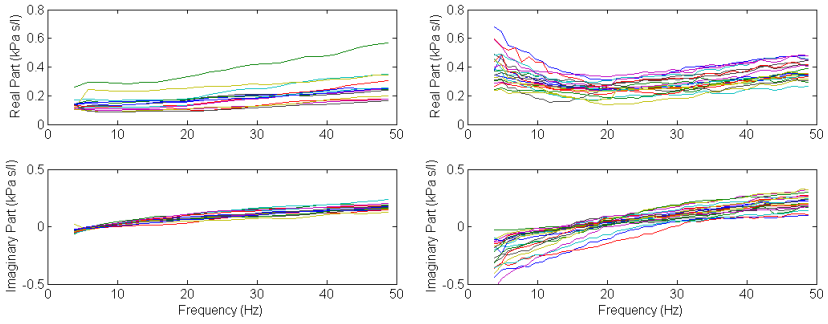

Figure 6.1: *Impedance plots for the healthy (left) and for the COPD (right) groups.*

Next, the models from (6.1)-(6.5) are fitted to these complex impedance values. Identification is performed using the System Identification Toolbox within the MatLab platform, i.e. the `lsqnonlin` optimization function (a nonlinear least squares algorithm). The estimated parameter values along with the modelling error values are given in table 6.2 for the healthy subjects, respectively in table 6.3 for the COPD patients.

Healthy	FO1	FO2	FO3	FO4
R_r	0.22 ± 0.09	0.22 ± 0.09	0.01 ± 0.01	-
L_r	-	$0.7 \cdot 10^{-3} \pm 0.1 \cdot 10^{-3}$	$19.3 \cdot 10^{-3} \pm 3.02 \cdot 10^{-3}$	$3.74 \cdot 10^{-3} \pm 3.11 \cdot 10^{-3}$
α_r	-	-	0.46 ± 0.07	0.43 ± 0.10
$1/C_r$	0	1.36 ± 0.98	0.99 ± 0.03	2.02 ± 1.47
β_r	0.99 ± 0.00	0.99 ± 0.01	0.72 ± 0.08	0.79 ± 0.16
E_R	0.05 ± 0.02	0.05 ± 0.02	0.02 ± 0.01	0.02 ± 0.01
E_X	0.12 ± 0.02	0.01 ± 0.00	0.01 ± 0.00	0.01 ± 0.00
E_T	0.13 ± 0.03	0.05 ± 0.02	0.02 ± 0.01	0.02 ± 0.01

Table 6.2: *Estimated model parameters and modelling errors for the healthy group in all candidate FO models.*

COPD	FO1	FO2	FO3	FO4
R_r	0.18 ± 0.08	0.26 ± 0.08	0.006 ± 0.01	-
L_r	-	$0.9 \cdot 10^{-3} \pm 0.1 \cdot 10^{-3}$	$7.7 \cdot 10^{-3} \pm 2.7 \cdot 10^{-3}$	$15.1 \cdot 10^{-3} \pm 8.1 \cdot 10^{-3}$
α_r	-	-	0.56 ± 0.06	0.59 ± 0.09
$1/C_r$	1.73 ± 3.32	5.20 ± 2.49	3.37 ± 1.73	2.94 ± 1.54
β_r	0.18 ± 0.36	0.83 ± 0.16	0.51 ± 0.08	0.52 ± 0.11
E_R	0.05 ± 0.01	0.04 ± 0.01	0.03 ± 0.01	0.03 ± 0.01
E_X	0.14 ± 0.02	0.02 ± 0.00	0.03 ± 0.01	0.02 ± 0.00
E_T	0.15 ± 0.02	0.05 ± 0.01	0.04 ± 0.02	0.04 ± 0.01

Table 6.3: *Estimated model parameters and modelling errors for the COPD group in all candidate FO models.*

From tables 6.2 and 6.3 one may observe that the models FO3 and FO4 give the smallest total error. This is due to the fact that two FO terms are present in their model structure, allowing both a decrease and increase in the real part of the impedance values. Although the FO2 model is the most commonly employed in clinical studies, it has to be used with care, since it provides higher modelling error in the real part of the impedance than the FO3 and FO4 models. The underlying reason is that the FO2 model can only capture a decrease in real part values of the impedance with frequency, whereas some patients may present an increase. In figure 2.9 was presented an example where one could visually compare the performance of the FO2 and FO4 models on a patient data. Another observation is that the resistance identified by FO3 was found to be very low in COPD patients, with values which were not statistically significant ($p < 0.26$) (Ionescu & De Keyser 2009*b*). Hence, it can be regarded as an indication that the FO3 model structure has an unnecessary parameter R_r, for the respiratory impedance in the 4-48 Hz frequency range.

This section presented a comparison of four candidate lumped models for the respiratory input impedance between 4-48 Hz frequency range. The results suggest that the two models broadly used in the clinical studies (i.e. FO1 and FO2) and reported in the specialized literature are suitable for frequencies lower than 15 Hz. However, in the transitional frequency range from compliance to inertance effects, two fractional orders are necessary in the model structure.

The multi-fractal model proposed here in (6.5) identifies significant values between the examined groups and has the best performance with the least number of model parameters. Hence, the remainder of this chapter will evaluate in detail the model performance in classifying between several groups of subjects.

6.3 Classification Indexes

Recalling here the identification procedure described in section 2.1 using (2.1), one obtains the complex impedance by means of its real and imaginary parts as a function of frequency. From the real and imaginary parts of the complex impedance, the model parameters of (6.5) were identified. The modeling errors were calculated with (2.2).

From the identified model parameters one can derive the tissue damping G_r and elastance H_r, defined as (Hantos *et al.* 1992*b*, *a*):

$$\begin{aligned} G_r &= \frac{1}{C_r \omega^{\beta_r}} \cos\left(\beta_r \frac{\pi}{2}\right) \\ H_r &= \frac{1}{C_r \omega^{\beta_r}} \sin\left(\beta_r \frac{\pi}{2}\right) \end{aligned} \tag{6.6}$$

both in (l/kPa). The hysteresivity coefficient η_r is defined as (Fredberg & Stamenovic 1989):

$$\eta_r = \frac{G_r}{H_r} \tag{6.7}$$

This parameter characterizes the heterogeneity of the lung tissue and has been shown to vary significantly with pathology. Since all these parameters from (6.6) and (6.7) are frequency-dependent, the identified values will represent an averaged value over the 4-48 Hz frequency range.

Apart from the identified model parameters, some additional parameters are introduced in this analysis. The real part of the complex impedance at 6 Hz ($R6$) can be used to characterize the total resistance at this frequency, a parameter often encountered in clinical studies. The resonant frequency ($Frez$) could also be used as a classifying parameter, since it has been shown that the balance between elastic and inertial properties change with pathology.

We introduce two dimensionless indexes, namely the quality factor at 6 Hz ($QF6$), denoted by the ratio of the reactive power to the real power:

$$QF6 = \frac{Im_6}{Re_6} = \tan \phi_z \tag{6.8}$$

where Re_6 and Im_6 denote the real and imaginary parts of the complex impedance evaluated at 6 Hz and ϕ_z denotes the phase angle at 6 Hz. From (6.8), one can calculate the corresponding power factor $PF6$:

$$PF6 = \sqrt{\frac{1}{QF6^2 + 1}} = \sqrt{\frac{Re_6^2}{(Re_6^2 + Im_6^2)^2}} = \frac{Re_6}{Re_6^2 + Im_6^2} = \cos \phi_z \tag{6.9}$$

In engineering, the quality factor QF compares the time constant for decay of an oscillating physical system's amplitude with respect to its oscillation period. In other words, it compares the frequency at which a system oscillates to the rate at which it dissipates its energy, also known as the damping factor. For a second order linear time invariant system, a system is said to be over-damped if $QF < 0.5$, under-damped for $QF > 0.5$ and critically damped for $QF = 0.5$. In other words, a low QF denotes a high energy loss, while a high QF denotes a low energy loss. For the power factor PF, we have that

for $PF = 0$ the energy flow is entirely reactive (hence the stored energy in the load returns to the source with each cycle), and if $PF = 1$, all the energy supplied by the source is consumed by the load.

Independent Student's t tests with unequal sample size were used to compute the confidence intervals. The classification results were considered significant if $p \leq 0.05$ (i.e. within 95% confidence interval).

The model parameters were compared between groups using `boxplots`. The lower and upper lines of the boxplot are the 25th and 75th percentiles of the sample group. The distance between the top and bottom of the box is the interquartile range. The line in the middle of the box is the sample group median value. If the median is not centered in the box, it is an indication of skewness. The whiskers are lines extending below and above the box. They show the extent of the rest of the sample group (unless there are outliers). Assuming no outliers, the maximum of the sample is the top of the upper whisker, respectively the minimum is the bottom of the lower whisker. An outlier is a value more than 1.5 times the interquartile range away from the top or bottom of the box, and they are denoted by plus signs. A side by side comparison of two or more boxplots provides a graphical way to determine which groups have significantly different medians (typical measure in classification studies).

6.4 Envisaged Subjects and Patients

In the remainder of this chapter, the term *subjects* will refer to healthy volunteers, whereas the term *patients* will refer to diagnosed volunteers. The forced oscillations lung function test (FOT) was employed to perform measurements of the input respiratory impedance, as described in section 2.1. The measurement was performed in the $f \in [4, 48]$ (Hz) frequency interval, respectively $\omega \in [25, 300]$ (rad/s).

Drop-out criteria were: i) technically biased measurements (swallowing, coughing, glottis closure); ii) fatigue and therefore reduced ability to breath spontaneously; and iii) irregular breathing period. All subjects and patients were in stable physical conditions at the time of the evaluation.

Written and/or oral consent was obtained from all participants, and in case of children, from both children and their parents. Further selection of the participants was performed by oral/written questionnaire ruling out any other respiratory disease than the one envisaged for the study at the time of mea-

surement or in the past 4 weeks. The remainder of this section presents the data for the participants to whom these inclusion criteria applied.

6.4.1 Healthy Subjects - Adults

The group evaluated in this study consists of 80 Caucasian volunteers (students) without a history of respiratory disease, whose lung function tests were performed in our laboratory, and table 6.4 presents their biometric parameters. The measurements were performed over the 2005-2009 time interval.

	Healthy (80)
female/male	31/49
Age (yrs)	27 ± 5
Height (m)	1.73 ± 0.17
Weight (kg)	69 ± 9.6

Table 6.4: *Biometric parameters of the healthy subjects. Values are presented as mean $\pm$ standard deviation.*

According to Pasker *et al.*, the real (Re) and imaginary (Im) parts of the impedance can be predicted from their biometric data as given below (Pasker *et al.* 1997):

$$
\begin{aligned}
&\textbf{Female}\\
&Re_0 = -0.4300 \cdot \underline{h} + 0.00165 \cdot \underline{w} - 0.00070 \cdot \underline{a} + 0.9312\\
&(RSD = 0.0619)\\
&Re_1 = 0.01176 \cdot \underline{h} - 0.000106 \cdot \underline{w} - 0.000045 \cdot \underline{a} - 0.00817\\
&(RSD = 0.00256)\\
&Im_0 = 0.2487 \cdot \underline{h} - 0.001700 \cdot \underline{w} - 0.00053 \cdot \underline{a} - 0.2158\\
&(RSD = 0.0406)\\
&\textbf{Male}\\
&Re_0 = -0.2454 \cdot \underline{h} + 0.001564 \cdot \underline{w} - 0.00055 \cdot \underline{a} + 0.5919\\
&(RSD = 0.0493)\\
&Re_1 = 0.01176 \cdot \underline{h} - 0.000106 \cdot \underline{w} - 0.000045 \cdot \underline{a} - 0.00817\\
&(RSD = 0.00197)\\
&Im_0 = 0.2487 \cdot \underline{h} - 0.001700 \cdot \underline{w} - 0.00053 \cdot \underline{a} - 0.2158\\
&(RSD = 0.0306)
\end{aligned}
\tag{6.10}
$$

where $\underline{h}$ denotes height in (m), $\underline{w}$ denotes weight in (kg), $\underline{a}$ denotes age in (yrs) and RSD is the residual standard deviation. The real and imaginary

parts of the impedance are fitted by the polynomial:

$$R_{rs} = \underline{D} f + \underline{E} \tag{6.11}$$

where f is the frequency. The coefficients calculated with (6.10) from their biometric parameters are then validated with the $\underline{E}$ and $\underline{D}$ coefficients resulting from the curve fitting. For the real part of the impedance, the coefficient $\underline{E}$ is validated with the coefficient Re_0, respectively the coefficient $\underline{D}$ is validated with the coefficient Re_1. For the imaginary part of the impedance, the coefficient $\underline{E}$ is validated with the coefficient Im_0. Since the volunteers were presumed healthy (but not guaranteed), the predicted values for terms in (6.11) were verified with the reference values from (Quanjer 1998). Only in 56 (from the initial 80) subjects, the identified values from (6.11) remained close to the predicted values of Re_0, Re_1 and Im_0, within the 95% confidence interval.

6.4.2 Patients with COPD

COPD (Chronic Obstructive Pulmonary Disease) denotes any disorder that persistently obstructs the bronchial airflow (Barnes 2000, Hogg *et al.* 2004). However, it mainly involves two related diseases – chronic bronchitis and emphysema. Both cause chronic obstruction of air flowing through the airways and in and out of the lungs. The obstruction is irreversible and progresses (becomes worse) over the time. Most cases of COPD develop after long-term exposure to lung irritants that damage the lungs and the airways (e.g. miners, smoke). Secondhand smoke (i.e. smoke in the air from other people smoking) can also irritate the lungs and contribute to COPD. Breathing in air pollution and chemical fumes or dust from the environment or workplace also can contribute to COPD.

The COPD group under study consisted of 47 Caucasian patients, diagnosed and under observation at the "Leon Danielo" Hospital in Cluj-Napoca, Romania. The patients were former coal miners from the Petrosani area in Romania. Their biometric and spirometric parameters are given in table 6.5. The measurements were performed in January 2006, Cluj Napoca, Romania.

6.4.3 Patients with Kyphoscoliosis

Kyphoscoliosis is a disease of the spine and its articulations, mostly beginning in childhood (McCool & Rochester 2008). The deformation of the spine characteristically consists of a lateral displacement or curvature (scoliosis) or

	COPD (47)
female/male	0/47
Age (yrs)	64 ± 13
Height (m)	1.74 ± 0.12
Weight (kg)	79 ± 12
VC % pred	84 ± 12
FEV_1 % pred	38 ± 8

Table 6.5: *Biometric and spirometric parameters of the COPD patients. Values are presented as mean $\pm$ standard deviation; % pred: predicted according to the asymptomatic males of the present study; VC: vital capacity; FEV_1: forced expiratory volume in one second.*

an antero-posterior angulation (kyphosis) or both (kyphoscoliosis). The angle of the spinal curvature called *the angle of Cobb* determines the degree of the deformity and consequently the severity of the restriction. Severe kyphoscoliosis may lead to respiratory failure, which often needs to be treated with non-invasive nocturnal ventilation.

This study was approved by the local Ethics Committee of the University Hospital Gent (UZGent) and informed consent was obtained from all volunteers before inclusion in the study. The study involved 9 adults diagnosed with kyphoscoliosis and their corresponding biometric and spirometric values are given in table 6.6. The measurements were performed during the June 2009 - August 2009 time interval.

6.4.4 Healthy Subjects - Children

This study was approved by the local Ethics Committee of the University Hospital in Antwerp (UZA) and informed consent was obtained from all volunteers before inclusion in the study. The study involved 16 healthy chidren and their corresponding biometric values are given in table 6.7. The measurements were performed in May 2009, at the St. Vincentius Basis School in Zwijnaarde, Belgium.

The healthy children had no history of pulmonary disease, and were selected using a specific questionnaire. The questionnaire verified the absence of dyspnoea, chronic cough, wheeze in the chest, etc.

	Kyphoscoliosis (9)
female/male	3/6
Age (yrs)	62.25 ± 10.12
Height (m)	1.55 ± 0.08
Weight (kg)	63.25 ± 15.62
VC % pred	33.25 ± 14.15
FEV_1 % pred	31.62 ± 11.30
FVC % pred	34.62 ± 12.12
Cobb angle (^{o})	75 ± 19.63
R_{aw} (kPa/l/s)	0.51 ± 0.12
C_{cw} pred* (l/kPa)	0.98 ± 0.29
VC % pred*	65.06 ± 10.48

Table 6.6: *Biometric and spirometric parameters of the adults diagnosed with kyphoscoliosis. Values are presented as mean±standard deviation values; % pred: predicted values; VC: vital capacity; FEV1: forced expiratory volume in one second; FVC: forced vital capacity; Cobb angle: the angle of spinal deformity (one patient was excluded for it has outlier value for Cobb angle, i.e.* 178^o*; C_{cw}: chest wall compliance; $pred*$: denotes values predicted from the Cobb angle, according to (McCool & Rochester 2008); R_{aw}: airway resistance from bodybox lung function test. All patients were on nocturnal ventilation.*

	Healthy (16)
female/male	13/3
Age (yrs)	9.66 ± 0.47
Height (m)	1.39 ± 0.07
Weight (kg)	32.3 ± 6.34

Table 6.7: *Biometric parameters of the healthy children. Values are presented as mean ± standard deviation values.*

In order to validate the measurements in healthy children, the real part of the complex impedance evaluated at 6 Hz (R6) was predicted from:

$$R6 = 0.0017 \cdot \underline{h}^2 - 0.5407 \cdot \underline{h} + 47.7323 \tag{6.12}$$

with $\underline{h}$ the height in (cm) (Duiverman *et al.* 1985). All subjects were within the 95% confidence interval values.

6.4.5 Children with Asthma

Asthma denotes a pulmonary disease in which there is obstruction to the flow of air out of the lungs, but the obstruction is usually reversible and between attacks of asthma the flow of air through the airways is usually good (Busse & Lemanske 2001, Vignola *et al.* 2004, Cavalcanti *et al.* 2006). Asthma is caused by chronic (ongoing, long-term) inflammation of the airways, making them highly sensitive to various triggers. Such triggers are usually: indoor and outdoor allergens, indoor and outdoor dust, exercise. In an asthma attack, the muscles in the airways contract (bronchospasm), causing narrowing of the airway walls. With proper treatment, people with asthma can have fewer and less severe attacks; while without treatment, they will have more frequent and more severe asthma attacks and can even die. Asthma can be controlled using specific medication (inhaled steroids).

This study was approved by the local Ethics Committee of the University Hospital Antwerp (UZA) and informed consent was obtained from all volunteers before inclusion in the study. The study involved 19 asthmatic children and their corresponding biometric and spirometric values are given in table 6.8. The measurements were performed during the December 2008 - March 2009 time interval.

The protocol in this clinical trial was as follows: initial measurements of FOT and spirometry were performed, followed by a bronchodilatator test. Typically, the spontaneous improvement of the symptoms mentioned above, after the bronchodilatator use, is also an indicative of asthma ($> 12\%$ improvement of forced expiratory volume for the 1 second (FEV1) predicted baseline after inhalation). For the bronchodilatation test, Ventolin 100 (4 x Salbutamol 100 mg) was administered. The patient has to breath in and breath out in a nebulizer 4 times the administered medication. A time interval of 12 minutes was allowed to pass after the inhalation, such that the airways have time to respond to the bronchodilatator. Repeated measurements of FOT and spirometry evaluated the patients after the bronchodilatation test.

	Asthma (19)	Healthy (16)
female/male	3/16	13/3
Age (yrs)	11.05 ± 4.7	9.66 ± 0.47
Height (m)	1.40 ± 0.17	1.39 ± 0.07
Weight (kg)	36.25 ± 15.58	32.3 ± 6.34
FEF/VC % pred	85.31 ± 31.15	NA
FEV_1/VC % pred	97.75 ± 12.83	NA
$MEF75/25$ (l)	2.12 ± 0.95	NA

Table 6.8: *Biometric and spirometric parameters of the asthmatic children and the healthy children used for comparison. Values are presented as mean $\pm$ standard deviation values; % pred: predicted values; VC: vital capacity; FEV1: forced expiratory volume in one second; FEF: forced expiratory flow; MEF75/25: mean expiratory flow at 75%, respectively at 25% capacity; NA: data not available.*

As additional information, allergy was determined based on specific positive reaction to inhaled allergen (house dust mite, birch tree, grass pollen, weed, dog/cat dander), and further details are given in table 6.9.

Medication	ICS: 12	LABA: 15	LRA: 8
Level of asthma control	PC: 6	C: 8	none: 5
Time of diagnose (years)	$<$1: 9	$<$2: 3	$<$5: 7
Allergic asthma	Yes: 17	No: 2	-

Table 6.9: *Number of the asthmatic children related to various asthma parameters: ICS: inhaled corticosteroid; LABA: long acting beta agonist; LRA: leukotriene receptor antagonist; PC: partially controlled; C: controlled.*

6.4.6 Children with Cystic Fibrosis

One of the most common severe genetic diseases, cystic fibrosis (CF) is characterized by the production of abnormal secretions, leading to mucous build-up, and persistent infections and inflammation in a variety of organs (Brennan *et al.* 2005, Rogers & Doull 2005). Inflammation and infection also cause injury and structural changes to the lungs, leading to a variety of symptoms and eventually to respiratory failure. Without treatment, CF results in death for 95% of affected children before the age of 5, hence early diagnosis is critical.

This study was approved by the local Ethics Committee of the University Hospital Antwerp (UZA) and informed consent was obtained from all volunteers before inclusion in the study. The study involved 10 children diagnosed with cystic fibrosis and their corresponding biometric and spirometric values are given in table 6.10. The measurements were performed during the December 2008 - March 2009 time interval.

	Cystic Fibrosis (10)	Healthy (16)
female/male	4/6	13/3
Age (yrs)	14.44 ± 6.21	9.66 ± 0.47
Height (m)	1.49 ± 0.15	1.39 ± 0.07
Weight (kg)	39.89 ± 11.67	32.3 ± 6.34
FEF/VC % pred	86.51 ± 36.12	NA
FEV_1/VC % pred	95.71 ± 9.42	NA
$MEF75/25$ (l)	2.08 ± 1.13	NA

Table 6.10: *Biometric and spirometric parameters of the children diagnosed with cystic fibrosis and the healthy children used for comparison. Values are presented as mean±standard deviation values; % pred: predicted values; VC: vital capacity; FEV1: forced expiratory volume in one second; FEF: forced expiratory flow; MEF75/25: mean expiratory flow at 75%, respectively at 25% capacity; NA: data not available*

The patients were clinically diagnosed and hospitalized at the time of measurement. Diagnosis was based on a sweat test and detection of a minimum 1 gene mutation responsible for cystic fibrosis.

6.5 Results

In the remainder of this chapter, the complex impedance will be depicted against frequency f in Hz, whereas its equivalent Bode plot representation will be depicted against angular frequency ω in rad/s.

6.5.1 Healthy vs COPD

The complex impedance values for the healthy and COPD patients obtained with (2.1) are similar to those presented in section 6.1; the equivalent Bode plots are given in figure 6.2. The real part denotes mainly the mechanical resistance of the lung tissue, which is generally increased in the COPD group,

resulting in a higher work of breathing. Also, the resistance at low frequencies is much increased in the COPD group, suggesting increased damping of the lung parenchyma (viscoelasticity is mainly analyzed at low frequencies).

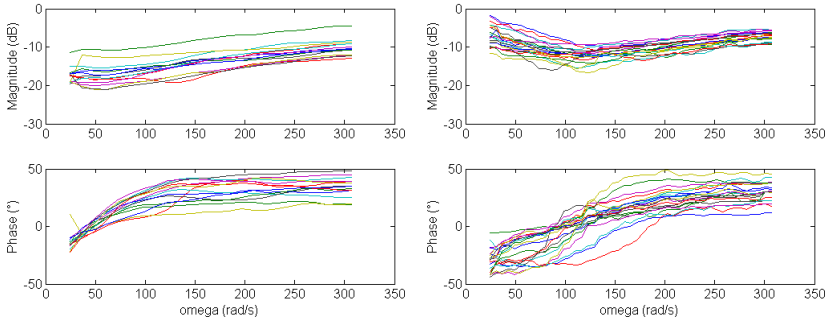

Figure 6.2: *Bode plots for the healthy (left) and for the COPD (right) groups.*

The estimated and derived model parameter values along with the real, imaginary and total error values are given in table 6.11 for the healthy subjects and for the COPD patients.

	Healthy	COPD
L_r	0.032 ± 0.029 (0.019,0.045)	0.016 ± 0.007 (0.013,0.019)
$1/C_r$	1.59 ± 1.10 (1.09,2.08)	2.81 ± 1.45 (2.15,3.47)
α_r	0.42 ± 0.08 (0.38,0.47)	0.56 ± 0.07 (0.53,0.60)
β_r	0.75 ± 0.11 (0.70,0.80)	0.52 ± 0.10 (0.47,0.56)
G_r	0.44 ± 0.15 (0.37,0.50)	1.77 ± 0.73 (1.43,2.10)
H_r	1.49 ± 1.14 (0.98,2.00)	2.15 ± 1.30 (1.55,2.74)
η_r	0.41 ± 0.21 (0.32,0.51)	0.99 ± 0.41 (0.80,1.18)
$R6$	0.13 ± 0.05 (0.11,0.16)	0.33 ± 0.07 (0.29,0.36)
$Frez$	10.48 ± 3.56 (8.75,13.87)	20.58 ± 8.98 (11.89,30.27)
$QF6$	0.09 ± 0.09 (0.02,0.17)	0.55 ± 0.24 (0.44,0.66)
$PF6$	0.99 ± 0.01 (0.98,0.99)	0.86 ± 0.08 (0.82,0.90)
E_R	0.02 ± 0.01	0.03 ± 0.01
E_X	0.013 ± 0.006	0.02 ± 0.006
E_T	0.02 ± 0.01	0.04 ± 0.01

Table 6.11: *Estimated and derived model parameters and modelling errors for the healthy and COPD groups. Values are given as mean $\pm$ standard deviation; values in brackets indicate the corresponding 95% confidence intervals.*

Tissue destruction (emphysema, COPD) and changes in air-space size and tissue elasticity are matched with changes in model parameters when com-

pared to the healthy group. The physiological effects of chronic emphysema are extremely varied, depending on the severity of the disease and on the relative degree of bronchiolar obstruction versus lung parenchymal destruction (Barnes 2000). Firstly, the bronchiolar obstruction greatly increases airway resistance and results in increased work of breathing. It is especially difficult for the person to move air through the bronchioles during expiration because the compressive force on the outside of the lung not only compresses the alveoli but also compresses the bronchioles, which further increase their resistance to expiration. This might explain the decreased values for inertance (air mass acceleration), captured by the values of L_r.

Secondly, the marked loss of lung parenchyma greatly decreases the elastin cross-links, resulting in loss of attachments (Hogg *et al.* 2004). The latter can be directly related to the fractional-order of compliance, which generally expresses the capability of a medium to propagate mechanical properties (Suki *et al.* 1994). The damping factor is a material parameter reflecting the capacity for energy absorption. In materials similar to polymers, as lung tissue properties are very much alike polymers, damping is mostly caused by viscoelasticity, i.e. the strain response lagging behind the applied stresses (Suki *et al.* 1994, 1992). In the FO model, the exponent β_r governs the degree of the frequency dependence of tissue resistance and tissue elastance. The increased lung elastance $1/C_r$ (elasticity) in COPD results in higher values of tissue damping and tissue elastance, as observed in figure 6.3. The loss of lung parenchyma (empty spaced lung), consisting of collagen and elastin, both of which are responsible for characterizing lung elasticity, is the leading cause of increased elastance in COPD. Given the results observed in Figure 6.4, it is possible to distinguish between tissue changes from healthy to COPD case from the variatons in the hysteresivity index η_r ($p << 0.01$). Since pathology of COPD involves significant variations between inspiratory and expiratory air-flow, an increase in the hysteresivity coefficient η_r reflects increased inhomogeneities and structural changes in the lungs.

Figures 6.3-6.4 depict the boxplots for the tissue damping G_r ($p << 0.01$), tissue elastance H_r ($p << 0.01$), tissue hysteresivity η_r ($p << 0.01$) and resistance at 6Hz $R6$ ($p << 0.01$) calculated with the parameters from Table 6.11. In emphysematous lung, the caliber of small airways changes less than in the normal lung (defining compliant properties) and peripheral airway resistance may increase with increasing lung volume. At this point, the notion of space competition has been introduced (Hogg *et al.* 2004), hypothesizing that enlarged emphysematous air spaces would compress the adjacent small airways, according to a nonlinear behavior. Therefore, the compression

would be significantly higher at higher volumes rather than at low volumes, resulting in blunting or even reversing the airway caliber changes during lung inflation. This mechanism would therefore explain the significantly marked changes in model parameters in tissue hysteresivity depicted in figure 6.4.

Many alveolar walls are lost by emphysematous lung destruction, the lungs become so loose and floppy that a small change in pressure is enough to maintain a large volume, thus the lungs in COPD are highly compliant (elastic) (Barnes 2000, Hogg *et al.* 2004, Ionescu *et al.* 2009*b*). This is observed in the high values identified for $1/C_r$.

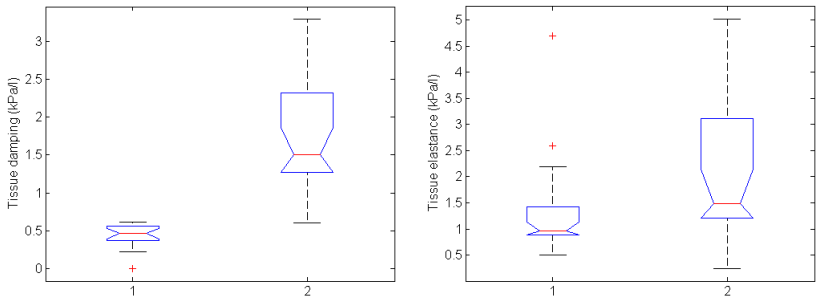

Figure 6.3: *Tissue damping G_r (left) and tissue elastance H_r (right) in 1: Healthy subjects and 2: COPD patients.*

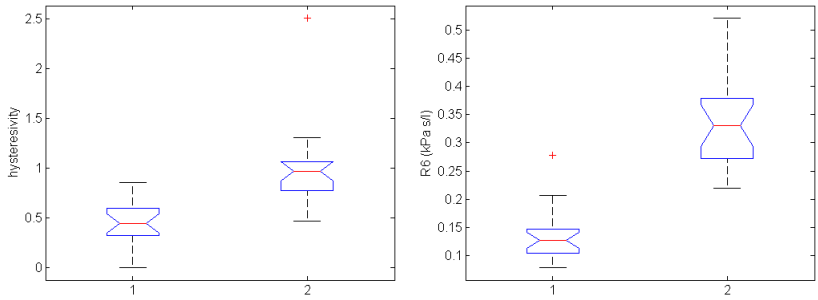

Figure 6.4: *Tissue hysteresivity η (left) and real part of impedance $R6$ evaluated at 6 Hz (right) in 1: Healthy subjects and 2: COPD patients.*

The quality factor $QF6$ is close to 0.5 in COPD, suggesting a critically damped tissue characteristic. As expected, the quality factor remained low in healthy, denoting the under-damped character of lung parenchyma. This will

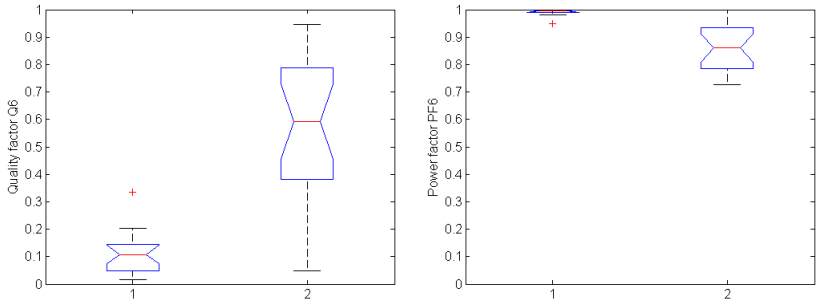

Figure 6.5: *Quality factor $QF6$ (left) and power factor $PF6$ (right) in 1: Healthy subjects and 2: COPD patients.*

then result in a high power factor for healthy and decreased power factor in COPD, hence increased work of breathing in COPD.

6.5.2 Healthy vs Kyphoscoliosis

The complex impedance values for the healthy and kyphoscoliosis patients obtained using (2.1) are depicted in figure 6.6 and the equivalent Bode plots are given in figure 6.7.

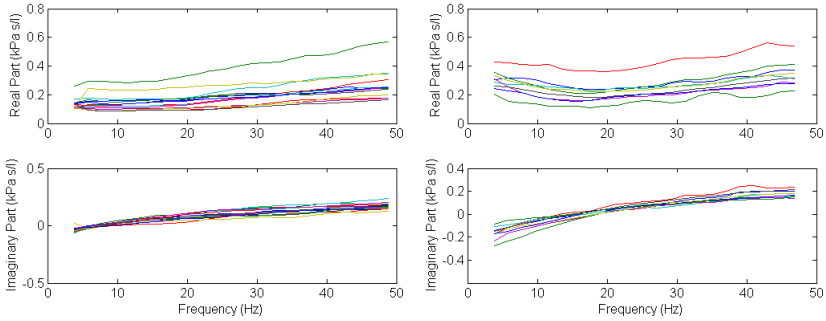

Figure 6.6: *Impedance plots for the healthy (left) and for the kyphoscoliosis (right) groups.*

Table 6.12 presents the results obtained from the identification of model parameters (2.4). There were significant variances between the groups for tissue damping G_r ($p << 0.01$), but not for tissue elastance H_r ($p < 0.75$), as observed from figure 6.8. The boxplots for the quality factor $QF6$ and

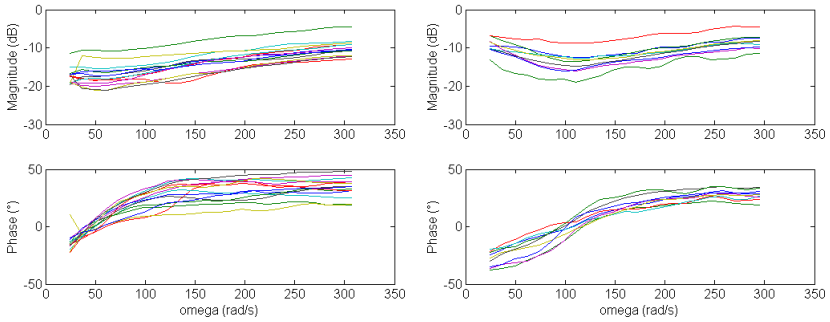

Figure 6.7: *Bode plots for the healthy (left) and for the kyphoscoliosis (right) groups.*

	Healthy	Kyphoscoliosis
L_r	0.032 ± 0.029 (0.019,0.045)	0.0173 ± 0.012 (0.007,0.02)
$1/C_r$	1.59 ± 1.10 (1.09,2.08)	2.47 ± 0.76 (1.85,3.10)
α_r	0.42 ± 0.08 (0.38,0.47)	0.54 ± 0.05 (0.49,0.58)
β_r	0.75 ± 0.11 (0.70,0.80)	0.55 ± 0.05 (0.50,0.59)
G_r	0.44 ± 0.15 (0.37,0.50)	1.55 ± 0.39 (1.25,1.86)
H_r	1.49 ± 1.14 (0.98,2.00)	1.91 ± 0.73 (1.34,2.48)
η_r	0.41 ± 0.21 (0.32,0.51)	0.85 ± 0.16 (0.72,0.98)
$R6$	0.13 ± 0.05 (0.11,0.16)	0.28 ± 0.06 (0.23,0.33)
$Frez$	10.48 ± 3.56 (8.75,13.87)	15.01 ± 2.08 (12.80,18.02)
$QF6$	0.09 ± 0.09 (0.02,0.17)	0.58 ± 0.15 (0.46,0.71)
$PF6$	0.99 ± 0.01 (0.98,0.99)	0.85 ± 0.05 (0.81,0.90)
E_R	0.02 ± 0.01	0.03 ± 0.008
E_X	0.013 ± 0.006	0.01 ± 0.005
E_T	0.02 ± 0.01	0.03 ± 0.008

Table 6.12: *Estimated and derived model parameters and modelling errors for the healthy and kyphoscoliosis groups. Values are given as mean $\pm$ standard deviation; values in brackets indicate the 95% confidence intervals.*

the power factor $PF6$ are given in figure 6.9, which were significantly different between the groups ($p << 0.01$). Finally, the boxplot for the real part of impedance at 6 Hz, $R6$ ($p << 0.01$), and for tissue hysteresivity η_r ($p << 0.01$) are given in figure 6.10.

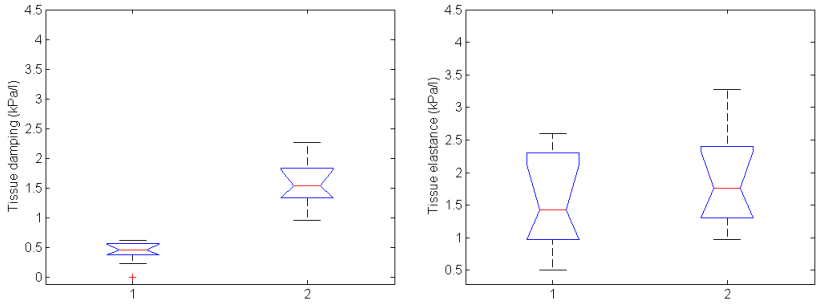

Figure 6.8: *Tissue damping G_r (left) and tissue elastance H_r (right) in 1: healthy and 2: kyphoscoliosis. See corresponding p-values discussed in text.*

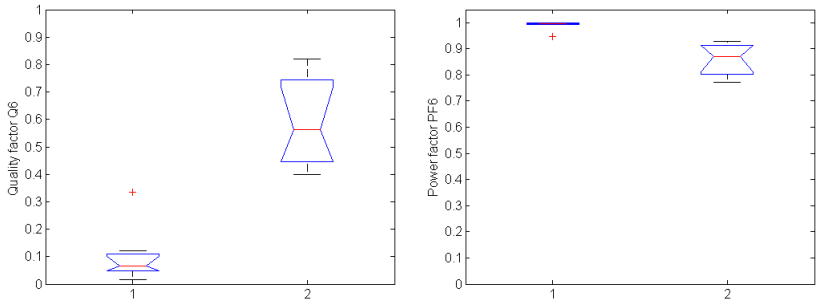

Figure 6.9: *Quality factors $QF6$ (left) and power factors $PF6$ (right) evaluated at 6 Hz in 1: healthy and 2: kyphoscoliosis. See corresponding p-values discussed in text.*

The total lung capacity can be markedly reduced in kyphoscoliosis, with a relative preservation of residual volume. Hence, the reduction in volume capacity (VC) is consequent. The fact that the predicted values in VC from the Cobb angle values were higher than measured, can be attributed to the fact that these patients may have secondary kyphoscoliosis, whereas the predicted values correlate better with idiopatic scoliosis (McCool & Rochester 2008). Similarly, a stiff chest wall (low C_{cw} values from Cobb angle) will diminish the resting position of the chest wall, which in turn, reduces the functional

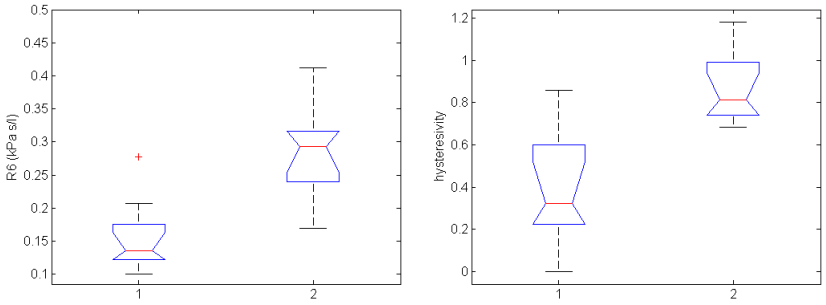

Figure 6.10: *Real part of impedance $R6$ evaluated at 6 Hz (left) and the tissue hysteresivity η_r in 1: healthy and 2: kyphoscoliosis. See corresponding p-values discussed in text.*

residual capacity. Stiffening of the chest wall leads as well to an overall reduction in the lung compliance (increased damping). One must keep in mind that these changes are not resulted from a diseased parenchyma, but a consequence of the relatively immobile chest wall.

The restrictive nature of the disease (from reduced lung volume) was confirmed by a significantly increased tissue damping G_r, airway resistance $R6$ and quality factor $QF6$. The latter suggested an over-damped dynamical system. The reduced lung and chest wall compliances increase the elastic load on the respiratory muscles and therefore increase the inspiratory pressure needed to inhale a given air volume. Consequently, the work of breathing is increased, reflected in the lower values for the power factor $PF6$.

Tissue elastance was not significantly different between the groups, but the tissue hysteresivity η_r provided a significantly increased heterogeneity in the lungs of the kyphoscoliosis group. Indeed, this result reflects the modified structure of the lungs as originated by the spinal deformity. For example, airway obstruction can occur in some cases as a consequence of changes in the geometry of the airways, or as a result of the aorta impinging on the tracheal wall.

6.5.3 Healthy vs Asthma in Children

Using a closed circuit spirometer (JAEGER MasterLab, Germany) measurements for forced vital capacity (FVC), forced expiratory volume in one second (FEV1), the ratio FEV1/FVC and the ratio of forced expiratory flow

(FEF) between 25% and 75% of FVC to FVC (FEF/FVC) were obtained for the asthmatic patients in a sitting position. These parameters were presented as raw data and percentile of the predicted values ($\%\ pred$) in a healthy subject with the same biometric details. Quality control of spirometry is given by the ATS criteria (American Thoracic Society), with the software allowing detection of non-acceptable manoeuvres. From the 19 patients with clinical diagnosis of asthma, 16 presented normal respiratory response by spirometry, and will be further referred to as normal-to-the exam (NE) patients. The underlying reason for this was that the patients had a *controlled asthma.*

The predicted values in $R6$ are very close to the measured values, in both healthy and asthmatic children, as depicted by figure 6.11. This then supports the spirometric data from Table 6.8, which shows values close to 100% from the predicted values in all subjects, thus denoting the NE patients. The high standard deviation values in Table 6.8 for the spirometric indexes are due to the few asthmatic patients which were not normal to the exam, also visible in figure 6.11 with $R6$ values higher than the rest of the group. As observed form figure 6.12, there was a linear dependence between the $FEV1/VC\%$ index and height in asthmatic children, in agreement with similar studies from literature (Duiverman *et al.* 1985, Peslin *et al.* 1984).

The complex impedance values for the healthy and asthmatic children obtained using (2.1) are depicted in figure 6.13 below. The equivalent Bode plots are given in figure 6.14. Table 6.13 presents the results obtained from the identification of model parameters.

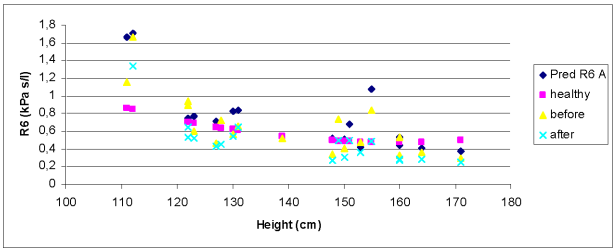

Figure 6.11: *The real part of impedance $R6$ evaluated at 6 Hz against the height in healthy (square), asthma before bronchial challenge (triangle) and asthma after bronchial challenge (crosses). Predicted values for $R6$ from (Duiverman* et al. *1985) (diamond).*

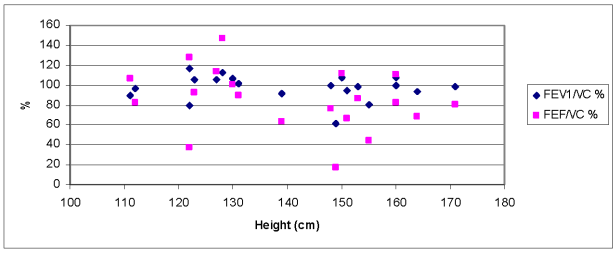

Figure 6.12: *The percent ratios $FEV1/VC\%$ (diamond) and $FEF/VC\%$ (square) against height.*

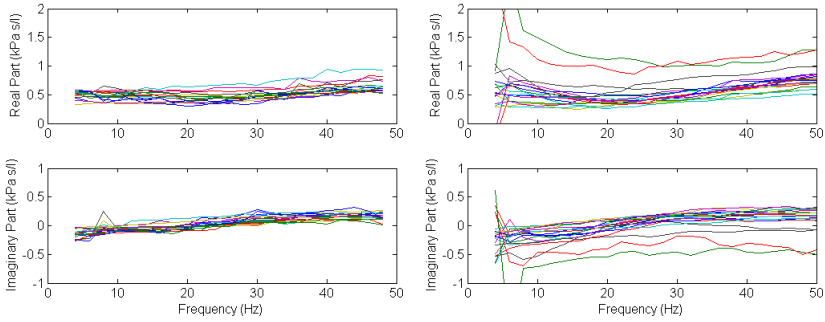

Figure 6.13: *Impedance plots for the healthy (left) and for the asthma (right) groups.*

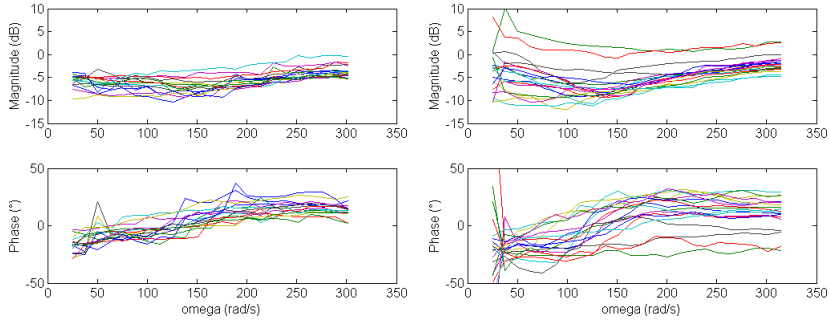

Figure 6.14: *Bode plots for the healthy (left) and for the asthma (right) groups.*

	Healthy	Asthma	Asthma (bc)
L_r	0.11 ± 0.08 (0.06,0.15)	0.13 ± 0.17 (0.03,0.23)	0.08 ± 0.04 (0.06,0.11)
$1/C_r$	4.73 ± 2.73 (3.2,6.2)	7.96 ± 3.16 (6.21,9.7)	7.95 ± 3.31 (6.13,9.78)
α_r	0.32 ± 0.11 (0.26,0.38)	0.32 ± 0.09 (0.27,0.38)	0.34 ± 0.10 (0.28,0.40)
β_r	0.63 ± 0.16 (0.54,0.72)	0.70 ± 0.13 (0.62,0.77)	0.76 ± 0.15 (0.67,0.85)
G_r	1.91 ± 0.68 (1.53,2.29)	3.21 ± 1.75 (2.25,4.18)	2.33 ± 0.90 (1.84,2.82)
H_r	4.10 ± 3.01 (2.44,5.76)	7.06 ± 3.18 (5.3,8.81)	7.47 ± 3.61 (5.34,9.39)
η_r	0.70 ± 0.38 (0.49,0.91)	0.53 ± 0.29 (0.37,0.70)	0.48 ± 0.66 (0.13,0.84)
$QF6$	0.41 ± 0.11 (0.35,0.48)	0.60 ± 0.17 (0.52,0.69)	0.61 ± 0.16 (0.52,0.7)
$PF6$	0.91 ± 0.03 (0.89,0.93)	0.85 ± 0.06 (0.82,0.88)	0.85 ± 0.06 (0.81,0.88)
$R6$	0.49 ± 0.06 (0.46,0.53)	0.61 ± 0.37 (0.42,0.8)	0.44 ± 0.24 (0.31,0.56)
$Frez$	21 ± 5.9 (17.81,24.18)	22.94 ± 12.29 (17.01,28.87)	16.66 ± 9.4 (11.98,21.34)
E_R	0.05 ± 0.01	0.09 ± 0.03	0.08 ± 0.02
E_X	0.04 ± 0.01	0.06 ± 0.04	0.04 ± 0.01
E_T	0.06 ± 0.02	0.12 ± 0.05	0.09 ± 0.03

Table 6.13: *The identified model parameters in the three groups; values are given as mean± standard deviation; (bc) denotes values after bronchial challenge; values in brackets denote the 95% confidence intervals.*

It can be observed that for the inductance L_r and its corresponding fractional-order parameter α_r, the confidence intervals are overlapping; hence, there are no significant differences from these parameters between the three groups. The elastance $1/C_r$ and its corresponding fractional-order parameter β_r were significantly different between the groups, leading to significantly different values for the tissue damping G_r ($p << 0.01$) and tissue elastance H_r ($p << 0.01$), as observed in figure 6.15. The corresponding boxplots for tissue damping G_r and tissue elastance H_r in the three groups: healthy, asthma before bronchial challenge and asthma after bronchial challenge test are given in figure 6.15. The boxplots for the quality factor $QF6$ and the power factor $PF6$ are given in figure 6.16. Finally, the boxplots for the real part of impedance $R6$ and resonant frequency η_r are given in figure 6.17.

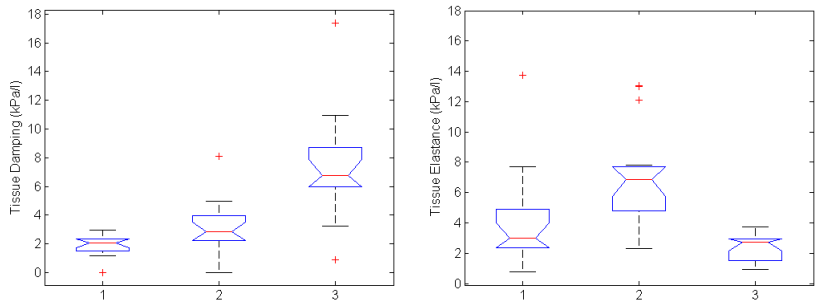

Figure 6.15: *Tissue damping G_r (left) and tissue elastance H_r (right) in 1: healthy; 2: asthma; and 3: asthma after bronchial challenge. See corresponding p-values discussed in text.*

There were no significantly different values obtained between the groups for the hysteresivity η_r ($p < 0.41$), perhaps due to prior medication of the asthmatic group. Indeed, in lung tissues, the frictional stress is almost invariably between 0.1 and 0.2 of the elastic stress, fraction known as hysteresivity. This means that for each unit of peak elastic strain energy that is stored during a cyclic deformation, 10 to 20% of that energy is lost irreversibly to heat. This fixed relationship holds at the level of the whole lung, isolated lung parenchymal tissue strips (Suki *et al.* 1994), and isolated smooth muscle strips (Yuan *et al.* 2000). The fact that in our case we do not have variations in histeresivity with bronchial challenge is explained by the fact that in all asthma patients, a spontaneous improvement higher than 12% was absent, due to prior medication intake (see Table 6.9). Nevertheless, the tissue damping and tissue elastance coefficients were sensitive to detect variations between the

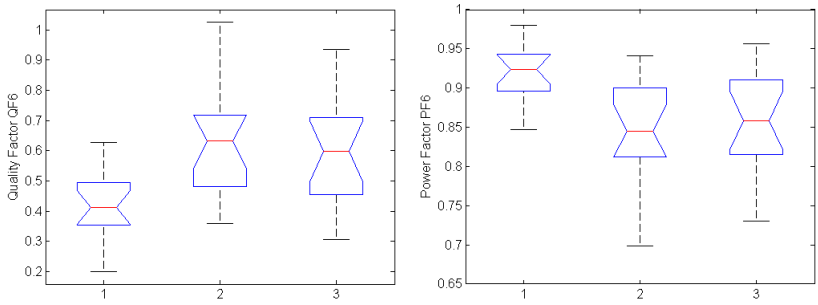

Figure 6.16: *Quality factors $QF6$ (left) and power factors $PF6$ (right) evaluated at 6 Hz in 1: healthy; 2: asthma; and 3: asthma after bronchial challenge. See corresponding p-values discussed in text.*

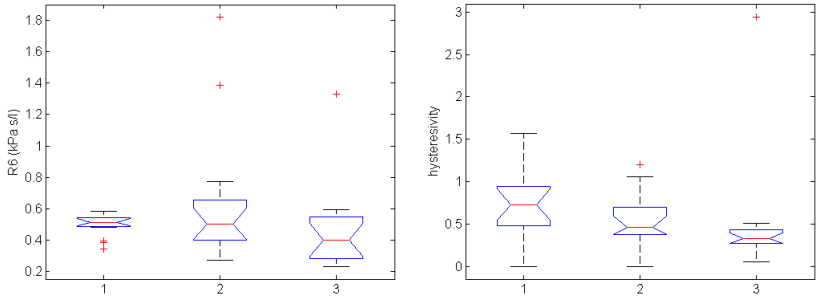

Figure 6.17: *Real part of impedance $R6$ evaluated at 6 Hz (left) and tissue hysteresivity η_r (right) in 1: healthy; 2: asthma; and 3: asthma after bronchial challenge. See corresponding p-values discussed in text.*

groups when evaluated independently. Tissue damping was higher in asthma and highest after bronchial challenge, than in healthy. Tissue elastance decreased in asthma after bronchial challenge, to values close to those found in the healthy group.

Lower $QF6$ values were obtained in the healthy group in figure 6.16 ($p << 0.01$), denoting that higher amount of air circulates in the lungs than in asthma. A slight decrease in $QF6$ values suggests an improvement in the air flow after bronchial challenge in asthma groups (decreased overall damping factor). The corresponding values for the $PF6$ show that in healthy lungs, the overall system is more efficient to use the available energy than in asthmatic lungs ($p << 0.01$), hence increased work of breathing in asthma.

The real values of impedance $R6$ ($p < 0.22$) and the tissue hysteresivity η_r ($p < 0.29$) were not significantly different between the groups. These findings are in agreement with similar studies in asthma groups, using forced oscillation lung function test (Cavalcanti *et al.* 2006). The authors also report no statistical significant differences between the control and NE groups in mean reactance, mean resistance and resonant frequency.

6.5.4 Healthy vs Cystic Fibrosis in Children

The complex impedance values for the healthy and cystic fibrosis (CF) children obtained using (2.1) are depicted in figure 6.18 below. The equivalent Bode plots are given in figure 6.19.

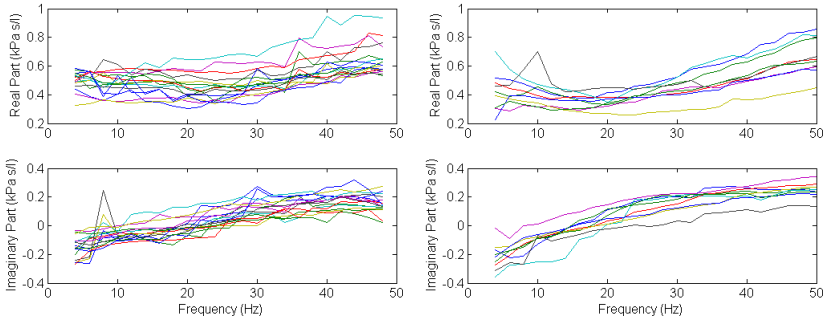

Figure 6.18: *Impedance plots for the healthy (left) and for the cystic fibrosis (right) groups.*

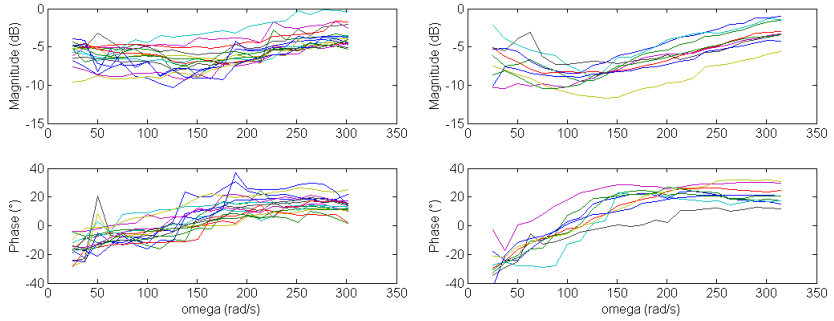

Figure 6.19: *Bode plots for the healthy (left) and for the cystic fibrosis (right) groups.*

	Healthy	Cystic Fibrosis
L_r	0.11 ± 0.08 (0.06,0.15)	0.07 ± 0.03 (0.05,0.10)
$1/C_r$	4.73 ± 2.73 (3.2,6.2)	8.67 ± 4.63 (5.11,12.23)
α_r	0.32 ± 0.11 (0.26,0.38)	0.38 ± 0.08 (0.31,0.44)
β_r	0.63 ± 0.16 (0.54,0.72)	0.77 ± 0.15 (0.66,0.89)
G_r	1.91 ± 0.68 (1.53,2.29)	2.07 ± 0.85 (1.41,2.73)
H_r	4.10 ± 3.01 (2.44,5.76)	8.26 ± 4.86 (4.52,12.00)
η_r	0.70 ± 0.38 (0.49,0.91)	0.38 ± 0.29 (0.15,0.61)
$R6$	0.49 ± 0.06 (0.46,0.53)	0.38 ± 0.08 (0.32,0.45)
$Frez$	21 ± 5.9 (17.81,24.18)	15.75 ± 4.71 (11.80,19.69)
$QF6$	0.41 ± 0.11 (0.35,0.48)	0.67 ± 0.18 (0.52,0.81)
$PF6$	0.91 ± 0.03 (0.89,0.93)	0.82 ± 0.06 (0.77,0.88)
E_R	0.05 ± 0.01	0.07 ± 0.03
E_X	0.04 ± 0.01	0.05 ± 0.04
E_T	0.06 ± 0.02	0.10 ± 0.05

Table 6.14: *The identified model parameters in the two groups; values are given as mean $\pm$ standard deviations; values in brackets denote the 95% confidence intervals.*

Table 6.14 presents the results obtained from the identification of model parameters. There were no significant variances between the groups for tissue damping G_r ($p < 0.46$) and tissue elastance H_r ($p < 0.17$), as observed from figure 6.20. The boxplots for the quality factor $QF6$ and the power factor $PF6$ are given in figure 6.21, which were significantly different between the groups ($p << 0.01$). Finally, the boxplot for the real part of impedance at 6 Hz, $R6$ ($p << 0.01$), and for tissue hysteresivity η_r ($p < 0.23$) are given in figure 6.22.

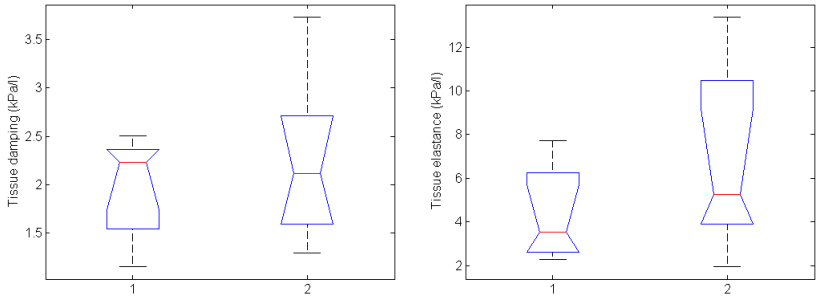

Figure 6.20: *Tissue damping G_r (left) and tissue elastance H_r (right) in 1: healthy and 2: cystic fibrosis. See corresponding p-values discussed in text.*

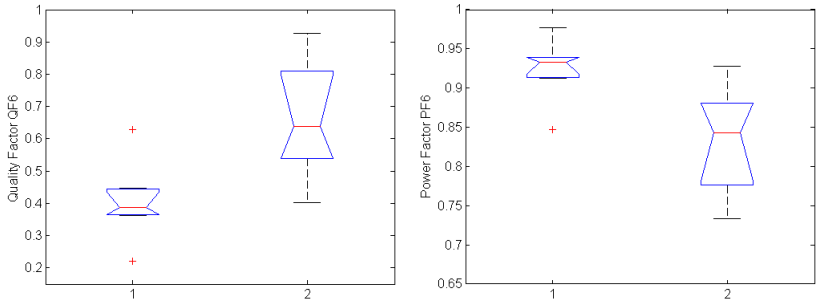

Figure 6.21: *Quality factors $QF6$ (left) and power factors $PF6$ (right) evaluated at 6 Hz in 1: healthy and 2: cystic fibrosis. See corresponding p-values discussed in text.*

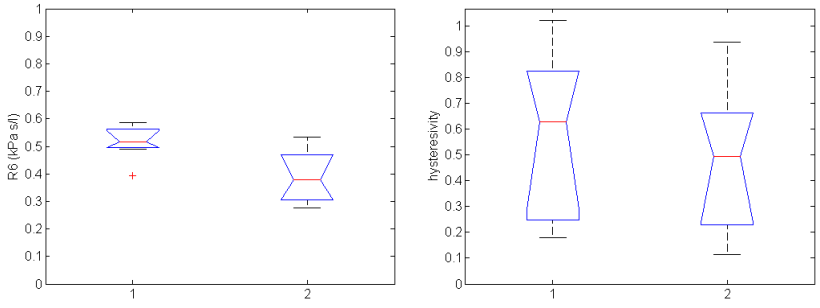

Figure 6.22: *Real part of impedance $R6$ evaluated at 6 Hz (left) and the tissue hysteresivity η_r (right) in 1: healthy and 2: cystic fibrosis. See corresponding p-values discussed in text.*

Lung disease in CF begins in the distal airways and should be therefore reflected in abnormalities of the intra-parenchymal airways and parenchymal mechanics. By its intrinsic nature, the identified FO4 model should be able to determine such changes. However, in order to partition the airway and parenchymal mechanics, one needs to measure at low frequencies, i.e. a decade lower than 5 Hz. Since in our study we are not envisaging such frequency range, it is not surprising that no statistical significant differences in tissue damping, elastance and hysteresivity were obtained. In a study over the 0.5-20 Hz frequency range using the model structure from (6.2), there was also no significant difference between the measures of lung function (airway or parenchymal) in infected or uninfected children with respiratory pathogen

(Brennan *et al.* 2005). Brennan *et al.* have shown that the FO2 model can provide separate estimates of the mechanical properties of the airways and pulmonary parenchyma in CF, but in a lower frequency decade than in this present study.

In the 4-48 Hz frequency range, the only parameters able to classify between healthy and CF children were those derived from the identified impedance at 6Hz: $R6$, $QF6$ and $PF6$. One should recall that the quality factor $QF6$ is related to the overall damping factor of the respiratory system, hence indirectly related to G_r. $QF6$ was significantly higher in CF than in healthy, denoting an over-damped tissue property. Consequently, the power factor $PF6$ was below than of healthy children, suggesting lower efficiency in breathing, thus requiring higher work of breathing.

Although one might expect increased airway resistance in CF than in healthy, the values for $R6$ were significantly lower in CF than in healthy. One of the reasons for this result might be that prior to the lung function exam, the CF patients undergone removal of retained secretions using specific physiotherapy which resulted in decreased airway obstruction and overall resistance (Rogers & Doull 2005).

The lung function measured by spirometry is insensitive to changes in airway structure, therefore it is not sufficient for early diagnosis of CF. We expect that the FO4 model is able to capture such changes, but in a lower frequency range.

6.6 Conclusions

This Chapter provided an evaluation of several candidate models in the 4-48 Hz frequency range. The specific information in this frequency range is the balance between elastic and inertial properties of the lung tissues. Hence, it is not surprising that the model with both fractional orders in the compliance and inertance terms gave the lowest modelling errors when fitted on the measured input impedance data.

Further on, we have shown the ability of this multi-fractal model to distinguish between healthy groups and other pathologic groups (COPD, kyphoscoliosis, asthma and cystic fibrosis) in this frequency range. Two novel indexes are introduced, the quality factor and the power factor, both evaluated at 6 Hz. These indexes proved to be sensitive for variations between all the groups. The identified values for the usual model parameters (tissue damping, elastance and hysteresivity) were in the same order of magnitude with

reported values in literature, but could not be compared since the model structure differs.

The results obtained in these investigations are encouraging for future clinical trials in groups with distinctive degrees of airway obstruction and other restrictive airway disorders.

Acknowledgment

I would like to acknowledge here the persons who supported administratively and technically in the clinical trials.

For the measurements on healthy adult subjects, I would like to thank Mr. Sven Verschraeven for the technical assistance for pulmonary function testing at the Department of Respiratory Medicine of Ghent University Hospital, Belgium.

For the measurements on healthy children, I would like to thank Mr. Principle Raf Missorten from St. Vincentius school in Zwijnaarde for allowing us to perform tests and to Mr Dirk Audenaert for providing the healthy volunteers. I would also like to thank Nele De Geeter and Niels Van Nuffel for further assistance during the FOT measurements.

For the measurements on COPD patients: many thanks to Prof Dr Dorin Isoc from Technical University of Cluj-Napoca and to Dr Monica Pop for the assistance in the University of Pharmacy and Medicine "Iuliu Hatieganu" from Cluj-Napoca, Romania.

For the measurements on asthmatic children, I would like to thank Rita Claes, Hilde Vaerenberg, Kevin De Sooner, Lutje Claus, Hilde Cuypers, Ria Heyndrickx and Pieter De Herdt from the pulmonary function laboratory in UZ Antwerp, for the professional discussions, technical and amicable support during my stay in their laboratory. I would also like to appreciate the many trips that Niels had made with his car to transport the medical devices.

For the measurements on kyphoscoliosis adults, I would like to thank Mrs. Hermine Middendorp for the assistance with the Ethical Committee request; to Philippe De Gryze, Frank De Vriendt, Lucienne Daman and Evelien De Burck for performing the spirometry tests and to Dr. Robert Gosselin for calculating the Cobb angles on the RX photos.

Chapter 7

Conclusions and Perspectives

In this Chapter, the main contributions of this thesis are emphasized. Some further research directions are mentioned as well.

7.1 Main Results

In this thesis, the airway tree geometry and morphology was engaged to find the origins of the fractional order appearance in impedance models of the respiratory system. These models pose the characteristic of having a constant phase over a frequency interval, suggesting a frequency independent mechanical efficiency of the lungs (i.e. constant-phase models). After a careful investigation in chapter 2 on the existing models from literature for the input impedance, we conclude that the fractional order models outperform integer order models. Hence, the natural question arises: *why?*

The work in this thesis is based on two characteristics of the respiratory system, in order to investigate the origins of the FO:

1. the geometrical structure, using the intrinsic recurrence of the respiratory tree and
2. the tissue structure, using the viscoelastic properties of lung parenchyma.

A mathematical model has been built in chapter 3, using the Navier-Stokes equations and Womersley theory, leading to a relation between the air pressure and air-flow in the airways, with respect to lung geometry, morphology and airway wall (visco)elasticity. Further on, following the two characteristics of the respiratory system, two analogues have been derived from this mathematical model:

1. an electrical analogue, based on the recurrent geometrical structure of the lung, and
2. a mechanical analogue, based on tissue viscoelasticity.

Chapter 4 shows that the electrical analogue leads to an equivalent structure of the respiratory tree, namely a ladder network. If approached with classic integer-order modelling, it results in a very high-order impedance model. However, a convergence analysis reveals that this recurrent ladder network can be well approximated by a low-order lumped impedance model containing a FO, over a limited range of frequencies. Similarly, chapter 5 shows that the mechanical analogue leads also to a ladder structure, whose low-order lumped model also contains fractional orders.

Therefore, it has been shown how at least two phenomena explain why the experimental data from chapter 2 is best approximated by lumped FO models. Furthermore, chapter 6 shows that in the envisaged frequency range (4-48

Hz) the selected best FO lumped impedance model is able to classify between healthy groups of subjects and several pathologies: Chronic Obstructive Pulmonary Disease, asthma, cystic fibrosis and kyphoscoliosis. Some typical indexes from literature, which were derived from the identified model parameters, as well as two novel indexes, are discussed for each of the groups in relation to the specific lung pathology. The results show good agreement with physiology and pathology of the lungs in all investigated groups.

The work presented in this thesis provides a mathematical basis for the results observed heuristically from experimental data. The thesis describes a physiologically consistent approach to model the respiratory tree and show the appearance of the fractional order impedance model and its typical constant phase characteristic. Rather than dealing with a specific case study, the modelling approach presents a general method which can be applied in many other similar systems (e.g. leaves, circulatory system, liver, intestines, brain). Although recurrence is linked to symmetry of the tree, we consider also the case when symmetry is not present, showing that the constant-phase behaviour is still present, hence justifying once again the use of fractional order models.

7.2 Subjects for further research

7.2.1 Relating the fractional order parameter values to pathology

It is significant to recognize the importance of relating the fractional order model parameter values to the changes occurring in lung pathology. Since these fractional orders are related to the physiology of the lungs, they might give insight on structural and morphological changes in the airways with the severity of the disease.

For instance, in chapter 4 it has been shown that the fractional order arises from the recurrence ratio of the resistance and compliance per level. Most of the obstructive and restrictive lung disorders have a crucial impact on the overall resistance and compliance of the lungs, hence it is clear that changes in these properties will lead to changes in the values obtained for the fractional orders.

A good starting point in this direction is the mathematical model developed in chapter 3, which allows various structural changes in the airways. Therefore, it provides the means to simulate various pathologies, which can be

further analyzed by means of the two analogue representations: electrical or mechanical ladder structures. The resulting fractional order values can then be related to specific changes in the airways.

7.2.2 Low Frequency Measurements

At present, the frequency range of 4-48 Hz used for gathering the measurements from patients is about one decade above the breathing frequency. This ensures that no signal distortion comes from the breathing in the measured frequency range. However, the viscoelastic properties can be analyzed at low frequencies, and one needs to measure closer to the breathing frequency. This will then bias the estimates due to the high noise level coming from the breathing signal itself. Hence, an interesting research direction is that of improving the low frequency identification, in the presence of nonlinear distortions coming from the breathing of the patient.

In order to apply the low frequency excitation signals (multisine, chirp, etc), the present FOT device needs to be revised and rebuilt in order to ensure that the signal to the patient is not distorted by hardware limitations. A preliminary version of the revised FOT device for low frequency measurements is already available, but with sub-optimal performance below 1 Hz. Once the low frequency measurements are available, the model described in chapter 5 can be further investigated, in relation to measured data.

7.2.3 Novel impedance estimation algorithms

In identification, the optimal design of the excitation signal is crucial. Another interesting research direction is the use of chirp signals instead of multisine signals to excite several oscillatory frequencies. By definition, the chirp signal excites a band of frequencies, by sending a sinusoidal signal whose frequency changes with time, but with a fixed amplitude and in a given time interval. The advantage is that a simple transfer function analyzer can be used on the input and output signals in order to identify the frequency response of a system.

The challenge is the interference with the breathing signal, which is superimposed on the chirp signal. In this manner, the classic transfer function analyzer algorithm cannot be used anymore and novel estimation algorithms have to be developed. Hitherto, several attempts have been done to perform such tests, but due to high interference with breathing, the estimation algorithm has to be revised.

Appendix A

Units for the Respiratory Impedance

For integer order models, the units for the impedance are given by the ratio between pressure (kPa) and flow (l/s), hence kPa/(l/s). In the case of fractional-order models, the units are not quite the same. For the model of Hantos *et al.* (Hantos *et al.* 1992*b*), we have that the impedance is given by:

$$Z_r(s) = \frac{P(s)}{Q(s)} = R_r + L_r s + \frac{1}{C_r s^{\beta_r}} \tag{A.1}$$

with P – pressure in kPa; Q – flow in l/s; Z_r – the respiratory impedance; R_r – airway resistance kPa/(l/s); L_r – inductance kPa/(l/s^2); $0 \leq \beta_r \leq 1$ the fractional order and s the Laplace operator. To determine the units of the capacitance C_r, we need to keep in mind the fractional order of the Laplace operator s^β.

The capacitance is defined as the ratio:

$$C_r = \frac{V(t)}{P(t)} \tag{A.2}$$

with $V(t)$ the volume in liters and $P(t)$ pressure in kPa. The term $\frac{1}{C_r s^\beta}$, can be re-written as $\frac{1}{C_r (j\omega)^\beta}$. The units for the angular frequency ω are no more *rad/second* but instead, are *rad/*$second^\beta$. The units for C_r will be given by:

$$C_r = \frac{V(t)}{P(t)} = \frac{1}{(\frac{d}{dt})^\beta} \frac{Q(t)}{P(t)} \tag{A.3}$$

which denote $(second^{\beta})\frac{l/second}{kPa}$ or $\frac{l \cdot second^{beta-1}}{kPa}$. In this context, the lung parenchyma can be considered as a *tissue with memory*. The correct units of the compliance for such model representations are not discussed in the literature, mainly because there is not enough information to provide a clear physiological explanation. In terms of viscoelastic properties, such memory effects could be associated with the slow motion of molecules at cellular level within the lung parenchymal strips.

In order to keep consistency with literature reports, we shall keep the units corresponding to an integer order model throughout the thesis (notice that other authors who use fractional order impedance also keep the same units). Presently, efforts are directed towards providing an interpretation of these units and their importance in characterizing the dynamics of the lung tissue.

Appendix B

Basic Principles for Estimating the Respiratory Impedance

For frequencies below 2Hz, the respiratory system can be represented mechanically as a series connection of a resistance R_e and a compliance C_e. The driving pressure $P(t)$ generates flow $Q(t)$ across the resistance and the volume $V(t)$ changes in the compliance. If $P_r(t)$ and $P_e(t)$ are the resistive and elastic pressure drops respectively, we have that:

$$R_r = \frac{P_r(t)}{Q(t)};\ C_r = \frac{V(t)}{P_e(t)} \text{ and } P(t) = P_e(t) + P_r(t). \tag{B.1}$$

It results that:

$$P(t) = R_r \cdot Q(t) + \frac{V(t)}{C_r} \tag{B.2}$$

This represents the first order equation in the motion-equation for a single compartment model of the respiratory system: a single balloon with compliance C_r on a pipeline with a resistance R_r. This system can be studied using the exponential decay of volume $V(t)$ as resulting from a step input V_0: $V(t) = V_0 e^{-t/\tau}$, where t is time and τ is the time constant which characterizes the system, denoted by the product of $R_r C_r$ (Hildebrandt 1969, 1970). However, in respiratory mechanics, the system is studied using a sinusoidal function at a given angular frequency ω. The pressure drop across the resistance is in phase with the flow, while the pressure across the elastic element is in phase with the volume. Using the exponential notation of sinusoidal functions, (B.2) can be re-written as function of flow:

$$P = R_r \cdot Q - j\frac{Q}{C_r \omega} \tag{B.3}$$

and division by Q results in the impedance formula:

$$\frac{P}{Q} = Z_r = R_r - j\frac{1}{C_r\omega}. \tag{B.4}$$

In this form, the resistance is the *in-phase* component, while the compliance is the *out-of-phase* component. The modulus is then defined by

$$|Z_r| = \sqrt{Re^2 + Im^2} \tag{B.5}$$

with Re and Im denoting the real, respectively the imaginary part of the complex impedance. The phase is defined by

$$\Phi = \tan^{-1}(Im/Re) = \tan^{-1}(\frac{-1}{R_rC_r\omega}) = \tan^{-1}(\frac{-1}{\tau\omega}). \tag{B.6}$$

When the pressure is oscillated at higher frequencies, an additional term, the inductance, must be introduced into the model to account for pressure changes in phase with the volume accelerations; resulting in the series RLC model structure (DuBois *et al.* 1956, Hildebrandt 1970, Hantos *et al.* 1992*b*, *a*).

The electrical impedance is given by

$$Z_r = |Z_r|\, e^{j\Phi} \tag{B.7}$$

with

$$|Z_r| = \sqrt{R_r^2 + (L_r\omega - \frac{1}{(\omega C_r)})^2} \tag{B.8}$$

and

$$\tan^{-1}\Phi = \frac{L_r\omega - 1/(\omega C_r)}{R_r} \tag{B.9}$$

Hence, Z_r varies with the frequency of the applied potential difference of the alternating current. At a certain frequency, the so-called *resonance frequency*,

$$L_r\omega - 1/(\omega C_r) = 0, \tag{B.10}$$

denoting the balance between the mechanical properties of the respiratory system. Depending on these properties, the resonance frequency varies with healthy and pathologic lungs.

Appendix C

Non-parametric Estimation of the Respiratory Impedance

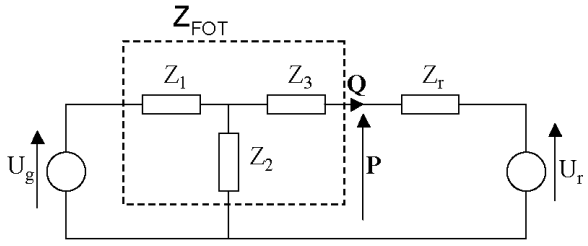

Figure C.1: *An electrical analogy of the FOT setup*

The global experimental set-up can be modelled by the electrical analogy from figure C.1, where: U_g denotes the generator test signal (known); U_r denotes the effect of spontaneous breathing (unknown); Z_r denotes the total respiratory impedance (to be estimated); Z_1 denotes the impedance (unknown) describing the transformation of driving voltage (U_g) to chamber pressure; Z_2 denotes the impedance (unknown) of both bias tubes and loudspeaker chamber; Z_3 denotes the impedance (unknown) of tube segment between bias tube and mouth piece (effect of pneumotachograph essentially).

Using the basic laws for analyzing electrical networks,the following relationships can be derived:

$$P = \frac{(Z_m - Z_3)Z_r}{(Z_m + Z_3)Z_1} U_g + \frac{Z_m}{Z_m + Z_r} U_r \tag{C.1}$$

$$Q = \frac{Z_m - Z_3}{(Z_m + Z_r)Z_1} U_g - \frac{1}{Z_m + Z_r} U_r \tag{C.2}$$

with $Z_m = Z_3 + \frac{Z_1 Z_2}{Z_1 + Z_2}$. This is a system with 2 inputs (U_g and U_r) and 2 outputs (P and Q) and the transfer matrix:

$$H = \begin{bmatrix} \frac{(Z_m - Z_3)Z_r}{(Z_m + Z_r)Z_1} & \frac{Z_m}{Z_m + Z_r} \\ \frac{Z_m - Z_3}{(Z_m + Z_r)Z_1} & \frac{-1}{Z_m + Z_r} \end{bmatrix} \tag{C.3}$$

all impedances Z being a function of the Laplace operator s. Define now the vectors:

$$S_{YU} = \begin{bmatrix} S_{PU_g} \\ S_{QU_g} \end{bmatrix} \tag{C.4}$$

and

$$S_{UU} = \begin{bmatrix} S_{U_g U_g} \\ S_{U_r U_g} \end{bmatrix} \tag{C.5}$$

containing the cross-prower-spectra $S_{YU}(j\omega)$ between two signals $y(t)$ and $u(t)$ and the auto-power-spectra $S_{UU}(\omega)$ of a signal $u(t)$. From well-known identification techniques and signal processing theory (Schoukens & Pintelon 2001), it follows that:

$$S_{YU}(j\omega) = H(j\omega) \cdot S_{UU}(j\omega) \tag{C.6}$$

In case of absence of breathing $U_r = 0$, the above expression reduces to:

$$\begin{bmatrix} S_{PU_g} \\ S_{QU_g} \end{bmatrix} = \begin{bmatrix} \frac{(Z_m - Z_3)Z_r}{(Z_m + Z_r)Z_1} \\ \frac{Z_m - Z_3}{(Z_m + Z_r)Z_1} \end{bmatrix} \cdot S_{U_g U_g} \tag{C.7}$$

and it would be *exact* to estimate the impedance of interest:

$$Z_r(j\omega) = \frac{S_{PU_g}(j\omega)}{S_{QU_g}(j\omega)} \tag{C.8}$$

the result being a complex variable. However, it is supposed that the test is done in normal breathing conditions, which may result in interference between the unknown breathing signal and the test signal U_g. From the point of view of the forced oscillatory experiment, the signal components of respiratory origin U_r has to be regarded as noise. Nevertheless, if $U_r$is designed to be uncorrelated with the test signal, then $S_{U_r U_g} = 0$ and our approach is still valid. This material has been published in (Ionescu & De Keyser 2003).

Appendix D

Nominal Recurrence in the Lungs

The anatomical parameters of the respiratory tree are designed to perform their natural function in an efficient manner. One may determine the ratio between parameters of consecutive airway levels and provide a mean and standard deviation value for each of these morphological parameters (i.e. radius, length). Since the respiratory tree is a dichotomously bifurcating structure, one may consider the parameter ratios in terms of powers of 2, as derived from morphological data of the symmetric representation of the lungs:

$$\begin{aligned} R_{m+1} &\cong R_m \cdot 2^{-0.17} \\ \ell_{m+1} &\cong \ell_m \cdot 2^{-0.18} \end{aligned} \tag{D.1}$$

where length is denoted by ℓ and airway radius by R; m represents the level of the branch. The detailed view of a branch bifurcation into two daughter branches is depicted in Figure D.1. In this figure, φ_b represents the bifurcation angle and b represents the bifurcation length.

The bifurcation angle can be found from Figure D.1 as following:

$$\cos\varphi_b \cong \frac{R_m}{2R_{m+1}} \Rightarrow \varphi_b \cong \arccos\left(2^{-0.83}\right) \approx 55^o \tag{D.2}$$

which is in agreement with other studies on bifurcation angles in lung (Sauret *et al.* 1999). The bifurcation length b in (m) is then given by:

$$\begin{aligned} b_{m+1} &\cong 2 \cdot R_{m+1} \sin\varphi_b \cong 2 \cdot R_1 \cdot 2^{-0.17m} \sin\varphi_b \cong \\ &\cong 0.016 \cdot 2^{-0.17m} \cdot 0.83 \cong 0.0132 \cdot 2^{-0.17m} \end{aligned} \tag{D.3}$$

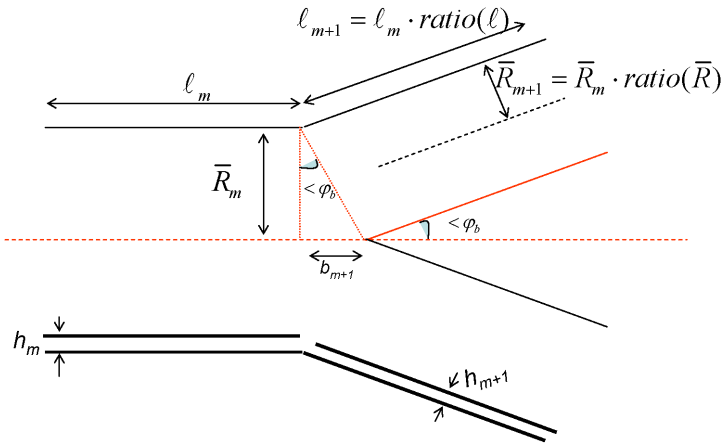

Figure D.1: *Schematic representation of a symmetric bifurcation.*

although in this contribution it will not be explicitly used. Taking into account that the airway radius is decreasing in each branch, the area of one branch will decrease too, while the total area per level will increase within the depth (2^{m-1} branches). From (D.1) follows the area in a single branch as well as the total area, respectively:

$$A^*_{m+1} \cong A^*_m \cdot 2^{-0.34} \rightarrow A_{m+1} \cong A_m \cdot 2^{0.66} \tag{D.4}$$

with m denoting the depth and $*$ denoting a single branch in the respective depth. Because the overall flow remains constant ($Q_{in} = Q_{out}$), it follows that $Q^*_m = 2Q^*_{m+1}$. From $w^*_m \cdot A^*_m = 2 \cdot w^*_{m+1} \cdot A^*_{m+1}$, with w^* the mean axial velocity in (m/s) of a single branch which is splitting in the next depth, we obtain that velocity is decreasing:

$$\frac{w^*_{m+1}}{w^*_m} = \frac{A^*_m}{2A^*_{m+1}} \cong 2^{-1} \cdot 2^{0.346} \cong 2^{-0.66} \tag{D.5}$$

Introducing the Poiseuille equation: $Q = \pi R^4 \Delta P / 8\mu\ell$, with μ - the dynamic viscosity of air and ΔP the pressure drop in (kPa), leads to:

$$\frac{\Delta P_m}{\Delta P_{m+1}} = 2\frac{R^4_{m+1} \cdot \ell_m}{R^4_m \cdot \ell_{m+1}} \cong 2 \cdot \left(2^{-0.17}\right)^4 \cdot 2^{0.18} \cong 1.40 \tag{D.6}$$

This observation tells us that the variation of the pressure will decrease with each depth in a singular branch, which is in accordance with similar studies (Olson *et al.* 1970, Pedley *et al.* 1971). Notice that these relations do not refer to the pressure itself, but its gradient, and are valid only in case of laminar flow conditions.

Appendix E

List of Symbols

Defined in Chapter 1:

P	pressure
Q	flow
Z_r	respiratory impedance
R_r	respiratory resistance
L_r	respiratory inertance
C_r	respiratory capacitance
β_r	fractional order
n	fractional order
j	the imaginary number $= \sqrt{(}-1)$
ω	angular frequency $= 2\pi f$, f the frequency in Hz
E^*	complex modulus of elasticity
σ	stress
ε	strain
E_S, E_D	storage and dissipation moduli, respectively
E	spring/elastic constant
η	damper/viscous constant

Defined in Chapter 2:

U_g	generated input/signal
U_r	breathing input/signal
Z_1	impedance describing voltage-pressure conversion
Z_2	impedance describing the loudspeaker and bias tube
Z_3	impedance describing the pneumotachograph effect
S_{PU}, S_{QU}	cross-correlation spectra between various signals
E_R	error calculated from the real part of impedance
E_X	error calculated from the imaginary part of impedance
E_T	total error
Re	the values of the real part of the impedance
Im	the values of the imaginary part of the impedance
α_r, β_r	fractional orders
$CP4$	the constant-phase model from literature in 4 parameters
$CP5$	the proposed constant-phase model in 5 parameters
N_S	total number of samples

Defined in Chapter 3:

δ	Womersley parameter $= R\sqrt{\omega\rho/\mu}$
$\varepsilon_0, \varepsilon_1, \varepsilon_2$	phase angles of the complex Bessel functions of the first kind and order 0 and 1
ϕ_P	phase angle for pressure
γ	complex propagation coefficient
κ	cartilage fraction
μ	dynamic viscosity
ν_P	coefficient of Poisson (=0.45)
θ	contour coordinate
$\rho, \rho_{wall}, \rho_s, \rho_c$	density of air at BTPS, respectively of the airway wall, of the soft tissue and of the cartilage
ω	angular frequency
ζ	radial deformation
ϕ_b	angle of bifurcation
ΔP	pressure drop
b	bifurcation length
c_x	capacity per distance unit
d_x	distance unit
$\tilde{c}, \acute{c}_0$	the complex velocity of wave propagation, the effective/corrected Moens-Korteweg velocity
f	frequency in Hz
g_x	conductance per distance unit
h	wall thickness
j	complex unit $= \sqrt{-1}$
l_x	inductance per distance unit
ℓ	airway length
ℓ_m	length of an airway in a level m
m	airway depth or airway level
p	pressure
q	flow
r	radial direction, radial coordinate

r_x	resistance per distance unit
t	time
u	velocity in radial direction
v	velocity in contour direction
w	velocity in axial direction
z	axial direction, longitudinal coordinate
y	ratio of radial position to radius $= r/R$
R	airway radius
A_p, C_1	amplitude of the pressure wave
A_u	amplitude of the radial velocity wave
A_w	amplitude of the axial velocity wave
A_m^*, A_m	the cross sectional area in an airway, and in the level m respectively
Q_m^*, Q_m	the air-flow in an airway, and in the level m respectively
w_m^*, w_m	the axial velocity in an airway, and in the level m respectively
E, E_c, E_s	effective, cartilage and soft tissue elastic modulus, respectively
F_r, F_θ, F_z	forces in the radial, contour and axial directions
M_p	modulus of pressure wave
J_1, J_0	Bessel functions of first kind and order 1 and 0
M_0, M_1, M_2	the modulus of the complex Bessel functions of the first kind and order 0 and 1
Δ	asymmetry index
R_e	electric resistance
L_e	electric inductance, inertance
C_e	electric capacitance, compliance
Zl, Zt, Z_0	the longitudinal, transversal and characteristic impedances
$\|E\|$, ϕ_E	the modulus and angle of the elastic moduli
N_{RE}	Reynolds number

Defined in Chapter 4:

λ	ratio for resistance
$1/\alpha$	ratio for inertance
χ	ratio for capacitance
o	ratio for conductance
fD	fractal dimension
R_m	radius of an airway in a level m
$BTPS$	body temperature and pressure, saturated air conditions
R_{em}	electrical resistance in the level m
L_{em}	electrical inertance in the level m
C_{em}	electrical capacitance in the level m
R_{UA}, L_{UA}, C_{UA}	upper airway resistance, inertance and capacitance, respectively
R_{CG}, L_{CG}, C_{CG}	gas compression resistance, inertance and capacitance, respectively
Zl, Zt	longitudinal and transversal impedances, respectively
Z_N, Y_N	the total ladder network impedance, respectively admitance
N	total number of levels, total number of cells
I_m	current in cell m
U_m	voltage in cell m

Defined in Chapter 5:

n	fractional order
F	force
A	cross sectional area
σ	stress
ε	strain
$\Delta\ell$	longitudinal deformation
E_S, E_D	storage and dissipation moduli, respectively
τ	relaxation time
V	volume
B	damping constant (dashpot) from electrical equivalence
K	elastic constant (spring) from electrical equivalence
E	spring constant
η	damper constant
v	velocity
x	axial displacement
E_d, φ_d	dynamic moduli and its angle
W	energy

Defined in Chapter 6:

$VC\%$	vital capacity in percent (spirometry)
$FEV1\%pred$	forced expiratory volume in 1 second, in percent of predicted value (spirometry)
FEF	forced expiratory flow (spirometry)
$MEF75/25$	mean expiratory flow at 75/25 percent ratio (spirometry)
R_{aw}	total airway resistance (body plethysmography)
C_{cw}	chest wall compliance calculated from Cobb angle
$\underline{h}$, $\underline{a}$, $\underline{w}$	height (m), age (years) and weight (kg)
$QF6$	quality factor at 6 Hz
$R6$	real part of impedance at 6 Hz
$PF6$	power factor at 6 Hz
$Frez$	resonant frequency
G_r	tissue damping
H_r	tissue elastance
η_r	tissue hysteresivity
ϕ_z	phase angle at 6 Hz

Bibliography

Abramowitz, M. & Stegun, I. (1972), "Handbook of Mathematical Functions with Formulas, Graphs, and Mathematical Tables", New York: Dover Publications.

Adolfsson, K., Enelund, M. & Olsson, M. (2005), "On the fractional order model of viscoelasticity", Springer, Mechanics of Time- Dependent materials, 9, 15–34.

Avolio, A. (1980), "A multibranched model of the human arterial system", Med and Biol Eng and Comp, 18, 709–718.

Babik, B., Asztalos, T., Petak, F., Deac, Z. & Hantos, Z. (2003), "Changes in respiratory mechanics during cardiac surgery", Anesth. Analg., 96, 1280–1287.

Barnes, P. (2000), "Chronic obstructive pulmonary disease", NEJM, 343(4), 269–280.

Bates, J. (2007), "A recruitment model of quasi-linear power-law stress adaptation in lung tissue", Annals of Biomedical Engineering, DOI 10.1007/s10439-007-9291-0, –.

Battaglia, J., Cois, O., Puigsegur, L. & Oustaloup, A. (2001), "Solving an inverse heat conduction problem using a non-integer identified model", Int J of Heat Mass Transf, 44, 2671–2680.

Bennet, S., Eldridge, M., Puente, C., Riedi, R., Nelson, T., Goetzman, B., Milstein, J., Singhal, S., Horsfield, K. & Woldenberg, M. (2009), "Origin of fractal branching complexity in the lung: www.stat.rice.edu/ riedi/UCDavisHemoglobin/fractal3.pdf", Preprint.

Benson, D., Tadjeran, C., Meerschaert, M., Farnham, I. & Pohll, G. (2004), "Radial fractional-order dispersion through fractured rock", Water Resources Research, 40, W12416, DOI 10.1029/2004WR003314.

Brennan, S., Hall, G., Horak, F., Moeller, A., Pitrez, P., Franzmann, A., Turner, S., de Klerk, N., Franklin, P., Winfield, K., Balding, E., Stick, S. & Sly, P. (2005), "Correlation of forced oscillation technique in preschool children with cystic fibrosis with pulmonary inflammation", Thorax, 60, 159–163.

Busse, W. & Lemanske, R. (2001), "Asthma", New Engl J Med, 344(5), 350–362.

Cavalcanti, J., Lopes, A., Jansen, J. & Melo, P. (2006), "Detection of changes in respiratory mechanics due to increasing degrees of airway obstruction in asthma by the forced oscillation technique", Resp Med, 100, 2207–2219.

Coleman, T. & Li, Y. (1996), "An interior trust region approach for nonlinear minimization subject to bounds", SIAM Journal on Optimization, 6, 418–445.

Craiem, D. & Armentano, R. (2007), "A fractional derivative model to describe arterial viscoelasticity", Biorheology, 44, 251–263.

Daroczi, B. & Hantos, Z. (1982), "An improved forced oscillatory estimation of respiratory impedance", Int J Bio-Medical Computing, 13, 221–235.

De Geeter, N., Ionescu, C. & De Keyser, R. (2009), "A mechanical model of soft biological tissue - an application to lung parenchyma", in : IEEE Proc. of the Eng Med Biol Comp, Minneapolis, USA, 2863–2866.

De Keyser, R., Ionescu, C. & Lazar, C. (2009), "Frequency-response based CACSD for fractional order systems", New trends in nanotechnology and fractional calculus applications, -, Springer, 415–423, eds. Machado, Baleanu.

Diong, B., Nazeran, H., Nava, P. & Goldman, M. (2007), "Modelling human respiratory impedance", IEEE Engineering in Medicine and Biology, 26(1), 48–55.

Doehring, T., Freed, A., Carew, E. & Vesely, I. (2005), "Fractional order viscoelasticity of the aortic valve cusp: an alternative to quasilinear viscoelasticity", Journal of Biomechanical Engineering, 127(4), 700–708.

DuBois, A., Brody, A., Lewis, D. & Brugges, B. (1956), "Oscillation Mechanics of Lung and Chest in Man", Journal of Applied Physiology, 8, 587–594.

Duiverman, E., Clement, J., Van De Woestijne, K., Neijens, H., van den Bergh, A. & Kerrebijn, K. (1985), "Forced oscillation technique: reference values for resistance and reactance over a frequency spectrum of 2-26 Hz in healthy children aged 2.3-12.5 years", Clinical Resp Physiol, 21, 171–178.

Eke, A., Herman, P., Kocsis, L. & Kozak, L. (2002), "Fractal characterization of complexity in temporal physiological signals", Physiol. Meas., 23, R1–R38.

Elizur, A., Cannon, C. & Ferkol, T. (2008), "Airway inflammation in cystic fibrosis", Chest, 133(2), 489–495.

Elzbieta, G., Rybaczuk, M. & Kedzia, A. (2005), "Fractal models of circulatory system. Symmetrical and asymmetrical approach comparison", Chaos, Solitons and Fractals, 24), 707–715.

Farre, R., Peslin, R., Oostveen, E., Suki, B., Duvivier, C. & Navajas, D. (1989), "Human respiratory impedance from 8 to 256 Hz corrected for upper airway shunt", Journal of Applied Physiology, 67, 1973–1981.

Franken, H., Clément, J., Cauberghs, M. & Van de Woestijne, K. (1981), "Oscillating flow of a viscous compressible fluid through a rigid tube: a theoretical model", IEEE Transactions of Biomedical Engineering, 28(5), 416–420.

Fredberg, J. & Stamenovic, D. (1989), "On the imperfect elasticity of lung tissue", Journal of Applied Physiology, 67, 2408–2419.

Fung, Y. (1981), "Biomechanics: mechanical properties of living tissues", Springer Verlag, New York.

Guyton, A. (1986), "Textbook of Medical Physiology", –, –, W. Saunders, Philadelphia, 466–525, ed. D. Dreibelbis.

Habib, R., Chalker, R., Suki, B. & Jackson, A. (1994), "Airway geometry and wall mechanical properties estimated from sub-glottal input impedance in humans", J. Appl. Phyiol., 77(1), 441–451.

Hantos, Z., Adamicz, A., Govaerts, E. & Daroczy, B. (1992*a*), "Mechanical impedances of lungs and chest wall in the cat", J. Appl. Phys., 73(2), 427–433.

Hantos, Z., Daroczy, B., Klebniczki, J., Dombos, K. & Nagy, S. (1982), "Parameter estimation of transpulmonary mechanics by a nonlinear inertive model", Journal of Applied Physiology, 52, 955–963.

Hantos, Z., Daroczy, B., Suki, B., Galgoczy, G. & Csendes, T. (1986), "Forced oscillatory impedance of the respiratory system at low frequencies", J. Appl. Phys., 60(1), 123–132.

Hantos, Z., Daroczy, B., Suki, B., Nagy, S. & Fredberg, J. (1992*b*), "Input impedance and peripheral inhomogeneity of dog lungs", J. Appl. Phys., 72(1), 168–178.

Harper, P., Karman, S., Pasterkamp, H. & Wodicka, G. (2001), "An Acoustic Model of the Respiratory Tract", IEEE Transactions of Biomedical Engineering, 48(5), 543–549.

Hildebrandt, J. (1969), "Comparison of mathematical models for cat lung and viscoelastic balloon derived by Laplace transform methods from pressure-volume data", Bulletin of Mathematical Biophysics, 31, 651–667.

Hildebrandt, J. (1970), "Pressure-volume data of cat lung interpreted by a plastoelastic, linear viscoelastic model", Journal of Applied Physiology, 28(3), 365–372.

Hogg, J., Chu, F., Utokaparch, S. & et al. (2004), "The nature of small airway obstruction in chronic obstructive pulmonary disease", New Engl J Med, 350(26), 2645–2653.

Horsfield, K., Dart, G., Olson, D. & Cumming, G. (1971), "Models of the human bronchial tree", J. Appl. Phyiol., 31, 207–217.

Hou, C., Gheorghiu, S., Coppens, M., Huxley, V. & Pfeifer, P. (2005), "Gas diffusion through the fractal landscape of the lung", Fractals in Biology and Medicine, IV, Berlin, Birkhauser, 17–30, ed. Losa, Merlini, Nonnenmacher.

Ile, C. (2007), "Investigations towards correlating a fractional-order model to the anatomical structure of the human respiratory system", scriptie, UGent, ir08.

Ionescu, C. (2003), "Respiratory Impedance", scriptie, UGent, ir08.

Ionescu, C. (2008), "Modelling the mechanical properties for the symmetric respiratory tree based on airway morphology", Internal report, UGent, ir08.

Ionescu, C. (2009), "Respiratory impedance: an overview upon parametric models from literature", Internal report, UGent, ir08.

Ionescu, C., Caicedo, A. & De Keyser, R. (2007), "Total respiratory impedance analysis using ladder networks analogy for fractional-order models", Bulletin of Transilvania University of Brasov, 14(49), 227–234.

Ionescu, C. & Chirita, M. (2008), "Stress-strain properties of natural and biomimetical formed collagen constructs", Int J of Technology and Healthcare, 16(6), 437–444.

Ionescu, C. & De Keyser, R. (2003), "A Novel Parametric Model for the Human Respiratory System", in : Proc. of the IASTED Int. Conf. on Modelling and Simulation, Palm Springs, CA USA, 246–251.

Ionescu, C. & De Keyser, R. (2004), "Some Frequency Domain Considerations upon Human Respiratory Mechanics", Annals of "Dunarea de Jos" University of Galati - open source DOAJ, -, 74–79.

Ionescu, C. & De Keyser, R. (2006), "On the potential of using fractional-order systems to model the respiratory impedance", Annals of "Dunarea de Jos" University of Galati - open source DOAJ, -, 57–62.

Ionescu, C. & De Keyser, R. (2008*a*), "Model-free Adaptive Control in Frequency Domain: Application to Mechanical Ventilation", Frontiers in Adaptive Control, www.intechweb.org/books.php (open access), In-Tech, 253–270, ed. S. Cong.

Ionescu, C. & De Keyser, R. (2008*b*), "Parametric models for the human respiratory impedance", Medical Engineering and Technology, 32(4), 315–324.

Ionescu, C. & De Keyser, R. (2008*c*), "Time domain validation of a fractional order model for human respiratory system", in : Proc. of the 14th IEEE Mediterranean Electrochemical Conf (MELECON08), Ajaccio, Corsica, 89–95.

Ionescu, C. & De Keyser, R. (2008*d*), "The use of non-integer order modelling in a tracheal simulation study", Transactions on Automatic Control and Computer Science, 53(67), 201–208.

Ionescu, C. & De Keyser, R. (2009*a*), "Flow controlled artificial ventilation of a COPD patient", in : Proc. of the European Control Conference ECC09, Budapesta, Hungary, 23-26 August 2009, 2476–2481.

Ionescu, C. & De Keyser, R. (2009*b*), "Relations between Fractional Order Model Parameters and Lung Pathology in Chronic Obstructive Pulmonary Disease", IEEE Transactions on Biomedical Engineering, 56(4), 978–987.

Ionescu, C., De Keyser, R., Desager, K. & Derom, E. (2009*a*), "Fractional order models for the input impedance of the respiratory system", Recent advances in biomedical engineering, www.intechweb.org/books.php (open access), In-Tech, 1–20, -.

Ionescu, C., Derom, E. & De Keyser, R. (2009*b*), "Assessment of respiratory mechanical properties with constant-phase models in healthy and COPD lungs", Comp Meth and Prog in Biomed, DOI: 10.1016/j.cmpb.2009.06.006, –.

Ionescu, C., Desager, K. & De Keyser, R. (2009*c*), "Estimating respiratory mechanics with constant-phase models in healthy lungs from forced oscillations measurements", Studia Universitatis Vasile Goldis, Life Science Series, 19(1), 123–132.

Ionescu, C., Muntean, I. & De Keyser, R. (2009*d*), "The respiratory impedance in an asymmetric model of the lung structure", in : Proc. of the Int. Symp. on Understanding Intelligent and Complex Systems, 6p.

Ionescu, C., Muntean, I., Tenreiro-Machado, J., De Keyser, R. & Abrudean, M. (in print), "A theoretical study on modelling the respiratory tract with ladder networks by means of intrinsic fractal geometry", IEEE Transactions on Biomedical Engineering, DOI 10.1109/TBME.2009.2030496, –.

Ionescu, C., Oustaloup, A., Levron, F., Melchior, P., Sabatier, J. & De Keyser, R. (2009*e*), "A model of the lungs based on fractal geometrical and structural properties", in : Proc. of the IFAC Int. Conf. on System Identification, St. Malo, France, 994–999.

Ionescu, C., Segers, P. & De Keyser, R. (2009*f*), "Mechanical properties of the respiratory system derived from morphologic insight", IEEE Transactions on Biomedical Engineering, 56(4), 949–959.

Ionescu, C. & Tenreiro Machado, J. (in print), "Mechanical properties and impedance model for the branching network of the sapping system in the leaf of Hydrangea Macrophylla", Springer, Nonlinear Dynamics, -, DOI: 10.1007/s11071–009–9590–0.

Jesus, I., Tenreiro , J. & Cuhna, B. (2008), "Fractional electrical impedances in botanical elements", Journal of Vibration and Cont, 14, 1389–1402.

Jesus, I. & Tenreiro Machado, J. (2008), "Development of fractional order capacitors based on electrolyte processes", Springer, Nonlinear Dynamics, -, DOI 10.1007/s11071–008–9377–8.

Kundur, P. (1994), "Power system stability and control", Power System Engineering, -, Mc Graw-Hill, NY, 200–230, ed. Balu, Lauby.

Lai, S. & Hyatt, R. (2000), "Effect of age on elastic moduli", J. Appl. Phyiol., 89, 163–168.

Losa, G., Merlini, D., Nonnenmacher, T. & Weiber, E. (2005), "Fractals in Biology and Medicine, vol.IV", Birkhauser Verlag, Basel.

Lutchen, K. & Costa, K. (1990), "Physiological Interpretation Based on Lumped Element Models Fit to Respiratory Impedance Data: Use of Forward - Inverse Model", IEEE Transactions of Biomedical Engineering, 37(11), 1076–1086.

Maksym, G. & Bates, J. (1997), "A distributed nonlinear model of lung tissue elasticity", Journal of Applied Physiology, 82(1), 32–41.

Mandelbrot, B. (1983), "The fractal geometry of nature", NY, Freeman & Co.

Mauroy, B. (2005), "3D hydrodynamics in the upper human bronchial tree: interplay between geometry and flow distribution", Fractals in Biology and Medicine, IV, Berlin: Birkhauser, 43–54, ed. Losa, Merlini, Nonnenmacher.

McCool, F. & Rochester, D. (2008), "Non-muscular diseases of the chest wall", Fishman's Pulmonary Disease and Disorders, II, Mc Graw Hall Medical, New York, 1541–1548, ed. A. Fishman.

Mead, J. (1961), "Mechanical properties of lungs", Physiological review, 41, 281–330.

Muntean, I., Ionescu, C. & Nascu, I. (2009), "A simulator for the respiratory tree in healthy subjects derived from continued fractions expansions", American Institute of Physics – Conference Proceedings, 1117, 225–231.

Murray, C. (1926), "The physiological principle of minimum work applied to the angle of branching arteries", General Physiology, 9, 835–841.

Navajas, D., Farre, R., Canet, J., Rotger, M. & Sanchis, J. (1990), "Respiratory Input Impedance in Anesthetized Paralyzed Patients", Journal of Applied Physiology, -, 1372–1379.

Oldham, K. & Spanier, J. (1974), "The fractional calculus", Academic Press, London.

Olson, D., Dart, G. & Filley, G. (1970), "Pressure drop and fluid flow regime of air inspired into the human lung", J. Appl. Phyiol., 28, 482–494.

Olufsen, M. (2004), "On deriving lumped models for blood flow and pressure in the systemic arteries", Mathem Biosciences and Eng, 1(1), 61–80.

Oostveen, E., Macleod, D., Lorino, H., Farre, R., Hantos, Z., Desager, K. & Marchal, F. (2003), "The forced oscillation technique in clinical practice: methodology, recommendations and future developments", European Resp Journal, 22, 1026–1041.

Oustaloup, A. (1995), "La derivation non-entiere (in French)", Hermes, Paris.

Oustaloup, A., Cois, O., Lannusse, P., Melchior, P., Moreau, X., Sabatier, J. & Thomas, J. (2000), "A survey on the CRONE approach", in : Proc. of the IEEE Conf on Systems, Signals and Devices (SSD05), Tutorial.

Pasker, H., Peeters, M., Genet, P., Nemery, N. & Van De Woestijne, K. (1997), "Short-term Ventilatory Effects in Workers Exposed to Fumes Containing Zinc Oxide: Comparison of Forced Oscillation Technique with Spirometry", Eur. Respir. J., 10, 523–1529.

Pedley, T., Schroter, R. & Sudlow, M. (1971), "Flow and pressure drop in systems of repeatedly branching tubes", J. Fluid Mech, 46(2), 365–383.

Peslin, R., da Silva, J., Chabot, F. & Duvivier, C. (1992), "Respiratory mechanics studied by multiple linear regression in un-sedated ventilated patients", Eur Respiratory Journal, 5, 871–878.

Peslin, R., Duvivier, C. & Jardin, P. (1984), "Upper airway walls impedance measured with head plethysmograph", Journal of Applied Physiology: Respiratory environment exercise physiology, 57(2), 596–600.

Podlubny, I. (1999), "Fractional differential equations", Academic Press, San Diego.

Quanjer, P. (1998), "Referentiewaarden", Longfunktie Onderzoek (in Dutch), -, Leuven, Garant, 27–37, ed. Demedts and Decramer.

Ramus-Serment, C., Moreau, X., Nouillant, M., Oustaloup, A. & Levron, F. (2002), "Generalised approach on fractional response of fractal networks", Chaos, Solitons and Fractals, 14, 479–488.

Reyes-Melo, M., Martinez-Vega, J., Guerrero-Salazar, C. & Ortiz-Mendez, U. (2004), "Application of fractional calculus to modelling of relaxation phenomena of organic dielectric materials", in : IEEE Proc. Int Conf on Solid Dielectrics, 6p.

Rogers, D. & Doull, I. (2005), "Physiological principles of airway clearance techniques used in the physiotherapy management of cystic fibrosis", Current Pediatrics, 15, 233–238.

Salazar, E. & Knowles, J. (1964), "An analysis of pressure-volume characteristics of the lungs", Journal of Applied Physiology, 19, 97–104.

Sauret, V., Goatman, K., Fleming, J. & Bailey, A. (1999), "Semi-automated tabulation of the 3D topology and morphology of branching networks using CT: application to the airway tree", Phys Med Biol, 44, 1625–1638.

Schoukens, J. & Pintelon, R. (2001), "System identification: a frequency domain approach", IEEE press.

Segers, P., Stergiopulos, N., Verdonck, P. & Verhoeven, R. (1997), "Assessment of distributed arterial network models", Med and Biol Eng and Comp, 35, 729–736.

Suki, B., Barabasi, A. & Lutchen, K. (1994), "Lung tissue viscoelasticity: a mathematical framework and its molecular basis", J. Appl. Physiol., 76(6), 2749–2759.

Suki, B. & Frey, U. (2003), "Temporal dynamics of recurrent airway symptoms and cellular random walk", Journal of Applied Physiology, 95, 2122–2127.

Suki, B., Yuan, H., Zhang, Q. & Lutchen, K. (1992), "Partitioning of lung tissue response and inhomogeneous airway constriction at the airway opening", J. Appl. Phys., 82, 1349–1359.

Tenreiro Machado, J. & Jesus, I. (2004), "Suggestion from the Past?", Fractional Calculus and Applied Analysis, 7(4), 403–407.

Van De Woestijne, K., Desager, K. & Marshall, E. D. F. (1994), "Recommendations for measurement of respiratory input impedance by means of forced oscillation technique", Eur Resp Rev, 4, 235–237.

Van Noord, J. (1990), "Oscillations mechanics of the respiratory system: clinical applications and modelling", Doctoral Thesis, KUL, 189p.

Vignola, A., Paganin, F., Capieu, L., Scichilone, N., Bellia, M., Maakel, L., Bellia, V., Godard, P., Bousquet, J. & Chanez, P. (2004), "Airway remodeling assessed by sputum and high-resolution computer tomography in asthma and COPD", Eur Resp Journal, 24, 910–917.

Weibel, E. (1963), "Morphometry of the human lung", Berlin: Springer.

Weibel, E. (2005), "Mandelbrot's fractals and the geometry of life: a tribute to Benoit Mandelbrot on his 80th birthday", Fractals in Biology and Medicine, IV, Berlin, Birkhauser, 3–16, ed. Losa, Merlini, Nonnenmacher.

Welty, J., Wicks, C. & Wilson, R. (1969), "Fundamentals of momentum, heat and mass transfer", John Wiley and Sons, USA.

Womersley, J. (1957), "An elastic tube theory of pulse transmission and oscillatory flow in mammalian arteries", Wright Air Development Center, Technical Report WADC-TR56-614, –.

Yuan, H., Kononov, S., Cavalcante, F., Lutchen, K., Ingenito, E. & Suki, B. (2000), "Effects of collagenase and elastase on the mechanical properties of lung tissue strips", Journal of Applied Physiology, 89(3), 3–14.